



UNIVERSITÀ DEGLI STUDI DI PALERMO

Dottorato di ricerca in Energia e Tecnologie dell'Informazione
Dipartimento di Energia, Ingegneria dell'Informazione e Modelli Matematici.
Settore Scientifico Disciplinare ING-IND/31 - Elettrotecnica

POWER DENSITY OPTIMIZATION OF EMI FILTERS FOR POWER ELECTRONIC CONVERTERS

IL DOTTORE
Ing. Graziella Giglia

IL COORDINATORE
Prof.ssa Maria Stella Mongiovì

IL TUTOR
Prof. Ing. Guido Ala

IL CO-TUTOR
Prof. Ing. G. Costantino Giaconia

IL CO-TUTOR ESTERNO
(CNR-ISSIA)
Dr. Ing. Maria Carmela Di Piazza

CICLO XXIX
ANNO CONSEGUIMENTO TITOLO 2017

To the person I love the most,

My son Giuseppe

ACKNOWLEDGEMENTS

I would like first of all to express appreciation and gratitude to my advisors, Prof. Ing. Guido Ala, Dr. Ing. Maria Carmela Di Piazza and Prof. Ing. G. Costantino Giaconia, for their availability and competence, for their guidance and support throughout my PhD studies.

I would like also to express my gratitude to Dr. Ing. Gianpaolo Vitale and Dr. Ing. Massimiliano Luna for their kind cooperation during the PhD course.

I also thank the technicians Giuseppe Scordato and Antonio Sauro for their contribution in the realization of the prototypes and for their support during the tests performed in the EMC laboratory.

I would also like to acknowledge the Prof. Pericle Zanchetta who gave me the opportunity to spend a period of study and research at the Power Electronics, Machines and Control Research Group - University of Nottingham.

Finally and the most importantly, I would like to thank my husband Eugenio and my son Giuseppe. I appreciate their love, support, and sacrifice. My greatest wish is to balance work and family life better and be more present in their lives. I would like also my parents and the rest of the family for their continuous support over the years.

Thank you everyone,

Graziella

CONTENTS

LIST OF FIGURES	6
LIST OF TABLES	10
LIST OF ACRONYMS	11
INTRODUCTION.....	13
CHAPTER I – ELECTROMAGNETIC COMPATIBILITY AND POWER DENSITY	
ISSUES IN POWER ELECTRONIC CONVERTERS.....	15
1.1 EMC: GENERAL CONCEPTS AND DEFINITIONS	15
1.2 EMI ISSUES IN POWER ELECTRONIC CONVERTERS.....	18
1.2.1 EMI Mitigation Strategies.....	23
1.3 POWER DENSITY ISSUES IN POWER ELECTRONIC CONVERTERS.....	30
1.3.1 Scopes of action for the power density improvement	31
CHAPTER II – EMI ANALYSIS.....	35
2.1 INTRODUCTION	35
2.2 CONDUCTED EMI AND NOISE PROPAGATION PATHS	35
2.3 CM AND DM EMI SEPARATION TECHNIQUES	37
2.3.1 Separation technique using RF current probes	40
2.3.2 Hardware-based separation technique	42
2.3.3 Software-based separation technique	43
2.4 EXPERIMENTAL VALIDATION OF THE SOFTWARE BASED SEPARATION TECHNIQUE.....	44
CHAPTER III – EMI FILTER DESIGN	48
3.1 INTRODUCTION	48
3.2 CRITERIA FOR THE CHOICE OF EMI FILTER TOPOLOGY	48
3.3 REAL BEHAVIOR OF PASSIVE COMPONENTS	52
3.3.1 Capacitors behavior including parasitic effects.....	53
3.3.2 Inductors behavior including parasitic effects.....	54
3.4 EMI FILTER GENERAL DESIGN PROCEDURE.....	56
3.4.1 Design of CM choke and DM extra inductor	59
3.4.2 Considerations on magnetic cores saturation	62
3.4.3 Considerations on materials of the EMI filter components.....	63

CHAPTER IV – OPTIMIZED DESIGN OF HIGH POWER DENSITY EMI FILTER	72
4.1 INTRODUCTION	72
4.2 OPTIMIZED DESIGN PROCEDURE.....	73
4.3 ODEF APPLICATION.....	77
4.4 SUMMARY.....	82
CHAPTER V – EXPERIMENTAL VALIDATION OF THE OPTIMIZED EMI FILTER	
DESIGN PROCEDURE	84
5.1 INTRODUCTION.....	84
5.2 EXPERIMENTAL SETUPS.....	84
5.3 CASE STUDY #1: INVERTER-FED INDUCTION MOTOR DRIVE	90
5.4 CASE STUDY #2: INVERTER-FED SYMMETRIC LOW POWER RESISTIVE LOAD	98
5.5 CASE STUDY #3: DC MOTOR DRIVE SUPPLIED BY A DC/DC BOOST CONVERTER	102
5.6 CASE STUDY #4: DC MOTOR DRIVE SUPPLIED BY A DC/DC BUCK CONVERTER.....	108
CONCLUSIONS AND FUTURE DEVELOPMENTS.....	113
REFERENCES.....	115
PUBLICATIONS.....	124

LIST OF FIGURES

- Figure I.1 - Main elements in the EMC.
- Figure I.2 - Scheme of EMC Problems.
- Figure I.3 - Electromagnetic disturbances related to the frequency bands.
- Figure I.4 - Typical current or voltage waveform generated by an electronic power system.
- Figure I.5 - Discrete spectrum of a train of trapezoidal pulses with $T=2\tau$.
- Figure I.6 - Spectral envelope of trapezoidal pulse train in Bode diagram.
- Figure I.7 - Feedback type active filters. (a) Current detecting and voltage compensating. (b) Current detecting and current compensating. (c) Voltage detecting and current compensating. (d) Voltage detecting and voltage compensating.
- Figure I.8 - Feedforward type active filters. (a) Current detecting and current compensating. (b) Voltage detecting and voltage compensating.
- Figure I.9 - Generic scheme of a common air cooled power electronic system.
- Figure II.1 - CM and DM noise paths.
- Figure II.2 - CM/DM voltage and current generated by a single phase power electronic equipment.
- Figure II.3 - Conducted emissions measurement circuit.
- Figure II.4 - Circuit scheme of the high voltage (HV) AMN (dual LISN).
- Figure II.5 - Impedance ideal curve and measured impedance curve of the LISN 1.
- Figure II.6 - Separation of CM and DM current by using a current probe.
- Figure II.7 - Comparison between the ideal and measured CM (upper) and DM (lower) LISN impedance.
- Figure II.8 - Separation of CM and DM noise via hardware.
- Figure II.9 - Block diagram of the time domain EMI measurement method.
- Figure II.10 - Test bench used to conducted EMI measurements.
- Figure II.11 - Comparison between CM EMI obtained by the software-based separation technique and by RF measurement-based technique.
- Figure II.12 - Comparison between DM EMI obtained by the software-based separation technique and by RF measurement-based technique.
- Figure III.1 - EMI filter circuit configurations.
- Figure III.2 - Schematic representation of noise source and victim without (a) and with (b) filter.
- Figure III.3 - Equivalent circuit of capacitors.
- Figure III.4 - Bode plot of impedance $Z_c(f)$.

- Figure III.5 - Equivalent circuit of an inductor.
- Figure III.6 - Bode plot of impedance $Z_L(f)$.
- Figure III.7 - Generic EMI filter configuration (a), CM equivalent circuit (b) and DM equivalent circuit (c).
- Figure III.8 - Steps of EMI filter design.
- Figure III.9 - CM choke.
- Figure III.10 - Winding angle example.
- Figure III.11 - Electrical representation of a CM inductor.
- Figure III.12 - Magnetic properties for ferrites, iron powder and metal alloys: permeability vs. frequency.
- Figure III.13 - Magnetic permeability curves versus frequency (a), Magnetization curves (b) and the saturation induction versus temperature (c) of the VITROPERM 500F and a typical Mn-Zn ferrite.
- Figure III.14 - Hysteresis loop of VITROPERM 500F and a typical ferrite.
- Figure III.15 - Comparison of magnetization losses of typical materials for CM choke and DM inductance.
- Figure III.16 - CM choke set up by using an N30 ferrite core (left) and a VITROPERM core (right).
- Figure III.17 - 100 nF capacitor impedance (a) 250Vdc ceramic capacitor (measured data) and (b) 300Vac, 1000Vdc polypropylene capacitor (datasheet).
- Figure III.18 - Measured impedance module (upper) and phase (lower) of a 47 μ F electrolytic capacitor with nominal voltage equal to 160V and 400V.
- Figure III.19 - Measured impedance module (upper) and phase (lower) of a 47 μ F electrolytic capacitor with nominal voltage equal to 160V of different manufacturers and for different application fields.
- Figure IV.1 - Concept of the optimized EMI filter design procedure.
- Figure IV.2 - Flowchart of the optimized EMI filter design procedure.
- Figure IV.3 - Screenshot of the web page for ODEF application download.
- Figure IV.4 - Screenshot of ODEF application: *Noise Profile* tab.
- Figure IV.5 - Screenshot of ODEF application: *Computation* tab.
- Figure IV.6 - Screenshot of ODEF application: *Extra* tab.
- Figure V.1 - Scheme of the experimental rigs: (a) case study #1; (b) case study #2; (c) case study #3; (d) case study #4.
- Figure V.2 - Cyclone III FPGA Starter Board equipped with the Nial Stewart GPIB expansion board used in the experimental setups.
- Figure V.3 - Board with the display SSD used in the experimental setups.

- Figure V.4 - MIL-STD-461F: CE102 limit (EUT power leads, AC and DC) for all applications.
- Figure V.5 - CISPR 25: Limits for broadband conducted disturbances (peak detector).
- Figure V.6 - View of the PWM induction motor drive experimental setup.
- Figure V.7 - CM and DM EMI generated by inverter-fed induction motor drive.
- Figure V.8 - Photo of conventionally designed EMI filter (on the left) and optimized EMI filter (on the right), in case study #1.
- Figure V.9 - Comparison of optimized and conventionally designed EMI filter performance (case study #1).
- Figure V.10 - Distribution of all feasible configurations (case study #1).
- Figure V.11 - Distribution of the best 15 configurations (case study #1).
- Figure V.12 - Scatter plot of the best 15 configurations (case study #1).
- Figure V.13 - Volume of the best configuration for each number of stages (case study #1).
- Figure V.14 - Distribution of the best 100 configurations for different n. of stages (case study #1).
- Figure V.15 - Volume variation of the best design for increasing CM attenuation (case study #1).
- Figure V.16 - Number of stages of the best design for increasing CM attenuation (solid line). CM core index of the best design for increasing CM attenuation (dashed line). - case study #1.
- Figure V.17 - CM and DM EMI generated by inverter-fed symmetric low power resistive load.
- Figure V.18 - Photo of conventionally designed EMI filter (on the left) and optimized EMI filter (on the right), in case study #2.
- Figure V.19 - Comparison of optimized and conventionally designed EMI filter performance (case study #2).
- Figure V.20 - CM and DM EMI generated by a DC motor drive supplied by a DC/DC boost converter.
- Figure V.21 - Comparison of components used to EMI filters setup (case study #3).
- Figure V.22 - Comparison of optimized and conventionally designed EMI filter performance (case study #3).
- Figure V.23 - Distribution of feasible configurations without extra L_{DM} (case study #3).
- Figure V.24 - Distribution of the best 30 configurations without extra L_{DM} (case study #3).
- Figure V.25 - Scatter plot of the best 30 no extra L_{DM} configurations (case study #3).
- Figure V.26 - Volume of the best configuration for each number of stages (case study #3).
- Figure V.27 - Distribution of the best 100 configurations for different n. of stages (case study #3).
- Figure V.28 - CM and DM EMI generated by DC motor drive supplied by the DC/DC buck converter 1.

- Figure V.29 - CM and DM EMI generated by DC motor drive supplied by the DC/DC buck converter 2.
- Figure V.30 - Comparison between CM EMI generated by the DC motor drive supplied by the buck converter 1 (solid line) or by the buck converter 2 (dashed line).
- Figure V.31 - Comparison between DM EMI generated by the DC motor drive supplied by the buck converter 1 (solid line) or by the buck converter 2 (dashed line).
- Figure V.32 - Measured EMI with and without EMI filter (case study #4).

LIST OF TABLES

Table II.1	Performance indices.
Table III.1	Filter topology selection based on impedance mismatching criterion.
Table III.2	Tables of AWG wire sizes (solid wire).
Table III.3	Comparison of different magnetic cores characteristics to set up a LCM=0.8 mH.
Table V.1	Input data for ODEF application – Case study #1.
Table V.2	Comparison between optimized and conventionally-designed EMI filters (Case study #1).
Table V.3	Input data for ODEF application – Case study #2.
Table V.4	Comparison between optimized and conventionally-designed EMI filters (Case study #2).
Table V.5	Input data for ODEF application – Case study #3.
Table V.6	Comparison between optimized and conventionally-designed EMI filters (Case study #3)
Table V.7	Input data for ODEF application – Case study #4 with buck converter 1.
Table V.8	Features of the optimized EMI filter (case study #4).

LIST OF ACRONYMS

AEF	active EMI filter
AMN	artificial mains network
AWG	american wire gauge
CISPR	Comité International Spécial des Perturbations Radioélectriques (International Special Committee on Radio Interference)
CM	common mode
DAEF	digital active EMI filter
DFFT	discrete fast Fourier transform
DM	differential mode
DPDT	double pole - double throw
DSO	digital storage oscilloscope
EEPROM	electrically erasable programmable read only memory
EM	electromagnetic
EMC	electromagnetic compatibility
EME	electromagnetic emission
EMI	electromagnetic interference
EPC	equivalent parallel capacitance
EPR	equivalent parallel resistance
ESL	equivalent series inductance
ESR	equivalent series resistance
EUT	equipment under test
HF	high frequency
HSMC	high speed mezzanine card
HV	high voltage
IEC	International Electrotechnical Commission
IL	insertion loss
LISN	line impedance stabilization network
PLLs	phase-locked loop
PSD	power spectral density
PWM	pulse width modulation
QP	quasi peak

List of Acronyms

RCFMFD	random carrier-frequency modulation with fixed duty cycle
RF	radiofrequency
RPWM	random pulse width modulation
SMPS	switched mode power supply
SRF	self resonant frequency
SSD	seven segments display
SSRAM	synchronous static random access memory
VNA	vector network analyzer

INTRODUCTION

The switching power converters are used in a broad variety of applications, from the consumer electronics to the DC distribution systems, from the vehicle applications (road vehicles, marine vehicles, aircraft) to the industrial automation. In each of these application fields, the conversion systems which present more compact size and reduced weight, at the same power, are strongly required in relation to stringent design constraints. In this context, the optimization of the *power density* of the converter becomes an essential requirement. The increase of the switching frequency of the static devices allows an improvement of the power density, thanks to the possibility of reducing the sizes of the energy storage passive components (inductors and capacitors). On the other hand, the increase of the switching frequency determines, with high probability, the generation of more relevant conducted electromagnetic interferences (*EMI*) in the frequency range 150 kHz – 30 MHz. In particular, the high switching frequency is responsible for several serious problems affecting both the reliability and the electromagnetic compatibility of the systems of which the converter is part. For this reason, noise mitigation is, more than ever, one of the major issues in power electronic system design, particularly when dealing with stringent standard regard the maximum emission limits, which however are mandatory for the marketing of these systems.

EMI filters are the most efficient among the different possible solutions to mitigate the conducted electromagnetic interferences. On the other hand, EMI filters are part of the power electronic converters and they have significant impact on the overall converter volume and weight. In order to take on this issue, besides satisfying EMI limits, a further optimization in terms of filter size and weight during the design stage is advantageous to maximize the overall converter's power density. The identification of the configuration leading to the best power density, in terms of minimum volume/weight, is a nontrivial task. The conventional design of EMI filters disregards the power density issue. The trial and error approach requires a significant effort in terms of time spent and it does not guarantee the optimal choice of filter configuration in order to obtain the maximum power density. For this reason, an automatic optimized design procedure of discrete EMI filters has been developed. Once the power electronic converter characteristics are known and based on databases, suitably set up, of commercially available devices for the realization of EMI filters, the optimized procedure enables EMI engineers or scientists to obtain the best EMI filter configuration in term of power density.

On the basis of the developed automatic design procedure, an interactive software, ODEF (Optimized Design of EMI Filters), has been developed to make the new design procedure more

accessible to EMI designer. Moreover, the developed application is provided of a graphical interface which allows to analyze and compare simultaneously different EMI filter designs. The optimization algorithm can be used as a EMI filter design tool but also as a tool for the analysis of the EMI filters performance.

The thesis is organized as follows.

The first chapter gives an overview of the conducted electromagnetic interference issues and the power density issues in power electronic converters. A literature review and a summary of the main mitigation strategies adopted to suppress the conducted EMI are provided and the scopes of actions for a power density improvement are explained.

Chapter II discusses the characterization of the EMI noise, such as the difference between the common-mode (CM) and differential-mode (DM) noise. The CM and DM noise paths are evaluated and three CM and DM separation techniques are described. In particular, a software-based CM/DM separation technique, developed within the PhD work, has been validated by comparing the measured EMI spectra with those obtained by measurements coming from a high bandwidth radio-frequency current probe and a spectrum analyzer. Furthermore, the deviation of the results obtained by the two techniques has been computed in terms of normalized root mean square error and normalized average error.

Chapter III is dedicated to the conventional EMI filter design. In the first step, the criteria for the correct choice of EMI filter topology and the real high frequency behavior of filter components, that can heavily influence the filter performance, are discussed. Then the EMI filter general design steps are presented. Finally, the chapter ends with some considerations on the material of filter components and on their impact on filter performance and size.

Chapter IV presents the new optimized EMI filter design technique for the optimal and fast selection of discrete EMI filter components and configuration, aimed at obtaining the minimum volume/weight. A general description of the ODEF implementation and functionality is given as well.

The results of EMI filters designs according to the optimized and conventional procedure in four case studies are discussed in chapter V. A comparison of the obtained optimized filters with the conventionally designed ones, is carried out in terms of volume, weight and performance. Furthermore, an analysis of the feasible configurations returned by the algorithm is performed, for some of the case studies, by a series of comparative plots generated by ODEF application.

The end of the thesis contains the conclusions and the possible future developments.

CHAPTER I – Electromagnetic Compatibility and Power Density issues in Power Electronic Converters

This chapter starts with an overview of the general concepts and main definitions of the Electromagnetic Compatibility. It follows with the background of conducted electromagnetic interference issues in power electronic converters. Then, a literature review and a summary of main mitigation strategies adopted to suppress the conducted EMI are provided. Finally, also the power density issues in power electronic converters are treated and the scopes of action for a power density improvement are explored.

1.1 EMC: General Concepts and Definitions

Electromagnetic Compatibility (EMC) deals with electromagnetic problems existing between the “devices” and the environment in which they are located.

The legislative decree 05/18/2016 no. 80 implements the Directive 2014/30/UE, drafted in date 26/02/2014, which provides the definition of electromagnetic compatibility as follows: “Electromagnetic Compatibility is the ability of a device, equipment or system to function satisfactorily in its electromagnetic environment without introducing intolerable electromagnetic disturbance to anything in that environment”. According to the Directive 2014/30/UE, the term “devices” indicate all electrical and electronic devices together with equipments and systems containing electrical and/or electronic components.

The term EMC, covers both electromagnetic emission and electromagnetic susceptibility [1], [2]. The electromagnetic emission is referred to the disturbance level emitted by a device which can degrade the performance of other devices operating in the same environment; the electromagnetic susceptibility (or immunity) is the ability of a device to maintain the correct functional performance in presence of external EM interference. Then an electromagnetically compatible system must satisfy the following requirements:

- it does not cause interference with other systems;
- it must not be susceptible to electromagnetic radiation generated by other systems;
- it does not cause interference to himself.

The EMC study is focused on the generation, the transmission and the reception of electromagnetic energy intended as a disturbance in relation to the correct functioning of the "devices". Therefore a

problem related to electromagnetic compatibility requires the identification of a source or emitter, of a propagation path and the coupling channel and a receiver or victim, as shown in Figure I.1.

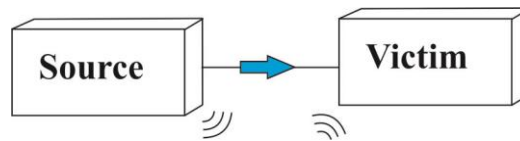


Figure I.1 - Main elements in the EMC.

It is possible to introduce a further distinction between natural (i.e. lightning, electrostatic discharge) and artificial sources; the latter can be classified as intentional and unintentional sources.

An intentional radiation source is specifically designed to generate radiation to perform a specific function (e.g. a mobile phone or a radio transmitter), while for an unintentional one, the emissions are an undesirable consequence (e.g., the radiation emitted by a computer or a monitor).

Concerning the effects that electromagnetic radiation causes on receivers, a similar distinction applies on them: if the received radiation generates a desired behavior it is called "useful signal" (intentional receiver); instead, if the received radiation generates a malfunction, it is called "interference signal" (unintentional receiver) or *Electromagnetic Interference* (EMI).

With regard to the electromagnetic interference effects, it is possible to observe that the EMI can determine a simple reduction of the devices/equipment/systems performance, or a malfunction or fault conditions of the same apparatus and, in certain critical applications, it can compromise irreparably things and/or people safety.

It must be remarked that the intentional sources and receivers can generate or receive electromagnetic radiation in frequency bands different from those typical of normal operation; even then they must comply the electromagnetic compatibility requirements.

On the basis of EMI propagation mode, the EMI are distinguished in conducted and radiated disturbances. The scheme in Figure I.2 summarizes electromagnetic compatibility problems [3]. It is common to define the EMI study into four different groups: conducted emissions, radiated emissions, conducted susceptibility and radiated susceptibility. The radiated emissions are the electromagnetic waves which propagate into the surrounding environment due to irradiation of the currents circulating in the conductor elements (e.g. cables or screens). It comes to radiated susceptibility if a component acts as an antenna that intercepts the emissions generated by other systems. The conducted emissions are undesired voltage or current signals which propagate from a system to another through the connection cables (power cables, signal and communication cables); the sensitivity of a component to this type of interference defines the conducted susceptibility. In fact, a variable signal that flows in a

conductor cable generates an EM field in the surrounding space and at the same time an EM field induces an electrical signal on a conductor. Then, conducted and radiated phenomena are related.

The EMI sources can be located inside the system (internal problem or intrasystem problem), or the interference can be generated by external sources (external problem or intersystem problem). A very common interference source, internal or external in the system, is due to a signal which, although specifically generated for a given circuit, also reaches one or more circuits in the system to which the signal itself is not dedicated.

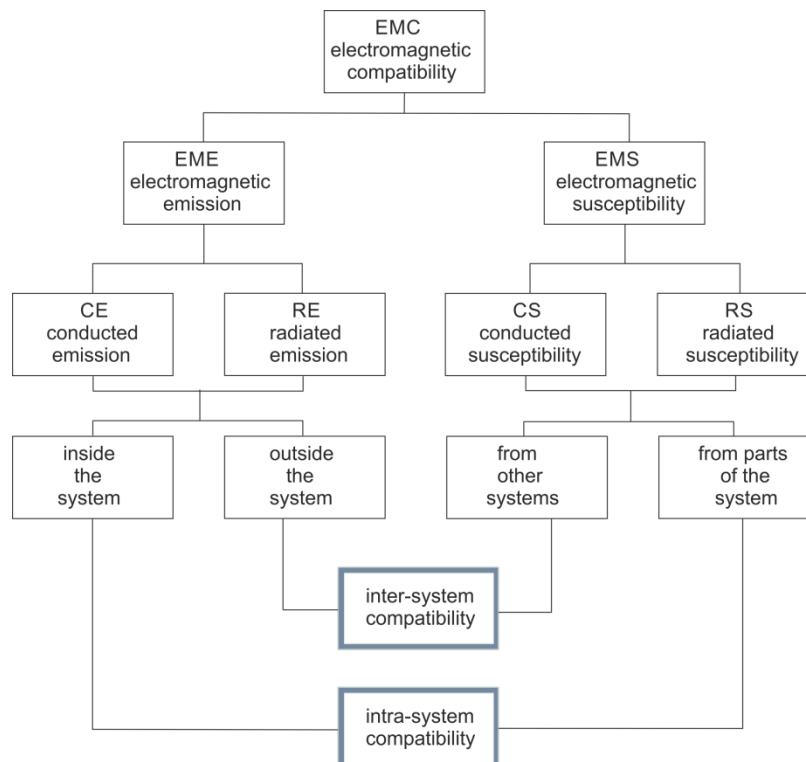


Figure I.2 - Scheme of EMC Problems.

According to the definitions listed above, the electromagnetic compatibility is related to the generation, the transmission and the reception of the electromagnetic energy between the source and the receiver by means a coupling path in which the interference is an unwanted phenomenon.

To prevent interference it is possible implement three strategies:

- to suppress the generated EMI;
- to make the coupling path less efficient as possible;
- to make the receiver less susceptible to interference.

It is therefore important to manage the generation of the electromagnetic radiation as well as the susceptibility to it, during the design phase of the device. If the noise sources and the possible

susceptibilities are not taken into account in the initial design, it can result underperforming, expensive and time-consuming procedures during the production and deployment process [4].

The standardization work on electromagnetic compatibility is spread mainly according to the following definitions:

1. a typical electromagnetic environment (public networks, residential or industrial environment, control areas plants, outdoor areas, etc.);
2. a compatibility level for each type of interference, given a specific interference level that has a defined probability of being exceeded in a given environment;
3. a susceptibility level, for different categories of devices, given by the maximum interference level that a device must be able to support maintaining its performance;
4. an emission limit level as the maximum interference level that a device can generate.

1.2 EMI issues in Power Electronic Converters

The power electronic converters can be used wherever it is necessary to modify the characteristics of the waveforms related to the electrical energy conversion, for example, varying the voltage and current levels, the waveform or the frequency [5], [6].

A power electronic converter is defined as the system consisting of one or more electronic switching devices and, if necessary, transformers, filters and other auxiliary devices necessary for the power electronic conversion. Electronic switching device is a component including one or more conductive paths in a single direction, not actuated or controlled in bistable mode [6]. Often the switching electronic devices used in power electronic converters are named as elementary conversion unit.

The main power electronic converters can be classified on the basis of their fundamental functions, on the basis of the converter switching mode and on the basis of the voltage (V) - current (I) plane quadrants in which they can work.

According to the first classification criterion, the power electronic converters can be identified as follows:

- rectifier (AC/DC converter);
- inverter (DC/AC converters);
- AC/AC converter;
- DC/DC converter.

The first two types of converter realize the conversion from AC to DC current and vice versa, respectively. Using the AC/AC and the DC/DC converters, it is possible to realize the voltage amplitude/polarity variation; furthermore the AC/AC converter makes also possible the variation of the frequency and of the number of phases.

A further distinction can be made among the AC/AC converters:

- AC power regulators to modify the current characteristics keeping constant the frequency.
- Direct frequency converters to modify the voltage, the frequency or the number of phases without an intermediate energy storage circuit.
- Indirect frequency converters that have an intermediate DC voltage connections. They modify the voltage, the frequency or the number of phases including an energy storage device in the intermediate circuit. In such converters, the output frequency is independent from the input one.

DC-DC converters are also referred as direct regulators of continuous current (also called chopper) and realize the DC voltage variation without employing any intermediate circuit. Except for some types of rectifiers, which can also operate in an uncontrolled way, all converters require a controllable elementary conversion unit.

With regard to the switching mode, it is possible to recognize the following types of converters:

- Natural switching converters in which the switching event is imposed by an external circuit and it occurs with a frequency equal to the network supply frequency.
- Forced switching converters in which the switching event is imposed by a control operation on the driving devices conditions of the converter. This event occurs with a frequency higher than the network supply frequency.
- Resonant or quasi-resonant converters in which the switching event occurs when the condition of zero voltage and/or zero current on the component is verified [2].

Finally, taking into account the operating quadrants of the converters on the plane V-I, it is possible to classify the following converters type.

- Converters which allow the power flux in a single direction, therefore their operation is only in the first quadrant.
- Reversible converters (also called current converters) whose operation can be represented in the first and second quadrant.
- Bidirectional converters are composed of two reversible converters with the electronic devices oriented in opposite direction, so as to obtain the possibility of reversal of both the current of the voltage; their operation may therefore be represented in all four quadrants of the V-I plane.

Power electronic converters are particularly interesting systems in electromagnetic compatibility. Due to non-linear effects of the static conversion devices and to the switching operation, power electronic converters generate a wide range of electromagnetic disturbances. The generated noise propagate towards the power supply network and to the load; then EMC problems occur [7].

In recent years, the power electronics development has contributed to progress in the power converters technology and in the market deployment evolution. In particular, the progress achieved in

the power electronic components control, during their power on/off phase, has allowed to obtain a drastic reduction of the turn-on and of the turn-off times of the switched voltage and current waveforms. Then a relative increase of the switching frequencies has been obtained. Indeed, some semiconductor power electronic devices controllable in turn-on and turn-off phase such as the GTO (Gate Turn-Off Thyristors) exhibit turn-on and turn-off time of tens of microseconds, and switching frequencies of some kHz. The BJT (Bipolar Junction Transistors) and the IGBT (Insulate Gate Bipolar Transistors) exhibit turn-on and turn-off time lower than microseconds and allowing switching frequency about to 100 kHz. Recently, power electronics market has been boosted by new high-speed MOSFET (Metal-Oxide-Semiconductor Field Effect Transistors), as the wide-band gap devices based on Silicon Carbide (SiC) or gallium nitride (GaN) [8], [9], allowing faster switching operation. These devices exhibit turn-on and turn-off time of tens of nanoseconds and switching frequency of the order of MHz. These devices are characterized by low switching losses and allow to obtain a beneficial effect on the reliability.

The increase of the switching frequency of static devices allows to reduce the dimensions of the energy storage passive elements (inductors and capacitors). Then, for the same power, more compact conversion circuits are obtained with an increasing of the system power density. However, the increase of the switching frequency leads to a significant extension in the harmonics frequency spectrum produced by power electronic converters. For this reason power electronic converters are considered unintentional sources of high frequency electromagnetic interference and they determine several problems affecting both the reliability and the electromagnetic compatibility of the systems of which the converter is a part.

Finally, it should be noted that the digital electronic devices of the control apparatus (in particular of the processor with an internal clock of the tens of MHz) can also determine the radio frequency interference emission. Even the driving circuits (drivers) of switching devices contribute to EMI emission because they amplify the high frequency signals and their connection, being traversed by high frequency current signals, radiate electromagnetic field.

Electromagnetic disturbances, in relation to their frequency content, can be related to well defined frequency bands (Figure I.3). Following a distinction into subharmonic frequencies (below 50 Hz), disturbances in the harmonic frequencies range (50 Hz to about 2 kHz), disturbances in the frequency band between the acoustic frequencies and the radio frequency, radio frequency conducted disturbances (in the frequency band 150 kHz - 30 MHz) and radiated interference (above 30 MHz).

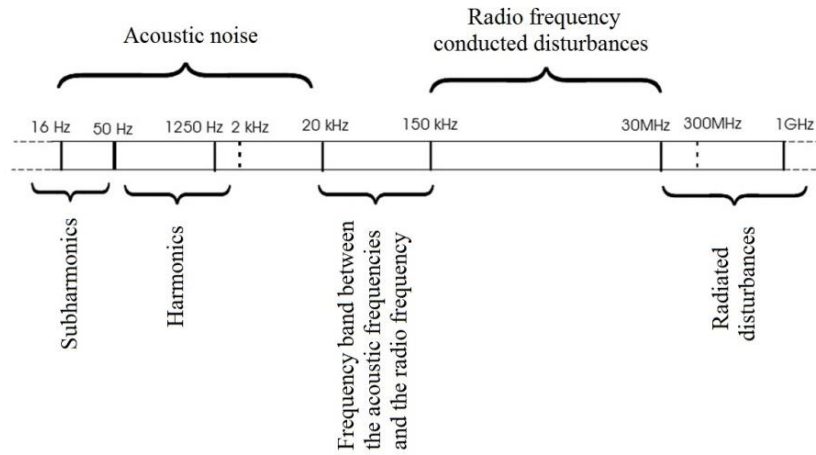


Figure I.3 - Electromagnetic disturbances related to the frequency bands.

In order to characterize the high frequency spectral content of the generated noise by a generic switching power electronic device, an analysis in the frequency domain of a series of trapezoidal pulses can be usefully performed [1].

The trapezoidal pulse, shown in Figure I.4, represents a typical current or voltage waveform generated by the power electronic circuits, where the variation speed of the signal is related to the switching speed of semiconductor devices.

Each trapezoidal pulse is described by the amplitude A , the rise time τ_r , the fall time τ_f and a pulse width τ of the 50% amplitude (Figure I.4). The time period of the pulse repetition is indicated as T .

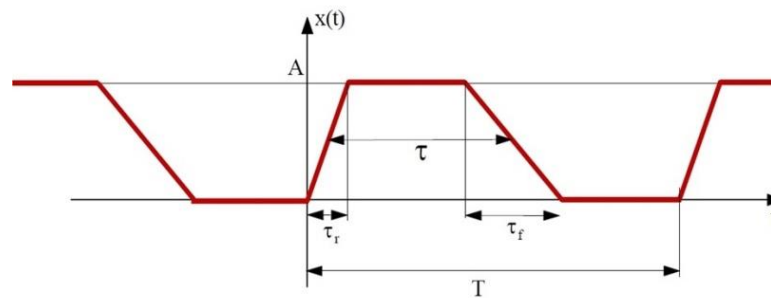


Figure I.4 – Typical current or voltage waveform generated by an electronic power system.

As it is well known, a periodic function $x(t)$ is expressible in Fourier series. The complex exponential form of the Fourier series of a periodic function $x(t)$ is defined as follows:

$$x(t) = c_0 + \sum_{n=1}^{\infty} c_n^+ \cos(n\omega_0 t + \phi_n) \tag{1.1}$$

where ω_0 is the angular frequency of the signal and

$$c_0 = A \frac{\tau}{T}$$

$$c_n^+ = 2|c_n| \quad \text{with positive integer } n$$

$$c_n = \frac{1}{T} \int_{t_1}^{t_1+T} x(t) e^{jn\omega_0 t} dt$$

For a trapezoidal pulses series, the expansion coefficients have the following expressions:

$$c_n = -j \frac{A}{2\pi n} e^{-jn\omega_0 \frac{(\tau+\tau_r)}{2}} \left[\frac{\sin(\frac{1}{2}n\omega_0\tau_r)}{\frac{1}{2}n\omega_0\tau_r} e^{jn\omega_0 \frac{\tau}{2}} - \frac{\sin(\frac{1}{2}n\omega_0\tau_f)}{\frac{1}{2}n\omega_0\tau_f} e^{-jn\omega_0 \frac{\tau}{2}} \right] \quad (1.2)$$

Equation (1.2) is not of immediate interpretation. By imposing that $\tau_r=\tau_f$ in (1.2), the expression of complex expansion coefficients c_n becomes:

$$c_n = A \frac{\tau}{T} \frac{\sin(\frac{1}{2}n\omega_0\tau)}{\frac{1}{2}n\omega_0\tau} \frac{\sin(\frac{1}{2}n\omega_0\tau_r)}{\frac{1}{2}n\omega_0\tau_r} e^{-jn\omega_0 \frac{(\tau+\tau_r)}{2}}$$

Since $\omega_0 = 2\pi/T$, it results:

$$c_n^+ = 2|c_n| = 2A \frac{\tau}{T} \left| \frac{\sin(n\pi \frac{\tau}{T})}{n\pi \frac{\tau}{T}} \right| \left| \frac{\sin(n\pi \frac{\tau_r}{T})}{n\pi \frac{\tau_r}{T}} \right| \quad (1.3)$$

Equation (1.3) allows to determine the discrete spectrum of the signal harmonics amplitudes when $\tau_r=\tau_f$. It is clear that this discrete spectrum contains spaced rows of intervals equal to $1/T$ and that the first zero occurs at $n/T=1/\tau$. Figure I.5 shows the trend of the trapezoidal waveform spectrum in case where τ/T ratio (i.e. the duty cycle) is equal to $1/2$.

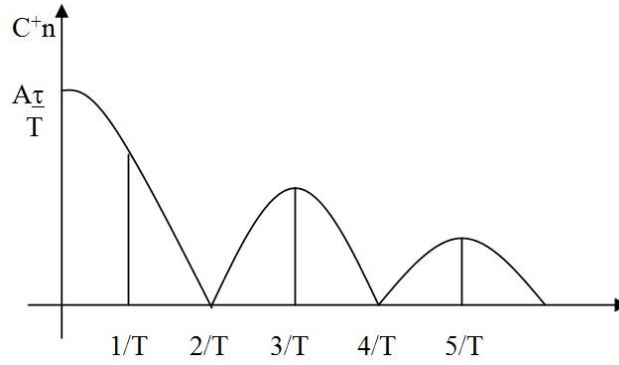


Figure I.5 – Discrete spectrum of a train of trapezoidal pulses with $T=2\tau$.

To obtain other information, the envelope of the spectrum previously identified can be analyzed by means of a Bode diagram. By replacing $f=n/T$, the conversion of the discrete spectrum in its continuous envelope versus frequency f is obtained with the following relation:

$$envelope = 2A \frac{\tau}{T} \left| \frac{\sin(\pi f \tau)}{\pi f \tau} \right| \left| \frac{\sin(\pi \tau_r f)}{\pi \tau_r f} \right| \quad (1.4)$$

The overall Bode diagram is the sum of the three diagrams:

$$diagram1 = 20 \log_{10} \left(2A \frac{\tau}{T} \right)$$

$$diagram2 = 20 \log_{10} \left(\left| \frac{\sin(\pi f \tau)}{\pi f \tau} \right| \right)$$

$$diagram3 = 20 \log_{10} \left(\left| \frac{\sin(\pi \tau_r f)}{\pi \tau_r f} \right| \right)$$

In the Bode plot the *diagram 1* has a slope of 0 dB/decade and a level of $2A\tau/T$. The *diagram 2* instead has two asymptotes, one with a slope of 0 dB/decade and a level equal to unity, the other with a slope of -20 dB/decade, the cutoff frequency equal to $1/(\pi\tau)$. The *diagram 3* likewise presents other two asymptotes, respectively with a slope of 0 dB/decade (level equal to unity) and of -20 dB/decade, with a cutoff frequency equal to $1/(\pi\tau_r)$. Therefore, the overall asymptote is composed of three segments (Figure I.6): the first with a slope of 0 dB/decade, the second with a slope of -20 dB/decade and finally the third with a slope of -40 dB/decade.

Since $\tau_r < \tau$, the first spectral envelope cutoff frequency will be equal to $1/(\pi\tau)$ therefore related to the trapezoidal pulse width τ . Instead the second cutoff frequency will be related to the rise time τ_r .

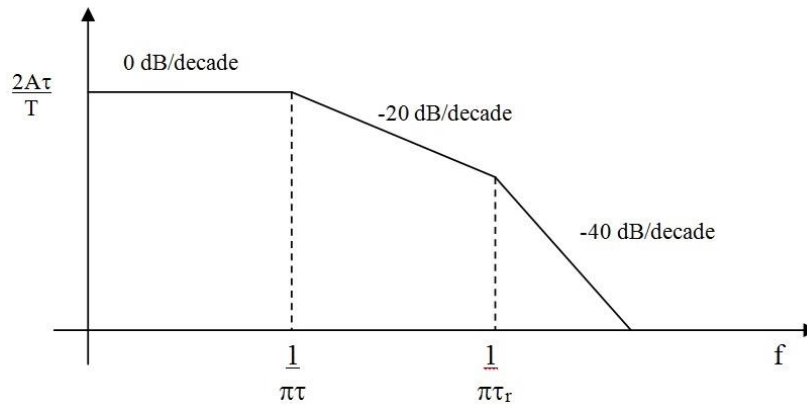


Figure I.6 - Spectral envelope of trapezoidal pulse train in Bode diagram.

By the Bode diagram shown in Figure I.6, it is deduced that:

- the spectral envelope overall level of a trapezoidal pulses train depends on both the amplitude A and the duty cycle τ/T of the pulses sequence;
- the behavior of the spectral envelope at low frequencies depends on the pulse width τ ;
- the behavior at high frequencies is related to the rise time τ_r and fall time τ_f of the pulses.

By consideng for example the CMF20120D device which is a Silicon Carbide Power MOSFET with high speed switching. This device exhibits the $\tau_r = 38$ ns and the $\tau_f = 24$ ns (datasheet data). According to the analysis performed above, it results that this device generates high frequency harmonics up to tens of MHz due to its rise time value. So, more relevant conducted EMI are generated at high frequencies. From this perspective, the implementation of a proper mitigation technique is a very crucial requirement.

1.2.1. EMI Mitigation Techniques

Due to the switching operation, the power electronic converters are unintentional sources of high frequency electromagnetic interference for equipment placed nearby. Therefore, EMI attenuation systems are necessary to ensure both the reliability and the electromagnetic compatibility of the system of which the power electronic converter is part. In particular, EMI containment techniques should be developed to ensure the compliance with the emission limits imposed by the technical standards which are binding for the marketing of those systems.

Technical literature provides a large number of contributions concerning the reduction of electromagnetic noise [10]. One way to reduce the level of conducted noise is by ensuring that less noise is generated by the noise source itself. On the other hand, the noise can be mitigated along the noise propagation path by filtering and other means.

The noise generation can be reduced by a proper design of circuit layout and selection of circuit components, a better switching-control scheme, and soft-switching transition technique.

The selection/design of appropriate components and/or better physical layout of the circuit to minimize the EMI generation, require a particular attention during the initial design stage.

About the switching-control scheme, it is possible to select a low switching frequency resulting in lower noise spectrum contribution at the high frequencies or to apply the more appropriate modulation technique. A common compromise is to set the switching frequency value lower than the half of the considered standard lower frequency limit [11], [12]. Of course, the proper operation of the switching devices imposes the limitations on the increase of the transition times. In [13] the impact of the used modulation technique on the generated EMI level in dc–dc power converters is analysed. A comparative investigation is performed into the use of different random modulation schemes as against the classic pulse width modulation (PWM). The effectiveness of randomization on spreading those dominating frequencies, that normally exist in constant frequency PWM schemes, is evaluated by power spectral density (PSD) estimations in the low-frequency range. Limited speed PWM driving of the power switches with appropriate snubber circuits guarantees reduced conductive EMI. However, this investigation shows that, among all the random schemes under consideration, the random pulse width modulation (RPWM) and the random carrier-frequency modulation with fixed duty cycle (RCFMFD) produce a minimum low-frequency harmonic spectrum and are, therefore, considered the best choice for dc–dc converter applications.

Moreover it is possible to improve the current and voltage waveforms associated with the switching of the power devices to reduce the EMI generated by the noise source. Snubbers, gate-drive modifications and soft-switching techniques all fall under this category. Snubber circuits could be considered as low-pass filters; they allow to soften the switching transitions and also to aid in damping the high frequency waveform oscillations during the switching. However the snubbers produce a slight increase in overall power loss. In [14] and [15] the reduction of the generated EMI is obtained by the implementation of the active voltage control (AVC); it is applied and improved successfully to define IGBT switching dynamics with a smoothed Gaussian waveform. The general idea of AVC is to use a high-speed feedback to force the collector–emitter voltage to follow a well predefined reference. In this way a constant control of the collector–emitter voltage and voltage clamping may be achieved. The high-performance proportional–derivative and multiple-loop AVC controller provides a practical solution to force the IGBT voltage to follow a smoothed Gaussian reference, so reducing the high-frequency EMI generation. In fact, the Gaussian reference implies a very high dv/dt in the middle slope, but the duration is short, and it is part of the S shape. The switching speed is not limited by the Gaussian reference but mainly by the drive capability of the driver. The successful shaping of IGBT switching is dependent on two aspects: the controller and the quality of the reference. The Gaussian

shaping requirement for the controller is very stringent. The Gaussian waveform sampling is limited by the FPGA and the digital-to-analog conversion rate. A high-quality reference generation might further improve the shaping performance.

Another method of reducing di/dt and dv/dt in order to reduce EMI generation is to use soft-switching techniques. The soft-switched converters have generally reduced conducted EMI. However, the soft-switched converters may require auxiliary resonant circuits and extra devices with additional control complexity that can increase the converter cost, can decrease its reliability, and can create extra losses that can adversely affect the efficiency [16].

A different solution to limit the EMI would be to make the receiver less susceptible to the interference. In other words, rather than to limit the signals amplitude that interfere with the noise receiver, it could make sure that they have the minimum possible effect on the correct operation of the receiver.

Another EMI mitigation strategy would be to make the coupling path as less efficient as possible. This could be achieved by placing the receiver in a metal box (shield) or by using the shielded cables to realize all connections between the devices. However, this solution is very expensive and the obtained performance are often below the expectations. The use of filters allows to modify more efficiently the characteristics of the noise propagation path so as to reduce the noise at the receiver end. This filter can be a separate unit kept on the front end or it can be integrated into the power converter itself. This leads to a further subdivision into external EMI filters and internal filters. In the internal filters, the noise currents are internally circulated within the converter itself by layout or topology modifications. The external EMI filters are adopted more frequently and they can be further classified into passive and active filter types [17] - [26]. Typically, an external EMI filter acts as a low-pass filter. It has a negligible effect at the power frequency, while it offers large attenuation to the noise currents in the conducted EMI frequency range.

The discrete passive EMI filters are generally realized with capacitors and inductors connected according to different topologies in single or multi-stage configuration. Each filter configuration can result useful for some applications while it can not ensure the required performance for others applications. Therefore, it is important to choose the filter configuration depending on the system in which it will be adopted. The main advantage of passive filters is the relative “simplicity” of the design and their practical implementation while their main limitation is related to their high frequency performance degradation due to the parasitic phenomena [27] - [29]. Moreover, the passive EMI filter performance are closely related to the EMI source and the EMI receiver impedances. The passive EMI filter design is considered a “black art” because little is known about the EMI source; the interaction between the EMI source and the EMI filter impedances can cause poor noise attenuation. A proper

EMI filter design must suitably take into account the criterion of maximum impedance mismatching between the source and the receiver [19], [69] - [71].

The active EMI filters (AEFs) use active electronic circuits to cancel or suppress the conducted noise and they are possible alternatives to bulky passive EMI filters. There can be numerous ways of implementing active filters in different applications, but the same theory of operation applies. The function of an active filter is the detection and the compensation of the noise signal (current or voltage) from the noise source or receiver. Different active filters topologies have been proposed in technical literature, depending on the method of compensation. There are two groups of active filters: the first one, referred as the feedback-type active filter, detects noise at the receiver while the other one, referred as the feedforward-type active filter, detects the noise at the noise source. Active filters can vary in type according to different detection and compensation signals. Figure I.7 and Figure I.8 show, respectively, possible configurations of feedback and feedforward type active filters according to different measures of detection and compensation signals. In the figures, z_s is the impedance of a noise receiver, which measures noise power caused at the noise source i_n ; z_n is an internal impedance of the noise source i_n , i_c and v_c are the compensation signals. The impedance relationship between source and receiver must be taken into account when selecting and locating various active filters.

In the systems employing the power electronic converters, the active EMI filters have been employed for both the input and output EMI mitigation compensation [22].

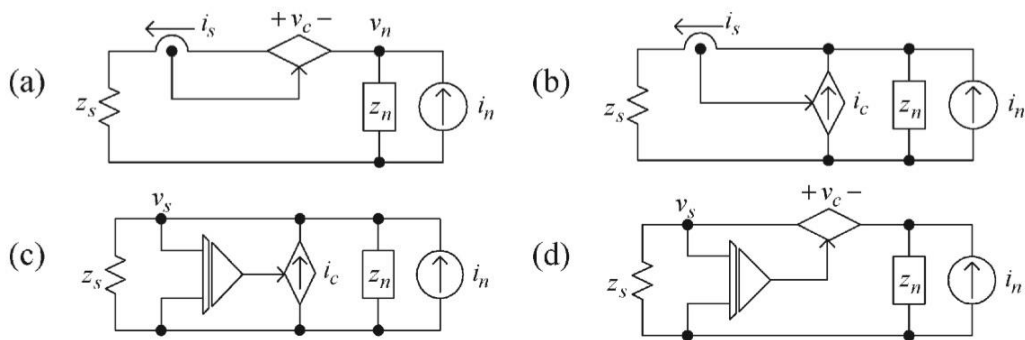


Figure I.7 - Feedback type active filters. (a) Current detecting and voltage compensating. (b) Current detecting and current compensating. (c) Voltage detecting and current compensating. (d) Voltage detecting and voltage compensating. [20]

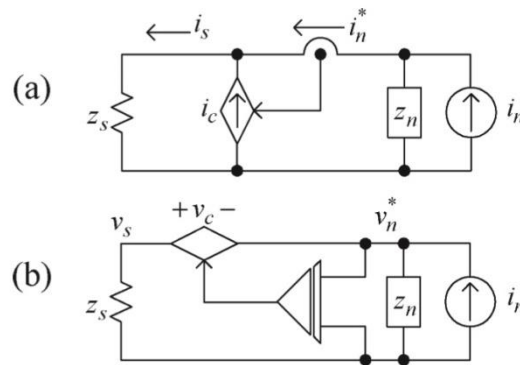


Figure 1.8 - Feedforward type active filters. (a) Current detecting and current compensating. (b) Voltage detecting and voltage compensating. [20]

The main advantage of the active filters is their very compact dimensions due to their small size integrated components; however the high frequency performance is limited by the bandwidth of the operational amplifier (op-amp) that makes the filtering action less efficient. Some studies have in fact shown that the active filters have good performance only up some MHz. In [24] the operational amplifier is used at unity gain to maintain its maximum bandwidth and the desired gain of the active filter can be achieved by the injection transformer. However, depending on the type of the operational amplifier selected for the application, there is always a minimum phase error and a distortion of the input signal at very high frequencies due to the parasitic elements inherent in the operational amplifier itself. Since the AEF requires op-amps with good high frequency characteristics and wide bandwidth, the traditional active EMI filters are expensive. A recent paper [24] proposes an improved topology structure for an active filtering with ordinary op-amps to suppress the CM interference. It includes two same closed-loop feedback circuits. Besides, the cost is less, the filtering effect and stability of the two-stage active filter are better.

Instead in [26] a method to enhance the op-amp gain bandwidth product is presented to improve the active EMI filter performance.

Another disadvantage is related to the possible instability of the entire system that can limit the filter dynamic performance [30], [31], [38], [39]. It should be noted that, generally, the presence of active components reduces the filter reliability. Furthermore, it is necessary a carefully design of the entire filtering system so avoiding possible interaction between the sensing/injector circuits and the input/output of the active filter [25].

Even if the AEFs are more compact, their high speed active components require an additional power supply, which in turn, will increase the size and weight of the active filter and their integration is difficult. Therefore, active EMI filters are still not widely accepted by the industry. To solve the problem related to the power supply of the active components, a novel AEF topology used for DC-DC

power converters is proposed in [37]. The most distinguished feature of this filter is that it shares the same power supply with the DC-DC converter; no power is supplied to the active part of the proposed filter, only the passive components are used. The size of the filtering circuit as well as its power supply cell is very small and compact. It is easy and feasible to be integrated in the future commercial large scale manufacture.

The performance versus cost reduction trends of the digital circuits has made possible their application for power converters digital controller techniques. They are usually based on FPGA technology that exploits their mathematical oriented resources. Some authors propose FPGA-based EMI suppression techniques, referred to as digital active EMI filter (DAEF) [32] - [34]. The DAEF presents stronger competitive application in medium to high current converters. The size and the losses of the passive EMI filter are proportional to the rated current and voltages of the power converter. Hence, the DAEF provide a feasible solution to overcome these drawback with good attenuation performance. The conducted noise signal is the noise voltage that is sensed through an RC high-pass circuit with the cutoff frequency tuned to the lower spectrum frequency of the conducted emission standard. The sensed noise voltage is sampled by using high-speed analog-to-digital converter (ADC) in order to be processed through a phase reversal algorithm. The discrete-time noise signal is then reconstructed by using a digital-to-analog converter (DAC). The output signal of the DAC is then electrically injected at input leads of the power converter, for the EMI noise suppression; by an injection circuit which is a simple low-pass filter tuned to the higher frequency spectrum of the conducted emission standard (30 MHz). ADC and DAC devices with high bit resolution are necessary to achieve an adequate signal sampling. If this requirement is not satisfied, a phase error between the sensed signal (sampled) and the injected signal (reconstructed) occurs, and consequently, a significant degradation in the DAEF performance will result. However, the cost of the DAEF remains an important disadvantage as compared to the passive EMI filter counter-part.

Finally, it is possible to combine more than one approach to come up with a “hybrid” mitigation approach. For example, the active and passive filtering techniques may be combined to develop a “hybrid” filter [35] - [39]. In the hybrid filters, the active filtering part mitigate the conducted EMI at low frequencies (it provide good noise attenuation for the first several harmonics of the switching frequency) and the passive filtering part to mitigate the conducted EMI at high frequencies. This approach allows to exceed the limits related to the passive and active filters with satisfactory results about the filter performance and the realization of a compact layout. Thus, the active filter can significantly reduce the size of the passive filter whose cut-off frequency can be set at much higher frequency. However the hybrid filters imply an inevitable increase in the complexity of the filtering system.

Taking into consideration the EMI mitigation techniques described above, it is possible to conclude that an external front-end passive filter is the most-established method to meet the EMI standards and it is extensively used at present. The main drawback of a passive filter is its large volume.

1.3 Power Density issues in Power Electronic Converters

The more increasing development of the power electronic converters in a wide range of applications requires, besides the electromagnetic compatibility compliance, some improvements in terms of higher efficiency, lower losses, lower volume, lower weight and lower production costs. A high efficient power converter ensures a good utilization of the energy resources and a low operating cost. Low losses are basic requirement to enable a compact realization, which also allows a flexible deployment of the converter system.

The integration of the power electronic converters in the final application is very common in many applications such as the variable speed drives, that are used in a range of the industrial systems, in the hybrid vehicles and in the More Electric aircraft. This trend allows to reduce the installation cost but the converter volume is strongly limited by the main dimensions of the load system. In addition to the low volume requirement also the low weight is very important in mobile systems applications to facilitate the installation, handling and maintenance operations of the power converter [84]. High power density power electronic converters become increasingly essential for future markets.

The converter design is a complex engineering due to the interaction of many aspects: a designer must choose the more appropriate design among various possible designs and technologies, finding the optimal allocation of each component in terms of its mass and its volume and for each component must meet the electrical and thermal specifications. Therefore, an efficient design considers simultaneously the system-wide electrical, mechanical and thermal problems; it is not enough to design each component individually based on its electrical specification alone. A generic power electronic converter is composed of :

- the power semiconductor devices,
- the modulation and control circuits,
- the power passive components (filters and transformers),
- the cooling system,
- the interconnections and the packaging.

It is necessary to introduce the power density concept. Power density of power electronics is a Figure of Merit (FoM) to compare the technological status and performance of power electronic converters. This parameter serves to characterize the degree of compactness of a converter or the volume required for realization at a given rated power. The power density, ρ , is defined by the ratio of

the power output, P_o , by the total volume, Vol , where the total volume is typically a factor of two more than the sum of the partial volumes ΣVol_i .

$$\rho = \frac{P_o}{Vol} = \frac{P_o}{\Sigma Vol_i} \quad (2.1)$$

A side view of a common air-cooled power electronic converter is shown in Figure I.9. It is evident that the passive components (capacitors and inductors) and the cooling system, if air volume is not taken into account, have major impact on the bulky power electronic system [40]-[42]. They are regarded as the main barriers to the improvement power density. However a proper evaluation of the power density of a power converter should take into account also the volume requirements of the EMC filter, the power semiconductors with driver circuitry and auxiliary power supply, as well as the control electronics and the housing in the construction volume Vol [44], [45]. Unfortunately, in the literature the heatink is often not taken into account or the EMI filter is omitted.

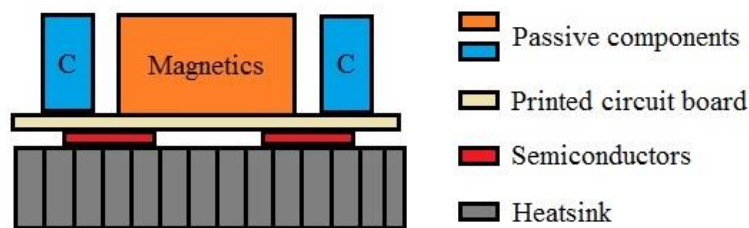


Figure I.9 – Generic scheme of a common air cooled power electronic system.

1.3.1 Scopes of action for the power density improvement

Since 1970, power density of power electronic converters has been approximately doubled every decade. This evolution was mainly driven by the increase of the switching frequency by a factor of 10 every ten years [84]. At present, an ever more radical increase of power density continue to be required.

One of the possible action regards the power inductors design in the switched-mode power supply (SMPS). The losses and the consequent temperature rise are the main intrinsic issues of power inductors operation. Commonly, the inductors are designed so that they can work in the weak saturation region but, in recent years, inductor saturation has been the subject of several scientific investigations. Some authors have experimentally verified that smaller volume inductors working in partial saturation, could help in achieving more compact SMPSs with an acceptable amount of power losses; in this context, it is necessary to assess the inductor saturation effects. No useful information on

the real magnitude of the current ripple for inductors working in partial saturation and how to efficiently analyze the sustainability of such operating conditions are given in the scientific literature and in the inductors datasheets. Recently, some authors have proposed [46] a method for ripple analysis of saturated inductors, in order to allow the investigation of effective SMPS design solutions with minimum size inductors, as well as the identification of optimum design tradeoff of the parameters of the inductors. In [47], the potential impact on the reduction of the volume and the weight of power inductors allowed by the adoption of partial saturation operation in Aerospace Power Supply Units, is described. Although a traditional bigger core non-saturated inductor presents lower power losses, current ripple and temperature rise, a smaller core inductor working in a partial saturation may operate with acceptable power losses, current ripple and temperature rise.

Another scope of action regards the use of power devices with higher switching speed [40]. The switching frequency increase allows to decrease the volume and weight of the passive energy storage elements (inductors and capacitors) and thus to decrease the converter's global volume.

However, the switching frequency increase determines a power losses increase of the power semiconductors and of the magnetic materials; this choice can finally leads to a thermal limit since a minimum volume is reached and no more energy can be dissipated from the surface area [43]. The power losses lead to worst performance, to a cost increase and to a minor power density of the converters. The power devices normally take large share of system losses and they are directly coupled to the cooling system; then they have major influence on the cooling system size. Advanced magnetic materials, dielectric materials, wide bandgap devices with better electrical and thermal properties are investigated to allow a wider operating frequency range.

Besides the power losses increase, higher switching frequency can determine more relevant high frequency conducted EMI, since the higher magnitude harmonics (1st, 2nd, etc) of the generated noise to be attenuated are located close to or within the frequency range limited by the reference EMC standards.

In [45] the implication of the switching frequency and the power rating on the converter weight is shown. In particular, the relationship between the per-unit weight of EMI filter, the switching frequency and the power level is analysed: for the same switching frequency, as the power rating increases, the EMI filter weight increases; for the same power level, the weight is not linearly dependent on the switching frequency. Then the optimal switching frequency could be chosen taking into consideration the EMI filter weight: for a power level higher than 10 kW, the tradeoff between cooling and passive components is more important for converter weight.

Instead in [48], based on the low frequency attenuation requirement, a smaller EMI filter size can be obtained by pushing the switching frequency higher. However, in the hardware implementation the real limitation comes from the spectrum at high frequencies. In fact the EMI filter performance are less

effective at 20 MHz - 30 MHz range due to the variation of the permeability of the magnetic material with the frequency, due to the parasitics phenomena of the EMI filter and to the inter-component coupling.

The current ripple influences the harmonic content, increasing the noise amplitude. In [49] an analysis towards the influences of the current ripple and the switching frequency on the overall losses, the minimization possibility and the EMI filter design is presented.

The EMI filters can contribute substantially to the volume and the weight of the power converter; then the optimization of the EMI filter size is an important requirement in the design stage. There are some scopes of action to improve the EMI filter power density and consequently of the power converter. They are listed in the following.

- *Choice of the converter topology based on EMI filter volume and weight.* Each converter topology generates different EMI, harmonics and it is characterized by different loss performance and therefore it has different impact on the convert power density [50].
- *Optimal switching frequency.* Depending on the application field and then on the EMC standard frequency range, the switching frequency value can have a major impact on the EMI spectrum amplitude, and then on the EMI filter size, if the fundamental and the other harmonics are inside the standard frequency range. The choice of the optimal switching frequency allows to reduce the EMI filter size and weight [12].
- *Optimal number of filter stages.* The optimum number of filter stages depends on the required attenuation value, on the design frequency and on the rated power [90]. A multistage EMI filter configuration can occupy a smaller volume than a single stage one. Then the evaluation of the optimal number of the EMI filter stages allows to increase its power density.
- *High performance magnetic materials for the inductance implementation.* The use of high performance magnetic materials allows to achieve high inductance value with a smaller number of turns and consequently a reduction of the number of stages, the size and the weight of the filter [86].
- *Integrated EMI filter.* These integrated structures use the printed circuit board technology to realize the filter components, implementing techniques to cancel or to compensate the parasitic phenomena, and they use appropriate packaging technologies to obtain better performance at high frequencies and more compact layout [51]-[59]. The distinctive feature of the integrated filters is a planar structure that integrates inductors and capacitors. This structure consists of alternating layers of conductors, dielectrics, insulators and magnetic materials with characteristics similar to the discrete components ones. The integrated EMI filter presents some limits due to the materials, the electromagnetic aspects, the structure and the limits related to the material processing technologies. These problems have to be

considered during the design stage of integrated EMI filters. However, the integrated EMI filter could not ensure good performance in the overall frequency range.

On basis of the considerations given in this section, it is evident that the power converter design oriented to the power density is very complex. In fact, an approach can improve the power density of a converter component but it can also deteriorate the performance or cause the size increase of other converter components.

It is of considerable importance the correlation between the electromagnetic compatibility and the power density issues in the power electronic converters. The implementation of a technique to solve these two issues at the same time has been the subject of the research activity conducted during the PhD course. It will be described in the following chapters.

CHAPTER II – EMI analysis

2.1 Introduction

Electromagnetic interference (EMI) emission is an important matter for any electric and electronic equipment. When the noise emission of an equipment fails to satisfy the Standard limits, it is necessary to adopt solutions to reduce the noise emission level. Measured emissions are a mixture of common mode (CM) and differential mode (DM) noise. Furthermore, the design procedure for EMI filters is usually divided in CM and DM filters design. Therefore, it is very important to measure separately the two modes in order to design an efficient EMI filter.

In this chapter the CM and DM noise paths are evaluated and CM and DM separation techniques are described. They can be roughly classified into three main groups: separation technique using RF current probes, hardware-based separation technique and software-based separation technique. In particular, the validation of the software-based CM/DM separation technique has been done by comparing the results with those obtained by measurements coming from a high bandwidth RF current probe and a spectrum analyzer. Furthermore, the deviation of the results obtained by the two techniques has been computed in terms of normalized root mean square error and normalized average error.

2.2 Conducted EMI and Noise Propagation Paths

The conducted EMI noise is usually decoupled and characterized by two noise components:

- Common Mode, defined as the noise flowing between the power circuit and the ground.
- Differential Mode, defined as the current flowing the same path as the power delivery.

The CM and DM noise propagation paths are shown in Figure II.1.

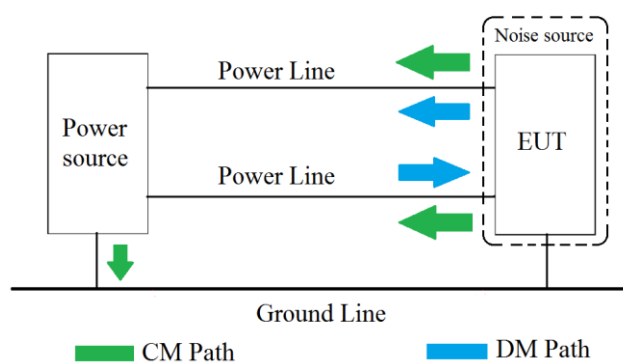


Figure II.1 – CM and DM noise paths.

Conducted EMI can propagate through a coupling channel given by metallic planes used for the equipment ground connection or through a coupling channel generated from the equipment power supply.

Regarding the emissions that propagate through the supply network, it is necessary to distinguish between internal network noise sources and external noise sources. For example, among the first, there are both impulsive and non-impulsive overvoltages, whereas lightning phenomenon and switching transients, due to electronic converters used for the network voltage regulation, are external noise sources.

To better understand the relationship between the CM and DM currents, a single-phase power application where the mains cable of the EUT (Figure II.2), can be considered. It consists of three parallel conductors: phase, neutral, and ground. The EUT is supplied by the power source by an artificial mains network (AMN), that consists of two line impedance stabilization networks (LISNs), described in section 2.3). Therefore, from the power flow point of view, the EUT is the load but from the conducted EMI point of view, the EUT is the source because it produces the noise.

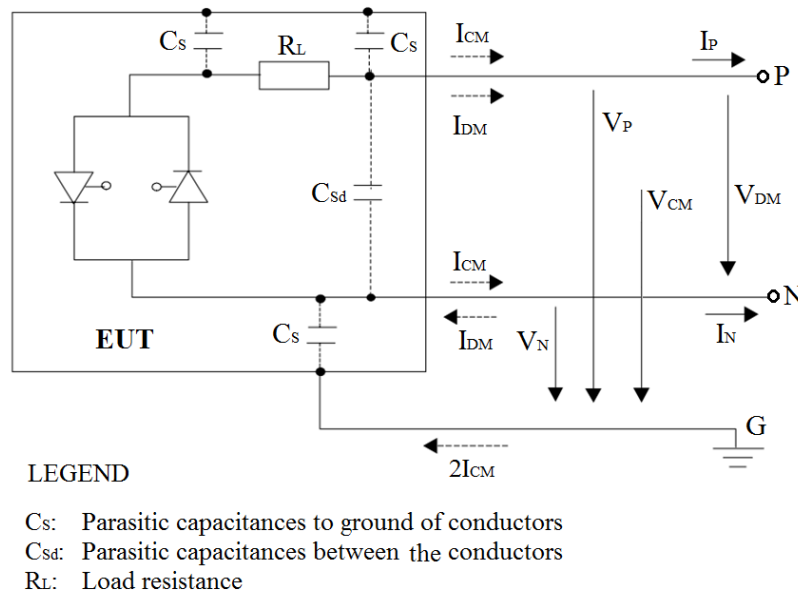


Figure II.2 – CM/DM voltage and current generated by a single phase power electronic equipment.

Sometimes the power cable might consist of only two conductors, phase and neutral, in which case the EUT is floating. The two wires P and N are characterized respectively by two voltage levels V_P and V_N and the currents flowing through the phase and neutral conductors are denoted with I_P and I_N , respectively. These currents can be decomposed into two components, which are referred as the CM current I_{CM} and the DM current I_{DM} . Then:

$$I_P = I_{CM} + I_{DM}, \quad I_N = I_{CM} - I_{DM}, \quad I_G = 2I_{CM}$$

$$I_{CM} = \frac{I_P + I_N}{2}, \quad I_{DM} = \frac{I_P - I_N}{2} \quad (2.1)$$

$$V_{CM} = \frac{V_P + V_N}{2}, \quad V_{DM} = V_P - V_N \quad (2.2)$$

Therefore the CM and DM emissions can be regarded as the two components of an electromagnetic disturbance. Indeed, given a conducted electromagnetic noise generated by a power electronic equipment, it is possible to identify:

- DM noise component (DM current) that flows from the P conductor closing on the N conductor, through the parasitic capacitances between the conductors;
- CM noise component (CM current) flowing on the P and N conductors and closes again on the ground line, through the parasitic capacitances between the aforementioned conductors and the equipment parts connected to the ground line.

On the basis of these considerations, it can be assessed that CM currents are equal in magnitude and have the same direction in both conductors while DM currents are equal in magnitude but opposite in direction in the two conductors.

2.3 CM and DM EMI Separation Techniques

In conducted noise compliance tests the CM and DM noise components are irrelevant. However, they are of basic importance in the design and in the analysis of passive EMI filters which are one of the most common possible solutions to mitigate conducted EMI. The components of an EMI filter attenuate CM and DM disturbances differently. For this reason, it is impossible to design or select an appropriate EMI filter without knowing the levels of the CM and DM noise.

In this section, the CM and DM EMI measurement methods are described.

Firstly it is necessary to focus attention on an essential circuit for the conducted EMI measurement: the artificial mains network placed between the power source and the EUT power supply cable (Figure II.3).

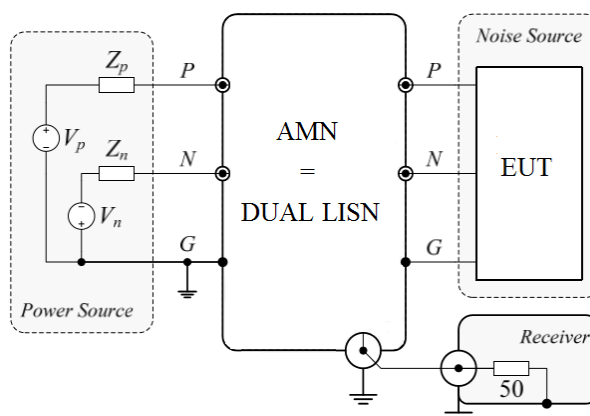


Figure II.3 - Conducted emissions measurement circuit.

The measurement of conducted emissions consists in evaluating the noise currents which are generated by an equipment and which propagate through its power supply cable. The measurement made with only a current probe is not sufficient to evaluate conducted EMI since it is necessary to obtain comparable measurements made at different environments. In fact, the power source impedance is variable from plant to plant and it depends on frequency value; the variability of the load connected to the EUT is a complication since it affects the intensity of the conducted interference. Consequently, it is necessary to stabilize the impedance seen from the EUT to make consistent and comparable measurements made at different environments and at a different time.

The LISN provides repeatability of the conducted EMI measurements by fulfilling several important functions.

Firstly, it allows to *obtain a constant impedance on the power supply of the EUT*; this impedance should also be constant for all frequencies of the conducted EMI measurement range. Generally, the LISN impedance value must be equal to 50Ω : i.e. it is the impedance value that the LISN must ensure between the phase/neutral conductor and the ground plane.

The amount of noise existing on the external network of the energy distribution varies from place to place; this external noise reaches the EUT via the power supply cable and, if it is not isolated in some way (such as through a filtering or via the intrinsic operation of the apparatus itself), it is added inevitably to the measured conducted emissions. The second objective of the LISN is to *block conducted emissions coming from the power supply, which are not due to the EUT in order to measure only conducted emissions generated by the equipment under test*.

Finally, the third objective of LISN is to *facilitate the power flow from the mains to the EUT*.

Figure II.4 shows the electrical circuit of AMN [60]. It is a dual circuit formed of two identical LISNs placed in the same metal enclosure, one for each DC power line (positive and negative wire, referred to ground). According to CISPR 25 standard requirements [61], each LISN has a $5 \mu\text{H}$

inductance, L , a $1 \mu\text{F}$ capacitor, C_1 , on the mains side, and a 50Ω resistance, R , as output to the measuring instrument, with a series connected coupling capacitor C of $0.1 \mu\text{F}$, on the EUT side. A 47 pF capacitor, parallel connected to the 50Ω resistance, allows the LISN impedance to follow the ideal impedance curve according to CISPR 25 in the whole frequency range of interest, as shown in Figure II.5. In the same plot, the LISN ideal impedance curve, with the upper and lower dotted line curves, defining the range of 10% admitted tolerance, is reported.

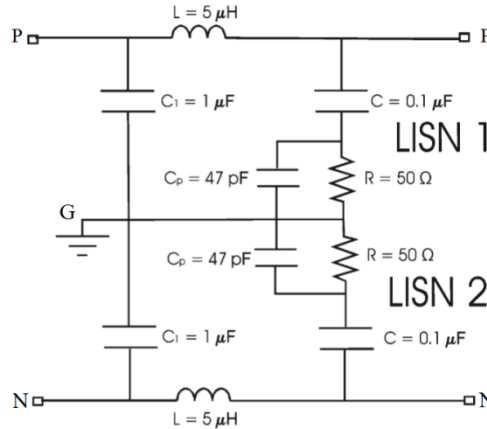


Figure II.4 - Circuit scheme of the high voltage (HV) AMN (dual LISN).

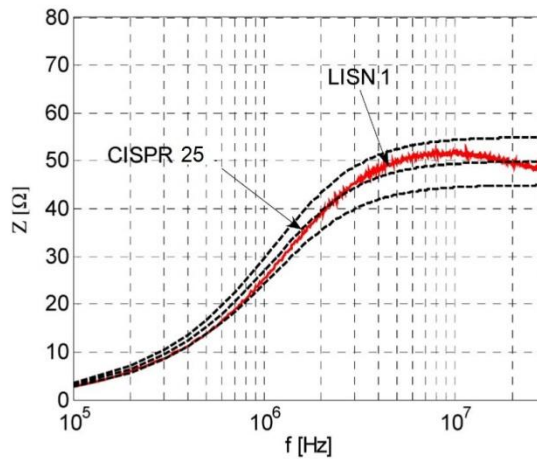


Figure II.5 - Impedance ideal curve and measured impedance curve of the LISN 1 [60].

As previously said, in order to properly design the EMI filter components, it is necessary to evaluate separately CM and DM noise component in the frequency range of interest.

As already stated, the total current in the phase/neutral conductors is given, respectively, by the sum and the difference of the CM and DM components:

$$I_{P/N} = I_{CM} \pm I_{DM}$$

If a noise component is predominant on the other, it is necessary to operate on those passive EMI filter components that act on the dominant component. This can take place on the whole frequencies range, on certain ranges or on specific frequencies.

To determine which of the current component is dominant at a given frequency, the CM and DM components should be known at every frequency in the range of interest. In this way, it can effectively operate on the passive components to act directly on the dominant component in the frequency range in which this occurs.

There are several CM and DM separation techniques; they can be roughly classified into three main groups:

1. Separation technique using RF current probes;
2. Hardware-based separation technique;
3. Software-based separation technique.

The three separation techniques of CM and DM components will be described in detail in the following sections.

2.3.1 Separation technique using RF current probes

The RF separation method is based on the use of a high bandwidth current probe to measure, via spectrum analyzer, the CM and DM noise between the LISN and the disturbance source. This separation method is a very reliable technique. It should be considered that, during the tests, the RF current probe is exposed to the typically high supply current. Therefore, saturation or sensitivity problems should be taken into account in the choice of a suitable current probe, especially in high power-low voltage applications. This involves the use of expensive RF current probes. [62]

The measuring principle is shown in Figure II.6.

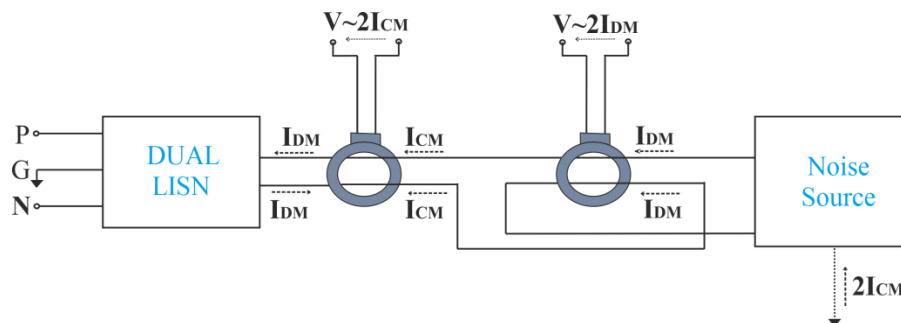


Figure II.6 - Separation of CM and DM current by using a current probe.

The spectrum analyzer (or EMI test receiver), connected to the current probe, measures twice the CM current and twice the DM current depending on the wire placement respect to the probe. The EMI instrument measures the voltage over a 50Ω resistor and scales it according to (2.3):

$$EMI[dB(\mu V)] = 20 \log_{10} V + 120 \quad (2.3)$$

In order to obtain the current level in $\text{dB}(\mu\text{A})$ it is necessary to add the correction factor k of the current probe to the voltage level in $\text{dB}(\mu\text{V})$:

$$I[dB(\mu A)] = V[dB(\mu V)] + k \left[dB\left(\frac{V}{A}\right) \right] \quad (2.4)$$

As well established, the LISN ideally provides a 50Ω load (per power wire) for the conducted EMI in the frequency range between 150 kHz and 30 MHz.

Considering the propagation paths of the CM/DM currents, the CM current flows on an impedance equal to 25Ω while the DM current flows on an impedance of 100Ω (corresponding to parallel or series connection of the two impedances from 50Ω). As a result, the CM and DM EMI components are defined by the following equations:

$$EMI_{CM} = 20 \cdot \log_{10} \left(2I_{CM} \cdot \frac{25}{2} \right) = 20 \cdot \log_{10}(2 \cdot I_{CM}) + 20 \cdot \log_{10}(12,5) \quad (2.5)$$

$$EMI_{DM} = 20 \cdot \log_{10} \left(2I_{DM} \cdot \frac{100}{2} \right) = 20 \cdot \log_{10}(2 \cdot I_{DM}) + 20 \cdot \log_{10}(50) \quad (2.6)$$

Although the LISN impedance should be equal to 50Ω in the frequencies range of interest, the CM and DM LISN impedance values may be subjected to some variations. Figure II.7 shows the CM and DM LISN impedances module values of Figure II.4, measured by a precision RLC meter Agilent 4285ALCR. It can be noted that the actual impedance of the LISN is not strictly constant within the frequency range of the conducted EMI.

Therefore, a suitable frequency-dependent conversion factor, corresponding to the CM and DM LISN impedance, respectively $Z_{CM_LISN}(f)$ and $Z_{DM_LISN}(f)$, must be used in order to obtain an accurate measurement of the evaluation of the CM/DM noise. Then,

$$EMI_{CM} = 20 \cdot \log_{10}(2 \cdot I_{CM}) + 20 \cdot \log_{10}\left(\frac{Z_{CM-LISN}(f)}{2}\right) \quad (2.7)$$

$$EMI_{DM} = 20 \cdot \log_{10}(2 \cdot I_{DM}) + 20 \cdot \log_{10}\left(\frac{Z_{DM-LISN}(f)}{2}\right) \quad (2.8)$$

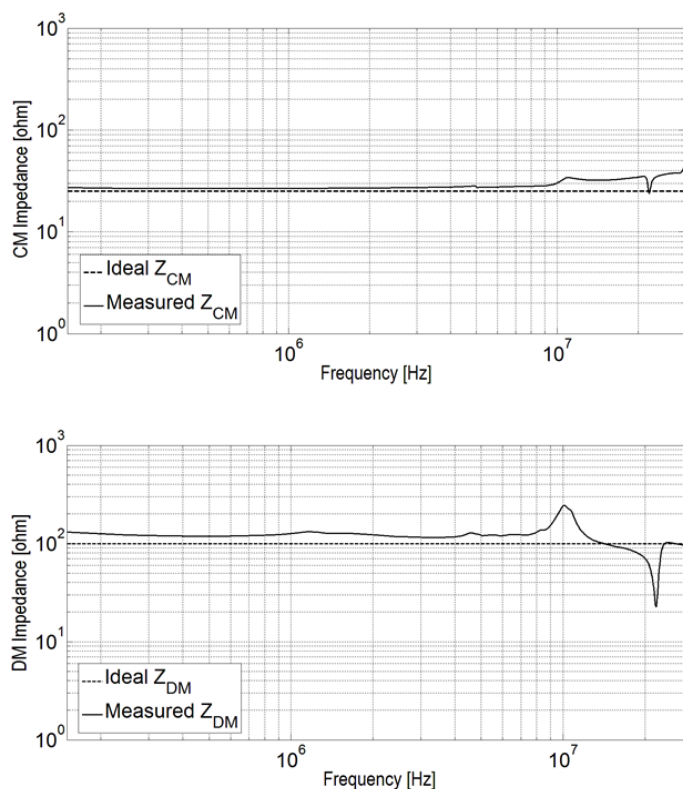


Figure II.7 - Comparison between the ideal and measured CM (upper) and DM (lower) LISN impedance.

2.3.2 Hardware-based separation technique

The second category of CM and DM noise separation techniques requires the use of a "noise separator" between the dual LISN and the spectrum analyzer (Figure II.8) [1], [63].

The device carries out the sum or the difference of the phase and neutral conductors voltages, by providing (obviously doubled value) only the CM or DM component. For this operation, the device uses two broadband transformers: on the primary windings of transformers are applied phase and neutral voltages on dual LISN outputs. The secondary windings of the transformers are connected in series and a DPDT (Double Pole Double Throw) reverses the neutral voltage polarity: with the switch in the normal position, the sum of the phase and neutral voltages is carried out, while after the switching, the difference of the same signals is carried out. The spectrum analyzer, spanning the whole

frequency range of interest, provides a view about the conducted measures, allowing to do all evaluations of the case study.

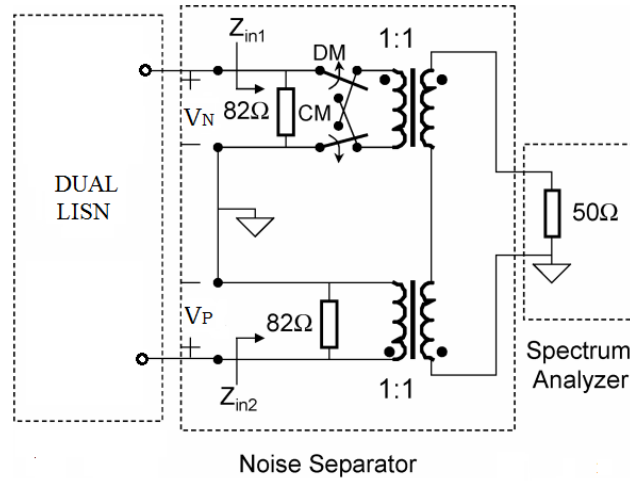


Figure II.8 - Separation of CM and DM noise via hardware.

The use of hardware separators (e.g., Paul Hardin separators, power combiners) may give phase coherency problems and results degradation without a good characterization of the unavoidable modal conversion of the complete set-up (i.e. the measured level at the DM output in case of pure CM excitation and vice-versa). Moreover the EMI separators are suitable for low-medium power levels, due to the saturation of their wideband transformer [63].

2.3.3 Software-based separation technique

Software-based separation techniques using time domain measurements are generally considered as easy and cost-effective methods for designing the EMI filters, provided that a multi-port digital oscilloscope with suitable sampling capability is available. Moreover, these techniques can reduce the phase coherency problems without any dedicated hardware.

The signals on the phase and neutral conductors of the dual LISN, are simultaneously measured by a multi-channel Digital Storage Oscilloscope (DSO) with a high sampling frequency. Figure II.9 shows a block diagram, synthesizing the software based CM/DM separation technique concept.

Considering that the signals retrieved from CH1 (V_P) and CH2 (V_N) are tied to CM and DM voltages, V_{CM} and V_{DM} , referring to Figure II.9, by relationships in (2.9) and (2.10), respectively,

$$2V_{CM} = V_P + V_N \quad (2.9)$$

$$V_{DM} = V_P - V_N \quad (2.10)$$

their separation can be achieved in time domain by simply summing and subtracting the measured signals. This operation is done by using the DSO processing features.

The concurrent signals measurement guarantees phase coherency; the high sampling frequency/processing speed of the instrument and the suitability of time domain signals to be processed by a DFFT (discrete fast Fourier transform) algorithm enables to obtain an accurate frequency spectrum of the CM and DM EMI in the range 150 kHz - 30 MHz. In particular, according to the Nyquist-Shannon sampling theorem [64], the DSO sampling rate should be at least two times that of the highest signal frequency. The DFFT algorithm can be simply executed on a PC or implemented on an embedded system as a part of an automated tool for EMI filter design.

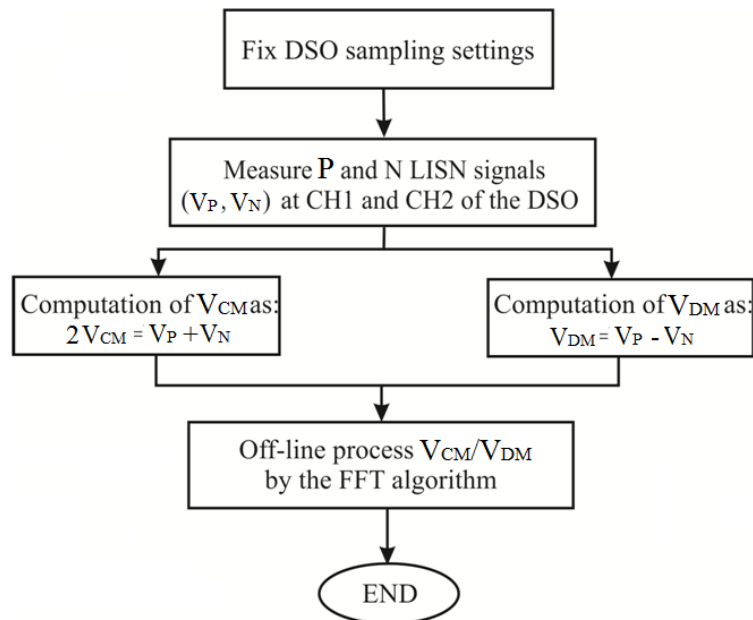


Figure II.9 - Block diagram of the time domain EMI measurement method.

2.4 Experimental Validation of the Software based separation technique

As described in the previous section, in software-based CM and DM noise separation techniques for conducted EMI, CM and DM signals are acquired in time domain and their frequency spectra are computed using a software-based post-processing. In particular Welch and Bartlett periodograms are proposed in [65] to represent the frequency spectra of CM and DM noise. In [66] a Labview-based measurement system is used. Both contributions state the advantage of the technique and show a qualitative comparison with RF measurement-based separation techniques in the case of low power

switched mode power supplies (SMPSs); on the other hand, the difference between CM and DM mode obtained by the different techniques is not quantified.

In this section the software-based separation technique is validated against a consolidated full experimental-based technique using a current probe, a spectrum analyzer and a correction factor of the DC LISN versus frequency that has been measured experimentally, instead of using the theoretical value of such a correction factor, which is constant. In this way the validation of the separation technique is more accurate.

Differently from other contributions in technical literature, the difference between the results obtained by the two techniques, has been evaluated in terms of normalized root mean square error (NRMSE) and of normalized average error (NAVE).

The test bench shown in Figure II.10 has been used and it is composed as follows. A PWM IGBT Voltage Source Inverter (VSI), equipped with a STGIPS10K60A module; an Altera Cyclone III FPGA board equipped with a Nial Stewart GPIB expansion board, implementing the PWM modulator; a 48V induction motor with a rated power of 1.1 kW. The VSI switching frequency is equal to 20 kHz. The use of an intelligent module for the VSI allows a very compact layout of the power electronic stage. A dual DC LISN with a voltage capability up to 600V has been set-up and used to measure the conducted EMI.

In particular, a Tektronix TDS7254B 2.5 GHz – 20 GS/s - 4 channels is used for the time domain measurements needed for the software-based CM/DM separation technique. A RF current probe R&S EZ-17 that allows measurements in the frequency range 20 Hz – 100 MHz with a maximum DC current of 300 A, and an Agilent E4402 (9 kHz – 3 GHz) spectrum analyzer have been employed for the RF measurement-based separation technique. A 10 kHz resolution has been chosen for both the measurement instruments to obtain directly comparable frequency spectra.

An accurate time triggering of the signals is done with the aim of capturing an integer number of the PWM switching periods. Moreover the DSO sampling rate and the length of measurement should be chosen so that the resulting resolution of the DFFT is the same of the RF based measurements. In this way the DFFT results can be directly compared with the RF measurements without the need of windowing techniques, used to reduce spectral leakage issues. In this way a simplification is obtained in the subsequent phase of EMI filter design since the use of appropriate margins to compensate the reduction of signal spectra amplitude due to windowing can be avoided.

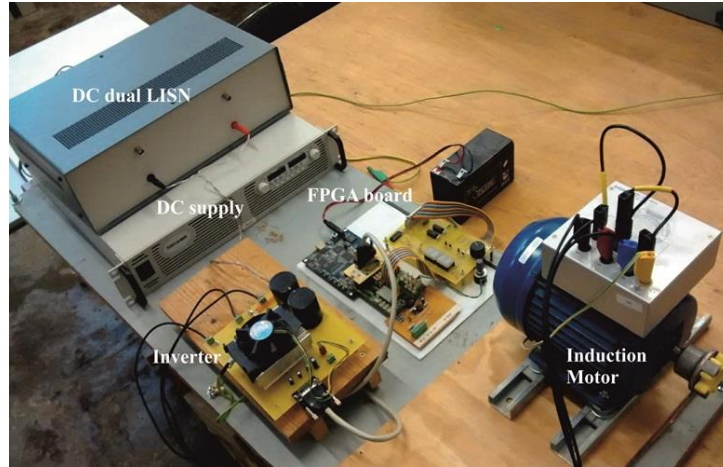


Figure II.10 – Test bench used to conducted EMI measurements.

Figure II.11 and Figure II.12 show the comparison between CM and DM EMI obtained with the separation techniques described in sections 2.3.1 and 2.3.3. It is possible to observe that the obtained results are very close to each other.

To quantify the difference of the software-based method results respect to the RF measurement-based ones, the NRMSE and the NAVE have been considered over the considered frequency range [67]. Such indices have been normalized with respect to the maximum amplitude of the RF measured emission, y_{max} , and they give a quantitative evaluation of the software based CM/DM separation technique. Table II.1 summarizes the obtained performance indices by Eq. (2.11) and (2.12):

$$NRMSE = \sqrt{\left(\frac{\sum_{i=1}^n (\hat{y}_i - y_i)^2}{n} \right)} / y_{max} \quad (2.11)$$

$$NAVE = \left(\frac{\sum_{i=1}^n (\hat{y}_i - y_i)}{n} \right) / y_{max} \quad (2.12)$$

where \hat{y}_i and y_i are respectively the RF emission amplitudes, measured to the i -th frequency, with the RF current probe and with the software based separation technique and n indicates the number of frequencies measured in the range of interest.

The low values of the performance indices demonstrate the goodness of the software based separation technique and allows to consider it as a valid tool for the noise mode separation in cases where high operating currents make critical the use of other methods.

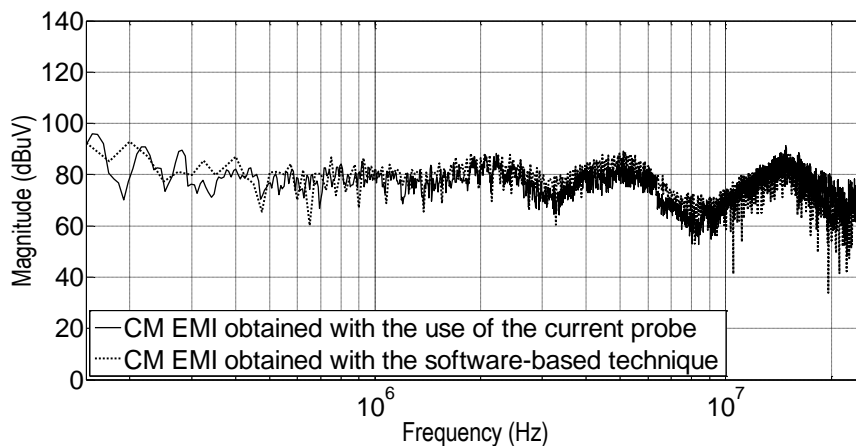


Figure II.11 - Comparison between CM EMI obtained by the software-based separation technique and by RF measurement-based technique.

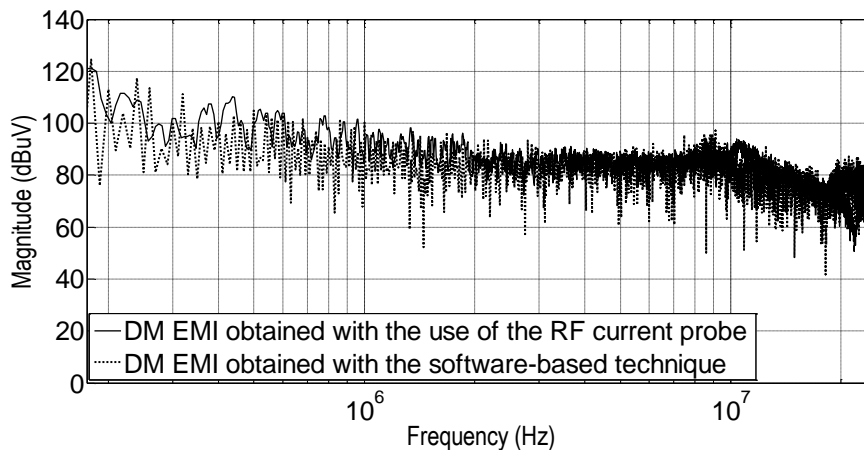


Figure II.12 - Comparison between DM EMI obtained by the software-based separation technique and by RF measurement-based technique.

Table II.1 PERFORMANCE INDICES.

Noise Mode	NRMSE (%)	NAVE (%)
CM	13.3	0.28
DM	2.3	0.24

CHAPTER III – EMI Filter Design

3.1 Introduction

Starting from the considerations of the previous chapters, it is evident that the use of EMI filters to reduce the conducted emissions has become necessary in various application fields. The EMI filters used for the attenuation of conducted emissions are generally low-pass type configuration; there are different circuit configurations with different characteristics obtained by the combination of passive components (capacitors and inductors).

Often the filter components are defined by a trial and error approach. This approach leads to oversizing of the components to obtain the desired performance of the EMI filter and therefore to an increase of the EMI filter volume and cost of realization. Appropriate considerations should be made during the design phase to avoid those advantages and they will be treated in this chapter.

In the previous chapter, the CM and DM noise paths have been evaluated and the noise separation techniques have been described.

The beginning of this chapter presents the criteria for the correct choice of EMI filter topology and the real HF behavior of filter components that can heavily influence the filter performance. Then the EMI filter general design steps, the design of CM choke and DM extra inductor with specific attention to the absence of magnetic core saturation are presented. Finally, the chapter ends with some considerations on the material of filter components and on their filter performance impact. In particular, the first part of this subsection deals with the available material technology that could help in reducing the volume of the filter, such as the nanocrystalline materials. Later on, the key parameters of the CM choke, such as the permeability, the saturation flux density and the magnetic losses of the magnetic material core, are analyzed and pushed to their limits. Also a study on capacitors is carried out in terms of the material performance, the nominal voltage and the application field. Lastly, the effect on the EMI filter performance due to the filter components tolerances is evaluated.

3.2 Criteria for the choice of EMI filter topology

EMI filters are generally low-pass passive filter realized with inductors and capacitors. The main adopted topology are the Γ , T and π configurations (Figure III.1). Each filter configuration can result useful for some applications whereas it could not ensure the required performance for others applications [68]. It is therefore important to choose the type of the filter depending on the application in which it will be used. As it can be seen in Figure III.1, each reactive element is arranged so as to

provide a theoretical attenuation of 20 dB/decade, in this way the π and T filters introduce a 60 dB/decade attenuation, on the other hand the Γ -filter theoretically provides a 40 dB/decade attenuation.

The term “theoretical attenuation” means the filter attenuation in the absence of parasitic effects. Really, parasitic phenomena occur at high frequencies resulting in a degradation of the filter performance.

With regard to the double stage configuration, it is noted that the intermediate capacitor in the π filter has a double value due to the parallel connection of the first stage output capacitor and the second stage input capacitor. Analogous consideration applies on the intermediate inductance of a T double stage filter.

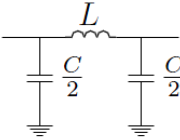
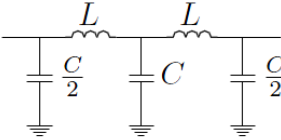
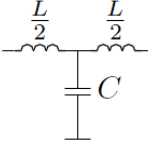
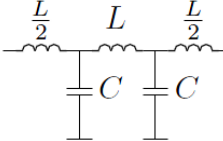
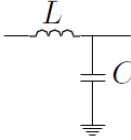
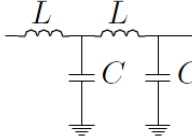
Type	Single Stage	Double stage
π	 <p>Attenuation = 60 dB/dec</p>	 <p>Attenuation = 100 dB/dec</p>
T	 <p>Attenuation = 60 dB/dec</p>	 <p>Attenuation = 100 dB/dec</p>
Γ	 <p>Attenuation = 40 dB/dec</p>	 <p>Attenuation = 80 dB/dec</p>

Figure III.1 - EMI filter circuit configurations.

The EMI filter design based only on the theoretical attenuation of the filter topology, without taking into account the source and the receiver impedances, generally does not allow complying with the limits imposed by the EMC standards.

The choice of the passive filter topology is closely related to the noise source and to the receiver impedances module, respectively Z_S and Z_L . Therefore, in addition to the theoretical attenuation value of the chosen filter configuration, a proper EMI filter design must suitably take into account the criterion of maximum impedance mismatching between the source and the receiver [69] - [71]. In fact,

the transfer of disturbance from the noise source to the victim (receiver or load) is dependent on the source/load impedance module ratio. In particular, if the system is schematised according to Figure III.2 (a), this transfer is described by (3.1), where V_L is the load voltage.

$$V_L = V_S \frac{Z_L}{Z_S + Z_L} \quad (3.1)$$

It is then evident that the condition

$$Z_S > Z_L \quad (3.2)$$

is required to have a load voltage attenuation. On the other hand, if this condition is not satisfied or the attenuation is not enough to comply with the standard limits, a filter should be interposed between the source and the load. In this case the corresponding scheme is that shown in Figure III.2 (b).

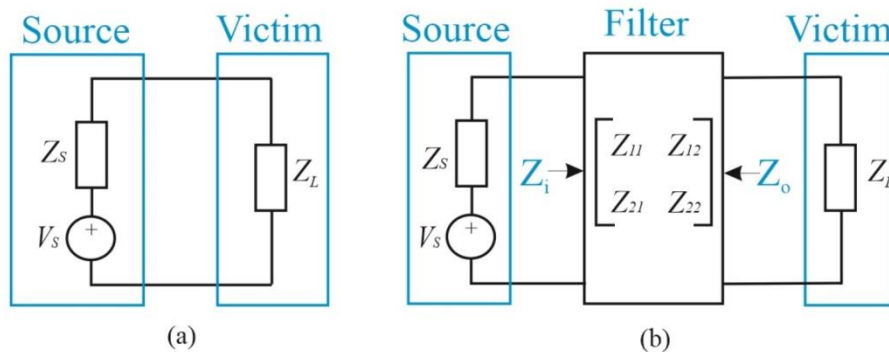


Figure III.2 - Schematic representation of noise source and victim without (a) and with (b) filter.

When the filter is inserted the source will “see” the impedance Z_i instead of Z_L and the victim will see the impedance Z_o instead of Z_S .

Then it is necessary to define the insertion loss of a filter (IL). This parameter is a figure of merit for a filter, it is defined as a ratio of the signal level in a test configuration without the filter (V_L) to the signal level with the filter (V_L'). This ratio is given in dB unit by the following equation:

$$IL_{dB} = 20 \log_{10} \left(\frac{V_L}{V_L'} \right) \quad (3.3)$$

For most filters V_L' will be smaller than V_L . Then, the insertion loss is positive and measures how much smaller the signal is after adding the filter. A high IL value means a good filter attenuation.

In the case shown in Figure III.2 (b), by means of impedance parameters, the IL equation becomes [72]:

$$IL = \frac{(Z_{11} + Z_S) \times (Z_L + Z_{22}) - Z_{12} \times Z_{21}}{(Z_S + Z_L) \times Z_{21}} \quad (3.4)$$

where Z_{11} , Z_{12} , Z_{21} e Z_{22} are the elements of the filter impedance matrix. From (3.4) it is evident that the IL is dependent on noise source impedance and load impedance, as well as on the intrinsic filter parameters. Eq. (3.4) can be rearranged as follows:

$$IL = \frac{\left(1 + \frac{Z_S}{Z_{11}}\right) \left(1 + \frac{Z_{22}}{Z_L}\right) - \frac{Z_{12}Z_{21}}{Z_{11}Z_L}}{\left(1 + \frac{Z_S}{Z_L}\right) \frac{Z_{21}}{Z_{11}}} \quad (3.5)$$

With reference to (3.5) it is possible to observe that the maximization of IL can be obtained if the two terms in round brackets appearing in the numerator are increased. This is obtained if the following conditions are imposed in the filter design:

$$\begin{cases} Z_S > Z_{11} \\ Z_L < Z_{22} \end{cases} \quad (3.6)$$

Table III.1 gives the filter topology to be used according to the noise source and load impedances. The following rules can be assessed:

- Filter series inductance should be connected to low impedance source or low impedance load.
- Filter parallel capacitors should be connected to high impedance source or high impedance load.

Table III.1 FILTER TOPOLOGY SELECTION BASED ON IMPEDANCE MISMATCHING CRITERION.

Z_L Z_S	High	Low
High	1	2
Low	3	4

3.3 Real behavior of passive components

Another important consideration on the EMI filter design and implementation regards the parasitic phenomena due both to non-ideal behavior of filter components and to the circuit layout. These aspects can heavily influence the filter performance.

Passive EMI filters components can have specific current and/or rating requirements, but they all must have good HF characteristics that are a purely capacitive behavior and purely inductive behavior, for capacitors and inductors respectively, up to high frequencies. Due to present parasitic phenomena, any suppression component resonates at a frequency, namely the self-resonant frequency f_r , given by:

$$f_r = \frac{1}{2\pi\sqrt{LC}} \quad (3.7)$$

where L and C are component's inductance and capacitance. For capacitors and inductors one of these parameters is the intrinsic characteristic while the other is a parasitic parameter. The f_r value of most suppression capacitors and inductors falls in the frequencies range 150 kHz – 30 MHz so it is necessary to choose passive components with a f_r as high as possible to obtain good HF characteristics. In the following subsections, an analysis of the real behavior of capacitors and inductors will be provided.

3.3.1 Capacitors behavior including parasitic effects

For low-frequency and DC signals, such as the supply currents in AC or DC power lines, a capacitor provides a high impedance path, but for HF signals, such as the noise currents in the 150 kHz – 30 MHz range, it provides a low impedance path. For this reason capacitors are connected in parallel with the noise source then they attenuate the conducted EMI by shunting them.

A real capacitor has not a purely capacitive behavior (even at low frequencies), since the leakage resistance of the isolation (R_{EPR}) and the equivalent series resistance (R_{ESR}) cannot be neglected in every case. At higher frequencies, the effect of stray inductance (L_{ESL}) is also to be considered. The characteristics of a real capacitor can be properly discussed in a relatively wide frequency range by means of the equivalent circuit shown in Figure III.3 [72].

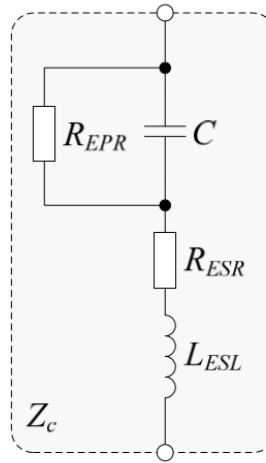


Figure III.3 – Equivalent circuit of capacitors.

The impedance of a capacitor, Z_C , is defined in (3.8):

$$Z_C = R_{ESR} + j\omega L_{ESL} + \frac{R_{EPR}}{1 + j\omega R_{EPR}C} = \frac{1 + \frac{R_{ESR}}{R_{EPR}} - \omega^2 L_{ESL}C}{\frac{1}{R_{EPR}} + j\omega L_{ESL}C + j\omega \left(\frac{L_{ESL}}{R_{EPR}} + R_{ESR}C \right)} \quad (3.8)$$

At DC and low frequency, the impedance of a capacitor is affected only by the resistive effects, $R_{ESR} + R_{EPR}$. With increasing frequency, the capacitive behavior predominates over the resistive one and Eq. (3.8) is simplified to the form below:

$$Z_C \approx R_{ESR} + j\omega L_{ESL} + \frac{1}{j\omega C} \quad (3.9)$$

Over f_r the inductive component predominates on capacitive one; then the real capacitor behave like an inductor at high frequencies. The impedance of a real capacitor is just R_{ESR} at f_r .

The Bode plot of the impedance as a function of frequency, defined by Eq. (3.8), with the following parameters: $C=10 \mu\text{F}$, $R_{ESR}=0.3 \Omega$, $R_{EPR}=10 \text{ k}\Omega$ and $L_{ESL}=96 \text{ nH}$, is shown in Figure III.4 as an example. As seen from the curve, the capacitor can be regarded as purely capacitance only in the angular frequency range $10 \div 10^6 \text{ rad/s}$.

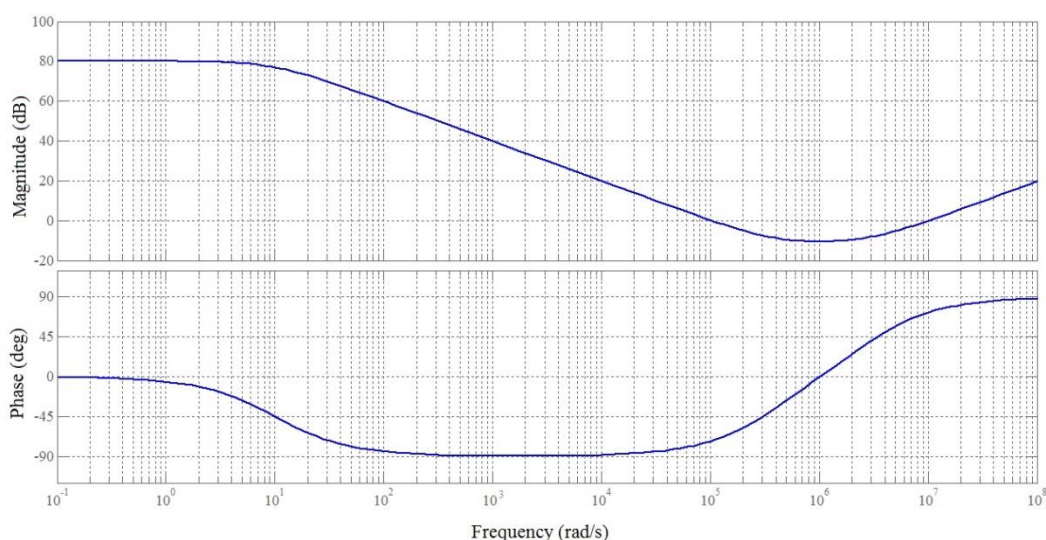


Figure III.4 - Bode plot of impedance $Z_c(f)$.

3.3.2 Inductors behavior including parasitic effects

Unlike capacitors, inductors provide a low impedance path for mains frequency signals, and high impedance for HF signals. There are two types of suppression inductors: DM inductors and CM chokes.

Suppression inductor is affected by disadvantages:

- it is bulky;
- the real inductance value can differ to the nominal value given by the manufacturer, due to high tolerance value;
- its HF characteristic depends on operating temperature or current (in fact the nominal inductance value decreases as a result of the core saturation).

In EMI filter design the Y-capacitor values are limited for safety reasons and the required CM attenuation must be achieved mainly by the inductive components of the filter. Despite the

disadvantages listed above, least one inductor is used in EMI filters implementation. In comparison with capacitors, inductors have non-linear characteristics and they can present more resonant frequencies.

To understand the terms that define the performance and limitation of inductors in the frequency range of conducted noise suppression, it is useful to consider the equivalent circuit in Figure III.5. The resistance R_{ESR} in the equivalent circuit represents the coils losses. Parasitic effects at higher frequencies, due to the stray capacitances between turns, cannot be neglected. Although the turn-capacitance is distributed, a parallel connected concentrated capacitor, C_{EPC} , provides a suitable approximation. [72]

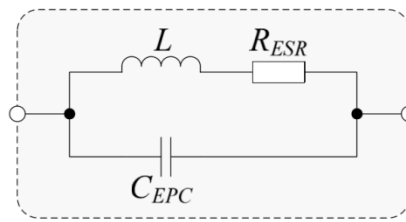


Figure III.5 – Equivalent circuit of an inductor.

The impedance of the inductor according to the equivalent circuit is:

$$Z_L = \frac{R_{ESR} + j\omega L}{1 - \omega^2 LC_{EPC} + j\omega R_{ESR} C_{EPC}} \quad (3.10)$$

The DC impedance is equal to R_{ESR} . At low frequencies, impedance Z_L is dominated by inductive component and its value increases proportionally with the frequency. At the resonance frequency, the inductor, L , resonates with the parallel capacitor, C_{EPC} , and the impedance reaches its maximum value. Over the resonance frequency the inductor impedance decreases because the capacitive contribution dominates and the inductor behaves like a capacitor.

The Bode plot of the impedance as a function of frequency, defined by Eq. (3.10), with the following parameters: $L=1$ mH, $C_{EPC}=10$ pF, and $R_{ESR}=10$ Ω , is shown in Figure III.6 as an example. The inductor can be regarded as purely inductance only in the angular frequency range $10^4 \div 10^7$ rad/s.

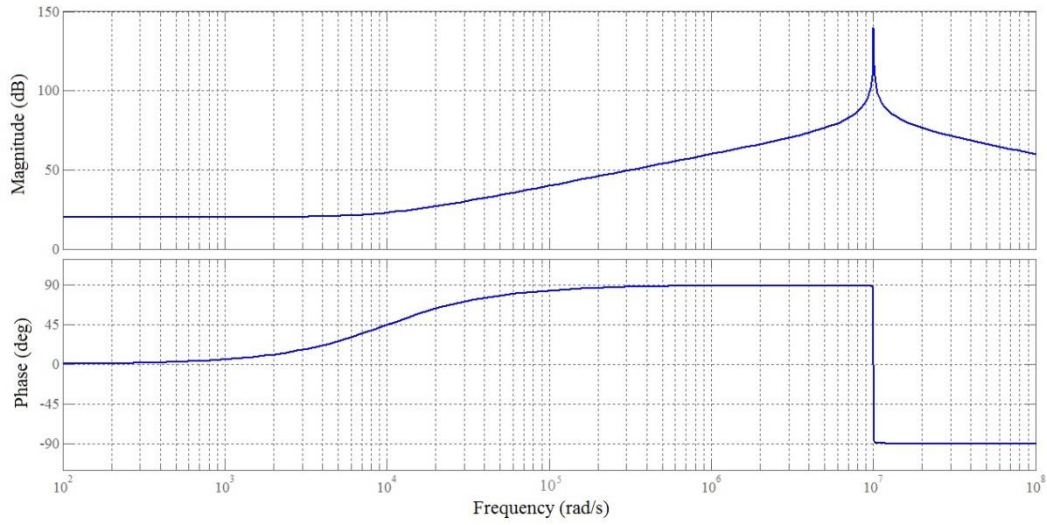


Figure III.6 - Bode plot of impedance $Z_L(f)$.

Finally, the inductor impedance at low frequencies (more precisely, in the frequency range below the resonance frequency) can be approximated as follows:

$$Z_L \approx R_{ESR} + j\omega L \quad (3.11)$$

At resonance frequency it is:

$$Z_L(f_r) \approx \frac{L}{R_{ESR} C_{EPC}} \quad (3.12)$$

Indeed, for frequencies higher than the resonant frequency, Z_L is approximated as follows:

$$Z_L \approx \frac{j\omega L}{\omega^2 L C_{EPC}} \approx \frac{1}{j\omega C_{EPC}} \quad (3.13)$$

3.4 EMI Filter General Design Procedure

As well established, the conducted electromagnetic emission can be decomposed in DM and CM noise. The generation and coupling mechanisms as well as the CM and DM EMI paths are different and therefore separated filter sections are needed in order to obtain suitable attenuation for EMC compliance. Both CM and DM filter components are usually embedded into a single filter configuration, as shown in Figure III.7 (a). In particular, a Γ type filter is used to attenuate CM noise,

as shown in Figure III.7 (b) (with capacitors placed on source side, assuming a high source impedance and a low load impedance), and a π type filter is used to DM noise mitigation, as shown in Figure III.7 (c). The filter is composed of passive components acting on CM or DM noise separately, and other elements simultaneously affecting both types of noise. Therefore, it is necessary to separately evaluate the two noise modes as a basic step to design an effective EMI filter [73].

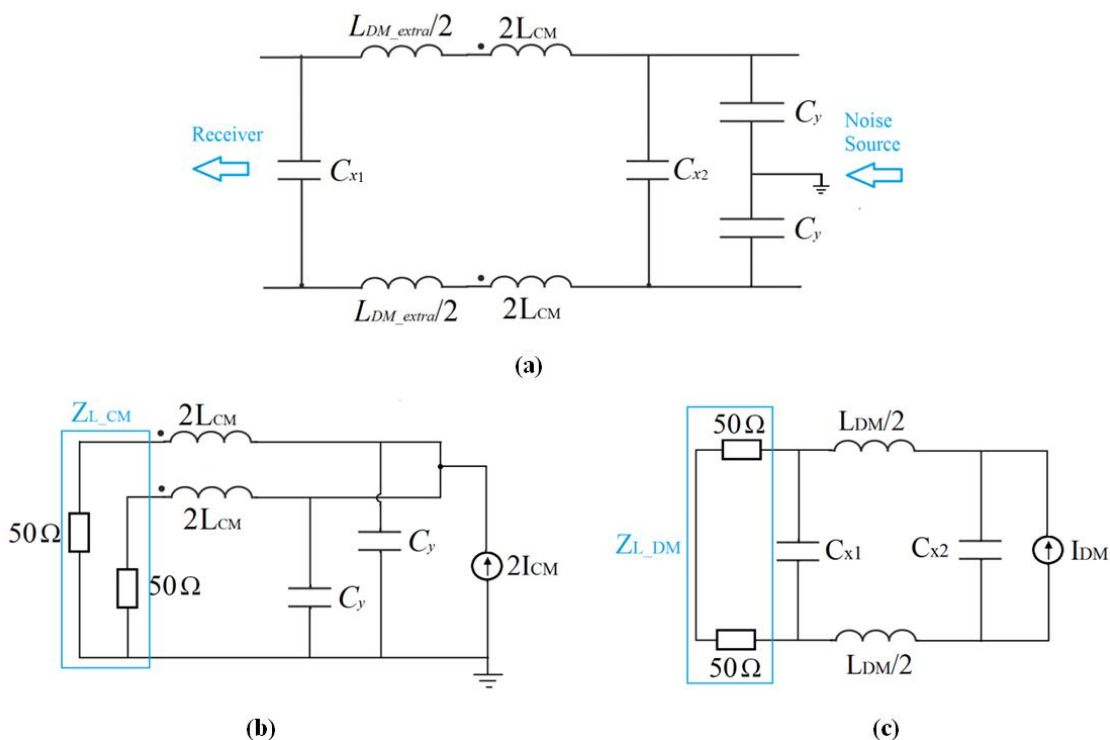


Figure III.7 - Generic EMI filter configuration (a), CM equivalent circuit (b) and DM equivalent circuit (c).

The capacitors C_y attenuate both CM and DM noise and they are generally in the order of magnitude of nF; their value is very small compared to that of C_{x1} and C_{x2} , which are in the μF range, so their effect on the DM noise is almost negligible. On the other hand, the capacitor C_x between the electrical lines only attenuates the DM noise. The bulkiest component of the filter is the common mode choke, L_{CM} , that ideally suppresses only the CM noise; however its leakage inductance ($L_{leakage}$) is usually sufficient to attenuate the DM noise as well [68]. Sometimes an additional inductance in series with the L_{CM} (L_{DM_extra}) might be useful to increase the total value of the DM inductance.

The procedure followed in designing the CM and DM filter components is shown schematically in the block diagram in Figure III.8 and it is described below.

The first step is the identification of the crucial point on the experimental curve of the EMI emission, i.e., the most relevant emission peaks or the emission peaks at the lowest frequency. Therefore it is necessary to measure the CM and DM components separately and to obtain their

frequency spectra. The required attenuation for the CM e DM noise, Att_{req_CM} e Att_{req_DM} , are calculated as follows:

$$Att_{req_CM} = A_{h_CM} - L + SM \quad (3.14)$$

$$Att_{req_DM} = A_{h_DM} - L + SM \quad (3.15)$$

where A_{h_CM} , A_{h_DM} are the amplitudes of the harmonic to be attenuated, L is the maximum amplitude allowed by the reference standard at the frequency of interest and SM denotes an additional safety margin usually set to $6 \text{ dB}\mu\text{V}$.

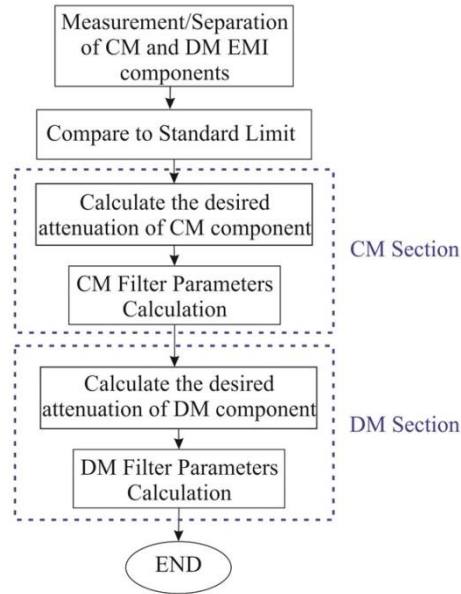


Figure III.8 – Steps of EMI filter design.

The cut-off frequency, f_o , of the CM or DM filter is given by (3.16):

$$\log_{10} \frac{f_{h_att}}{f_{o_CM/DM}} = \frac{Att_{req}}{Att_{filter}}, \quad f_{o_CM/DM} = \frac{f_{h_att}}{10^{\frac{Att_{req}}{Att_{filter}}}} \quad (3.16)$$

where f_{h_att} is the harmonic frequency to be attenuated and Att_{filter} is the filter theoretical attenuation, relating to its circuit configuration [68]. In order to improve the filter performance and to avoid any amplification of the switching frequency harmonics, the designer could choose to fix the f_o value lower than the converter switching frequency value (f_{PWM}).

When the both corner frequencies are known, the inductance and capacitance values of the CM/DM sections of the EMI filter can be determined according to (3.17) and (3.18).

$$L_{CM} = \frac{1}{C_{CM} (2\pi f_{o_CM})^2} \quad C_{CM} = n_{phase} C_y \quad (3.17)$$

where n_{phase} is the number of AC phases/DC lines of the power electronic system.

$$C_{DM} = C_{x1} = C_{x2} = \frac{1}{L_{DM} (2\pi f_{o_DM})^2} \quad (3.18)$$

From Eq. (3.17) and (3.18), it is necessary to define a value of filter components to obtain all the others. Usually firstly the CM parameters are defined. The CM capacitors, C_y , are connected from the line to the ground/chassis and the value of these specific capacitors is therefore regulated by standards for safety. Some of the possible choices for the designer are cited below:

- $C_y = 100$ nF (SAE AS 1831 - Society of Automobile Engineers [74]);
- $C_y = 100$ nF for 60 Hz equipment or $C_y = 20$ nF for 400 Hz equipment (MIL-STD-461F [75]).

With reference to DM parameters some degrees of freedom exist; in particular, by increasing the value of C_{DM} , the size of L_{DM} will be reduced and vice versa.

The DM inductance is usually obtained by the leakage inductance of the CM choke; in this case its value is approximately 0.1-2% of the CM inductance value, depending on the core material. Then, the required DM capacitance is defined on the basis of the cutoff frequency. On the other hand, if a higher L_{DM} value is preferred to reduce the value or the size of DM capacitors, then dedicated DM inductors can be considered in the filter design [76].

Once the values of the EMI filter components are defined, the chokes/inductors and capacitors should be accurately chosen to obtain an effective attenuation. In particular, with regard to magnetic cores, both geometrical dimensions and magnetic properties of the material must be appropriately selected to prevent magnetic saturation, as it will be described in subsections 3.4.1 and 3.4.2.

In subsection 3.4.3 some considerations on the impact of magnetic cores' and capacitors' material on filter performance will be presented.

3.4.1 Design of CM choke and DM extra inductor

Once the values of the filter inductive components are defined, it is necessary to perform the following analysis.

The first parameter that needs to be set is the windings wire section A . This parameter is defined by the value of the operating current I as: $A = I / J$ where J is the current density set equal to 4 A/mm^2 . The value of the wire section defines the wire AWG (American Wire Gauge), as in Table III.2. The AWG is a standardized wire gauge system used for the diameters of round, solid, nonferrous, electrically conducting wire.

The AWG of a stranded wire is determined by the cross-sectional area of the equivalent solid conductor. Because there are also small gaps between the strands, a stranded wire will always have a slightly larger overall diameter than a solid wire with the same AWG. The cross-sectional area of each gauge is an important factor to determine its current-carrying capacity.

Table III.2 TABLES OF AWG WIRE SIZES (SOLID WIRE).

AWG gauge	Conductor Diameter (mm)	Conductor Section (mm^2)
14	1.628	2.08
15	1.450	1.65
16	1.291	1.31
17	1.150	1.04
18	1.024	0.823
19	0.912	0.653
20	0.812	0.518

The next step is to choose a core size and material depending on the number of turns needed to implement L_{CM} .

To avoid saturation phenomena in the core material, due to high L_{CM} value (generally of the order of millihenries) and the current that runs through it, CM inductance is implemented with a *CM choke*.

Common mode inductors are wound with two or three windings with equal numbers of turns. The number of windings is the same as the number of phases. As depicted in Figure III.9, the windings are placed on the core so that the line currents in each winding create fluxes that are equal in magnitude but opposite in phase in the case of DM currents, and identical in the case of CM currents. The fluxes of DM currents are thus ideally cancelling out each other and the related current is not influenced by the inductors. It will be shown in section 3.4.2 that the cancellation is in practice not complete, and this is called leakage inductance. The fluxes due to CM currents, on the contrary, are accumulated inside the core. Therefore, the common mode choke coil works as an inductor against common mode current.

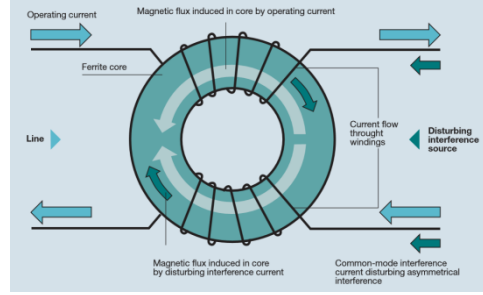


Figure III.9 – CM choke [98].

The inner circumference of the toroidal core, $I.C.$, the maximum number of achievable turns on toroidal core, N_{max} , and the required number of turns for $L_{CM/DM}$ implementation, $N_{required}$, are determined by the following equations in which $\sigma_{winding}$ represents the maximum angle that the winding subtends on half of the core. It is acceptable to assume $\sigma_{winding}$ equal to 145° , as shown in Figure III.10.

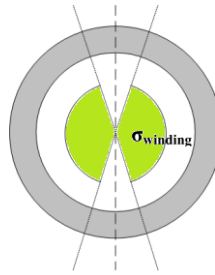


Figure III.10 - Winding angle example.

$$I.C. = \pi(ID_{core} - D_{wire})$$

$$N_{max} = \frac{2\sigma_{winding}}{360^\circ} \frac{I.C.}{D_{wire}}$$

$$CM \begin{cases} L_1 = 2 \cdot L_{CM} \\ N_{required} = 2\sqrt{\frac{L_1}{A_L}} \end{cases} \quad DM \begin{cases} L_1 = L_{DM} / 2 \\ N_{required} = \sqrt{\frac{L_1}{A_L}} \end{cases} \quad (3.19)$$

where ID_{core} is the inner diameter of the toroidal core, D_{wire} is the wire diameter, L_1 is the inductance value of a winding and A_L is the inductance value obtained with a turn realized on a specific core. Of course the condition $N_{required} < N_{max}$ must be verified.

3.4.2 Considerations on magnetic cores saturation

After having chosen a suitable toroidal core in terms of geometric dimensions to implement L_{CM} or L_{DM} , it's necessary verify the suitability of the core in terms of absence of magnetic saturation.

The design criterion for the magnetic core selection to implement L_{CM} and L_{DM} is based on the following analysis.

Let us consider the CM choke in Figure III.11. The maximum flux density (B_{max}) in the CM choke magnetic core depends on the flowing peak current in its inductors. If L_1 and L_2 are the inductance of the two windings of the CM choke and $M_{12}=M_{21}=M$ the mutual one, the currents flowing on such inductors are respectively $(I_{DM}+I_{CM})$ and $(-I_{DM}+I_{CM})$.

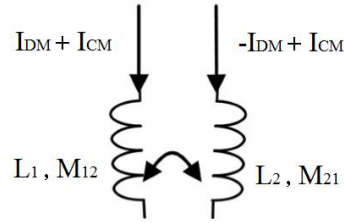


Figure III.11 - Electrical representation of a CM inductor.

The magnetic flux due to each of the two windings of the CM choke, ϕ_1 and ϕ_2 , is given by:

$$\begin{aligned}\phi_1 &= L_1 \cdot (I_{DM} + I_{CM}) + M \cdot (-I_{DM} + I_{CM}) = \\ &= (L_1 - M) \cdot I_{DM} + (L_1 + M) \cdot I_{CM}\end{aligned}\quad (3.20)$$

$$\begin{aligned}\phi_2 &= L_2 \cdot (-I_{DM} + I_{CM}) + M \cdot (I_{DM} + I_{CM}) = \\ &= (-L_2 + M) \cdot I_{DM} + (L_2 + M) \cdot I_{CM}\end{aligned}\quad (3.21)$$

Therefore, as an upper limit, the overall flux $\phi_{tot_CMchoke}$ on the core is given by:

$$\phi_{tot_CMchoke} = \phi_1 + \phi_2 = (L_1 - L_2) \cdot I_{DM} + (L_1 + L_2 + 2M) \cdot I_{CM}\quad (3.22)$$

The term proportional to the DM current is tied to the leakage flux. Moreover, having a coupling factor $k = \frac{M}{\sqrt{L_1 L_2}}$ close to unity, the following approximation can be done: $M=L_1=L_2$.

Then Eq. (3.22) can be rewritten as follows:

$$\phi_{tot_CMchoke} = L_{leakage} \cdot I_{DM} + 4L_1 \cdot I_{CM} \quad (3.23)$$

In the case of an extra DM inductor the magnetic flux is generated by a single winding and the peak current flowing on the same is composed of both the DC current that the noise current. So the magnetic flux due to DM inductor, $\phi_{tot_DMinductor}$, is given by:

$$\phi_{tot_DMinductor} = \frac{L_{DM}}{2} (I_{DC} + I_{DM} + I_{CM}) \quad (3.24)$$

Moreover the maximum magnetic flux can be expressed as:

$$\phi_{tot_max} = B_{max} \cdot S \cdot N \quad (3.25)$$

where N is the total number of turns of the windings, S is the cross section of the magnetic core, B_{max} is the maximum value of the magnetic flux density. Therefore,

$$B_{max} = \frac{\phi_{tot_max}}{(h \cdot (r_{out} - r_{int})) \cdot N} \quad (3.26)$$

where h , r_{out} and r_{int} are the height, the outer radius and the inner radius of the toroidal core, respectively.

Once the peak current is known, it is possible to suitably choose the toroidal core for the CM choke or DM inductor implementation, according to the condition $B_{max} < B_{sat}$ (B_{sat} is the saturation value of the magnetic flux density at the operating temperature).

3.4.3 Considerations on materials of the EMI filter components

For the implementation of the CM choke and the DM inductance, generally toroidal cores of magnetic materials are used.

The typical requirements of a common mode choke are: high permeability of the magnetic core, high saturation level and low magnetic losses.

Three basic materials used in the design of the traditional CM choke are ferrite cores, powder materials (iron) and metal alloys (nanocrystalline and amorphous structure). Other materials with high performance at high frequencies and high permeability are commercially available. Those materials allow to achieve high inductance value with a smaller number of turns and thus reducing the number

of stages, the size and the weight of the filter. The choice of materials has therefore a significant impact on the filter performance.

Figure III.12 presents an overview of the permeability as a function of the frequency of nanocrystalline, ferrites, iron and amorphous materials [77]. The permeability μ , as the ratio of the magnetic flux density B and the magnetic field H , is the most important parameter of magnetic materials. The highest permeabilities are found in nanocrystalline materials. Amorphous alloys have somewhat smaller values whereas iron powder cores have relatively low permeabilities. Ferrite cores can be used over a wide frequency range but exhibit a significantly lower level of saturation. Higher flux densities can be found in nanocrystalline and amorphous materials as well as in iron powder cores but are limited in the used frequency range. Nanocrystalline materials are a good alternative to the traditional chokes made of ferrite or iron powder. So, the main advantage is the high level of saturation and the resulting smaller size.

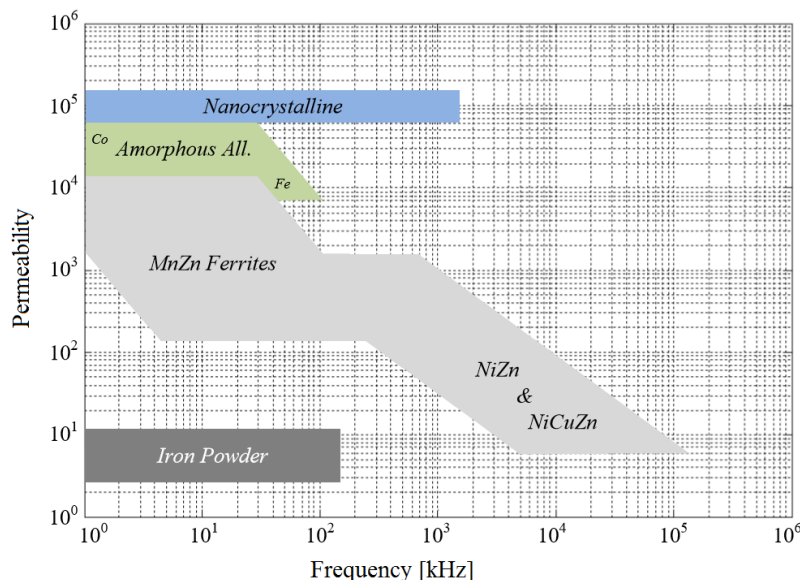


Figure III.12 - Magnetic properties for ferrites, iron powder and metal alloys: permeability vs. frequency.

A comparison of the magnetic characteristics of a nanocrystalline material and a common ferrite is given in Figure III.13. It shows the magnetic permeability curves versus frequency (a), the magnetization curves (b) and the saturation flux density versus temperature (c) of the VITROPERM 500F and of a typical Mn-Zn ferrite.

In Figure III.13 (a), it can be observed that the permeability of VITROPERM 500F is significantly higher than ferrite in the low frequency range. At higher frequencies the μ of the nanocrystalline material remains above that of ferrite. A high choke impedance is preferred for higher attenuation. This can be achieved more effectively by using high permeability core materials than by increasing the

number of turns, as a lower number of turns results in lower winding capacitance and hence improved HF properties. In Figure III.13 (b), the magnetization curve of VITROPERM 500F in comparison to typical Mn-Zn ferrite shows noticeable differences in permeability (slope of the curve) and saturation flux density (maximum value of the curve). In particular, as shown in Figure III.13 (c), the saturation flux density of the VITROPERM suffers of a small variation in the operating temperature range up to 150 °C, while the ferrite exhibits a decrease of about 40% at 100 °C, compared to the environment temperature value. The high Curie temperature of VITROPERM alloys (above 600 °C), allows short term maximum operating temperatures as high as 180 – 200 °C; then the VITROPERM is more suitable for applications with high operating temperatures.

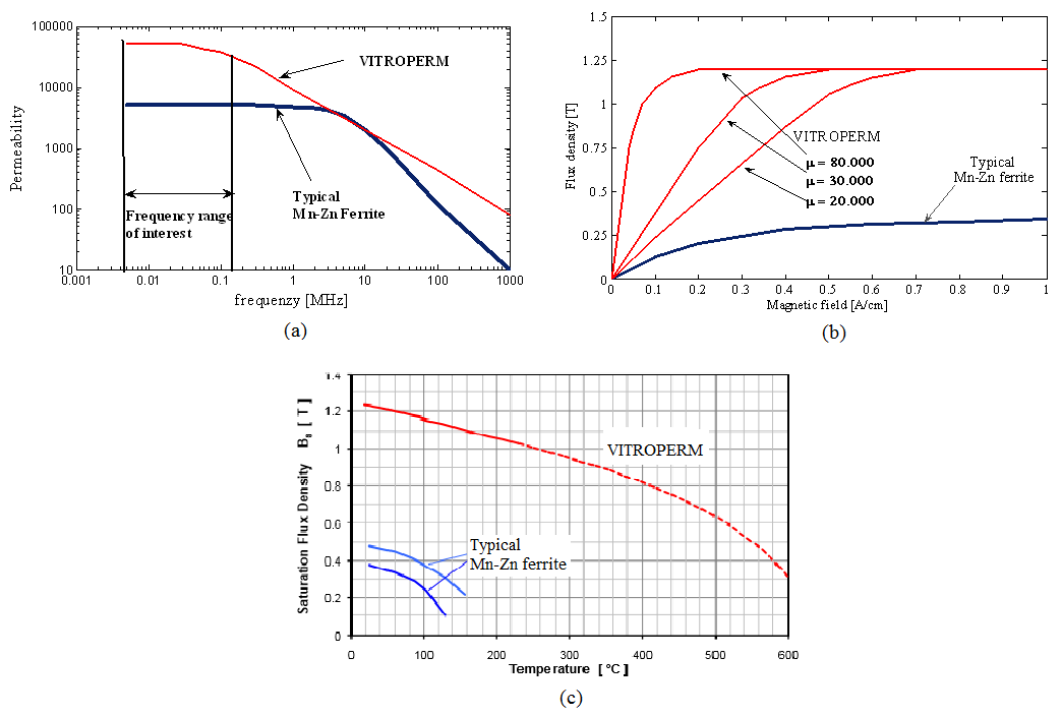


Figure III.13 - Magnetic permeability curves versus frequency (a), Magnetization curves (b) and the saturation induction versus temperature (c) of the VITROPERM 500F and a typical Mn-Zn ferrite.

Another feature to take into consideration is related to the power losses in the magnetic materials. These losses occur when the magnetic material is subjected to a time variable magnetic flux density. There are several specific losses that contribute to the total power loss due to the magnetic hysteresis phenomenon and to the eddy currents.

The magnetic hysteresis phenomenon occurs when a ferromagnetic material core is subjected to an alternative cyclic magnetization. This occurs, for example, when a ferromagnetic material core is subjected to a time variable magnetic field, as produced by a time variable current. The energy provided to the core during the magnetization phase is not entirely returned during the

demagnetization phase; at each cycle, a quantity of energy proportional to the area enclosed by the hysteresis loop (Figure III.14) is stored in the magnetic core. Therefore a dissipation of heat energy occurs in these cores; it is equivalent to the hysteresis power loss and it depends on the frequency f of the magnetizing current. The Steinmetz's equation allows calculating the specific hysteresis loss p_i per volume [W/m^3] or per mass [W/kg], depending on the expression of the constant k_{ist} , as follows:

$$p_i = k_{ist} \cdot f \cdot B_{max}^\alpha \quad (3.27)$$

where B_{max} is the maximum value of the magnetic flux density, α can range from 1.6 to 2, and k_{ist} is a coefficient depending on the magnetic material.

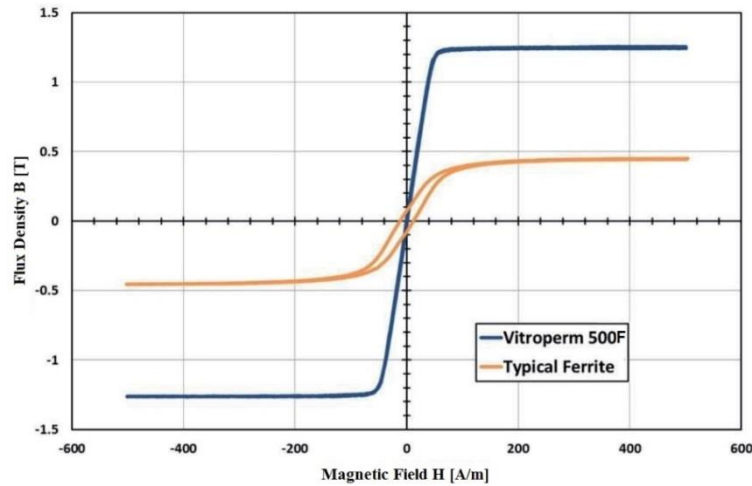


Figure III.14 – Hysteresis loop of VITROPERM 500F and a typical ferrite [78].

In addition to the hysteresis loss, the eddy currents in the cores mass induced by the variations of the magnetic flux cause a further dissipation of energy. This loss is determined by the electrical resistance ρ and the thickness δ of the core. The eddy currents loss p_c is calculated using the equation:

$$p_c = \frac{k'_c \cdot \delta^2 \cdot f^2 \cdot B_{max}^2}{\rho} = k_c \cdot f^2 \cdot B_{max}^2 \quad (3.28)$$

where k_c is a coefficient depending on the magnetic material.

For the nanocrystalline material VITROPERM 500F the coercitivity is very small and therefore the hysteresis loss is very low. The loss is much lower than in ferrite materials. VITROPERM 500F is a metallic material and it shows therefore eddy current losses. Because this loss depends not only on the conductivity but also on the ribbons thickness (Eq. 3.28), that is only $20 \mu\text{m}$ [80], minimal eddy currents loss is ensured.

The sum of hysteresis loss and eddy currents loss constitutes the total loss in the material. Manufacturers of ferromagnetic materials provide a very important technical data, known as *specific loss figure* C_p . Known the value of the specific loss figure, the evaluation of the total loss p_t in the ferromagnetic material, absorbed by a core of mass M subjected to a variable magnetic flux with a maximum flux density B_{max} and frequency f , is performed by means of the following semi-empirical relation:

$$p_t = C_p \cdot B_{max}^2 \cdot \left(\frac{f}{50}\right)^{1.2} \cdot M \quad (3.29)$$

Figure III.15 shows the comparison of magnetization losses in different materials. Just in the range of the operating frequencies of the switching power devices of 10 – 100 kHz, the nanocrystalline VITROPERM-alloys are superior to other magnetic materials by exhibiting lower losses. For this reason the VITROPERM is suitable to power applications from a few kW, e.g. medical or industrial applications, up to powers of MW used in the field of modern railway traction techniques [78].

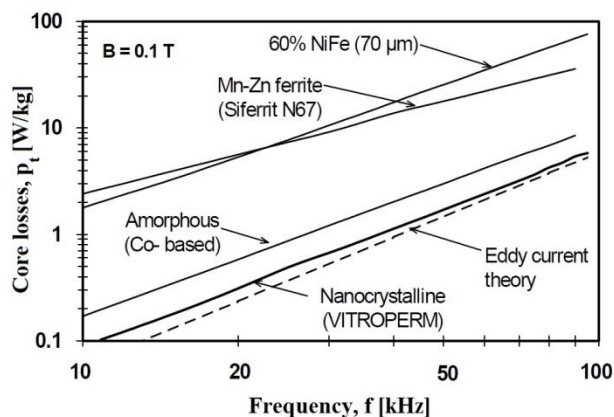


Figure III.15 – Comparison of magnetization losses of typical materials for CM choke and DM inductance [79].

On the basis of the considerations aforesaid, VITROPERM nanocrystalline alloys are optimized to combine highest permeability and lowest coercive field strength. The combination of very thin tapes and the relatively high electrical resistance ($1.1 - 1.2 \mu\Omega\text{m}$) ensures minimal eddy current losses and an outstanding frequency vs. permeability behavior. Along with saturation flux density of 1.2 T and wide operational temperature range, these features combine to make VITROPERM a universal solution for most EMC problems and it presents better performance in many aspects to commonly used ferrite and amorphous materials [80].

The choice of magnetic materials with high permeability allows achieving high inductance value with a smaller number of turns: a reduction of the number of stages, the size and the weight of the

filter is obtained. Two CM chokes with a CM inductance equal to 0.8 mH have been realized by using a N30 ferrite core and a VITROPERM 500F core. A comparison between the main geometrical and magnetic characteristics of the two cores is reported in Table III.3. The nanocrystalline core allows reducing the CM choke size of about 87.5% in volume respect to the ferrite core. Similarly, a reduction of the CM choke weight of 82.5% is obtained. The CM choke set up with ferrite and VITROPERM cores is shown in Figure III.16. The size reduction with the use of nanocrystalline material is evident.

Table III.3 COMPARISON OF DIFFERENT MAGNETIC CORES CHARACTERISTICS TO SET UP A $L_{CM}=0.8$ mH.

Parameter	Symbol	Ferrite N30	VITROPERM 500F
Toroidal core size		50x30x20 mm	25x16x10 mm
Volume	V	50 cm ³	6.25 cm ³
A _L value	A _L	8700 nH, 10 kHz	65.5μH, 10 kHz
Saturation flux density	B _s	0.45 T	1.2 T
Weight		114 g	20 g
N° of turns per winding	N	12	5



Figure III.16 - CM choke set up by using an N30 ferrite core (left) and a VITROPERM core (right).

[68] Suitable considerations must be complied about the capacitors. They are very critical components; an incorrect choice of the type to use can cause damage and malfunctions of the system. In particular, they are sensitive to overvoltages that may cause permanent damage to the insulation. The main specification for the capacitors is MIL-STD-15573. The capacitors must meet various voltage ratings and for AC capacitors, the level must be 4.2 times the RMS voltage of the system. For example, in a 220V RMS system, the capacitor must be designed to handle 924V, usually rounded up to 1 kV. For the DC capacitor, the multiplier is 2.5 times the system voltage. For example, in a 50V DC system, the DC capacitor must be designed to handle 125V DC. Moreover, the RMS peak voltage and the maximum applied DC voltage are used to determine this, not the nominal or average voltage. If this is a 120V AC system, then we can safely assume $\pm 10\%$; the peak value of 132V is multiplied by 4.2=554V, which is the final test voltage for the capacitor [68].

Noise suppression capacitors are typically made of metalized film. This choice has the advantage to increase the stability of the component versus time and temperature. They are also self healing: the

components repairs itself after a voltage spike: each layer acts as a single capacitor, if any of them is damaged the total capacitance can decrease slightly without affecting the performance of the part. In a worst case scenario the failure mode is an open circuit. This specific structure also allows high values of capacitance (several μF). These capacitors are more expensive than general purpose capacitors.

In most filters, if the capacitor value is reasonably higher, the filter will work much better and give more insertion loss (but that will not suffice if the value is limited). From that point of view, ceramic or polypropylene capacitors are generally preferred. In the following, the impedances module and phase of different capacitors measured by a precision RLC meter Agilent 4285ALCR are shown to perform a comparison on their high frequencies behavior. In Figure III.17 the impedances module of ceramic and polypropylene capacitors are shown: a capacitive behavior can be noted up to a few megahertz. The ceramic capacitors are characterized by a low parasitic inductance due to their small size. The polypropylene capacitors have low losses and can support overvoltages.

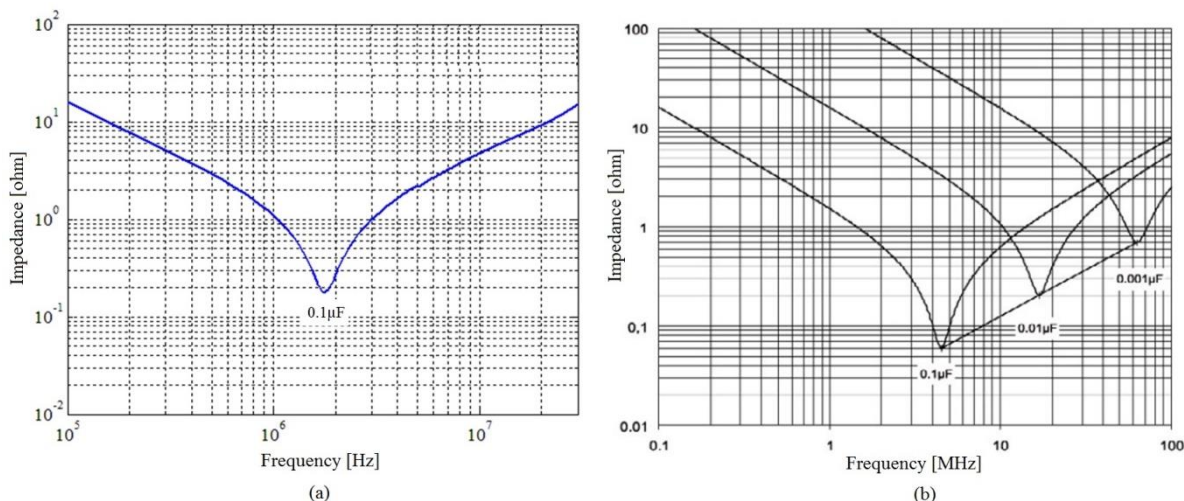


Figure III.17 – 100 nF capacitor impedance (a) 250V_{dc} ceramic capacitor (measured data) and (b) 300V_{ac},1000V_{dc} polypropylene capacitor (datasheet).

The DM capacitance is generally of the order of tens of microfarads. In these cases electrolytic capacitors are used even though their high frequency performance are not good compared to ceramic/polypropylene capacitors. As illustrated in Figure III.18, the capacitor behavior is generally capacitive until the tens of kilohertz range, and then become resistive and finally inductive after 1 MHz. In particular, in Figure III.18 and Figure III.19 it can be observed that, for a given capacitance value, the performance of an electrolytic capacitor varies both as a function of the nominal voltage and the application field. This confirms the importance of the choice of suitable capacitors for EMI mitigation.

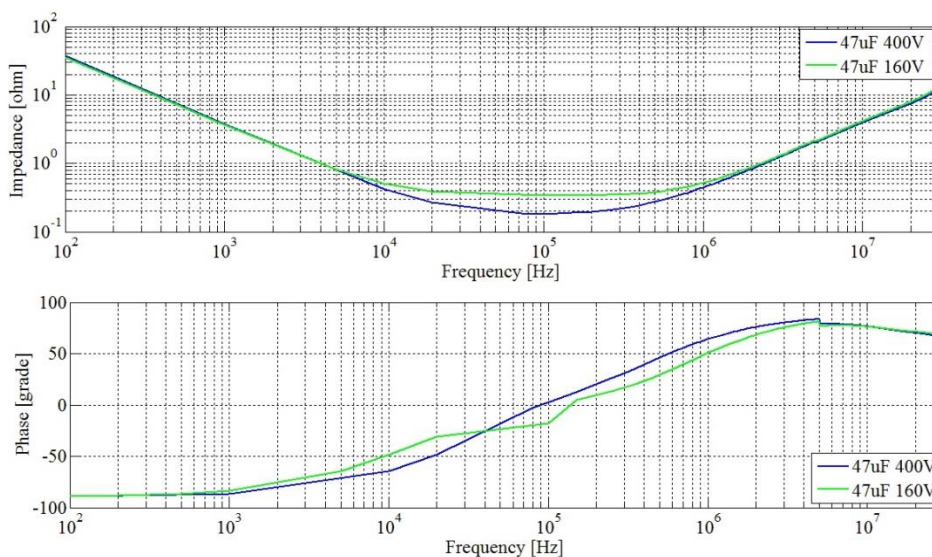


Figure III.18 – Measured impedance module (upper) and phase (lower) of a 47µF electrolytic capacitor with nominal voltage equal to 160V and 400V.

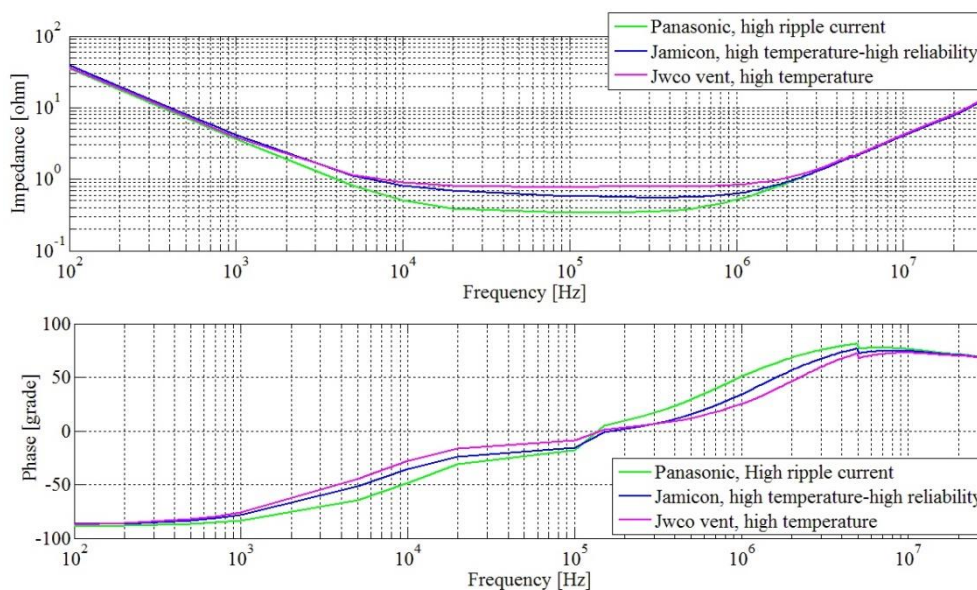


Figure III.19 – Measured impedance module (upper) and phase (lower) of a 47µF electrolytic capacitor with nominal voltage equal to 160V of different manufacturers and for different application fields.

Another feature that can influence the EMI filter performance is the tolerance of its components. The tolerance value is the extent to which the actual component is allowed to vary from its nominal value listed in the datasheet.

The cut-off frequency f_o of the EMI filter is described by the Eq. (3.27):

$$f_o = \frac{1}{2\pi\sqrt{LC}} \quad (3.27)$$

The deviation on the required f_o due to the inductor and capacitor tolerance is obtained as follows:

$$\Delta f_o = \left| \frac{\partial f_o}{\partial C} \right| \cdot \Delta C + \left| \frac{\partial f_o}{\partial L} \right| \cdot \Delta L \quad (3.28)$$

According to Eq. (4.27), the Eq. (4.28) can be rewritten as follows:

$$\Delta f_o = \frac{1}{4\pi\sqrt{LC}} \cdot \frac{\Delta C}{C} + \frac{1}{4\pi\sqrt{LC}} \cdot \frac{\Delta L}{L} \quad (3.29)$$

where $\Delta L/L$ and $\Delta C/C$ are the tolerance values of the inductor and capacitor respectively.

From the Eq. (3.30) that defines the deviation on f_o value in percent, it is evident that the inductor and capacitor tolerances determine a cut-off frequency value unlike the required one.

$$\frac{\Delta f_o}{f_o} \% = \frac{1}{2} \cdot \left(\frac{\Delta C}{C} \% + \frac{\Delta L}{L} \% \right) \quad (3.30)$$

Usually the tolerance rating is expressed as a percentage ($\pm\%$). The tolerance value of the capacitors can range anywhere from -20% up to +80% in some cases. Thus a 100 μ F capacitor with a $\pm 20\%$ tolerance could legitimately vary from 80 μ F to 120 μ F and still remain within tolerance. The tolerance value of the inductors depends to the A_L tolerance of the core magnetic material used to realize the desired inductance. For example, the A_L tolerance of a VITROPERM core can range from -25% to 45% while for a typical ferrite core it can range from -30% to 30%.

The negative tolerance percentage determines a negative impact on filter performance because it involves a real value of the component lower than the nominal value and consequently a cut-off frequency higher than the required one; hence the filter will begin to attenuate at different frequency than the desired one.

Depending the filter topology, the tolerances effect can not be neglected and it can be analysed by a Monte Carlo analysis or worst case method.

CHAPTER IV – Optimized Design of High Power Density EMI Filter

4.1 Introduction

Now that the baseline design, topology and guidelines for an accurate choice the EMI filter components have been revised, it is essential to look at the optimization of the EMI filter and especially at its size reduction to achieve a high power density.

Recently power electronics market has been boosted by new high-speed devices allowing faster switching operation as the wide-band gap devices based on Silicon Carbide (SiC) or Gallium Nitride (GaN) [8], [9]. On the other hand, their operation in power electronic converters leads to an increase of electromagnetic interference. For this reason noise filtering is, more than ever, one of the major issues in power electronic system design, particularly when dealing with stringent standard limits [81]-[83]. Besides satisfying EMI limits, a further optimization in terms of filter size and weight can be performed; in fact, the EMI filter can contribute up to 30% of the total size and weight of power electronic converters. Therefore, a filter design matching the maximum power density is strongly desired, especially for the applications (e.g. airplanes, electric vehicles, etc.) in which compactness and low weight are the primary constraints [84].

Scientific literature proposes several techniques dealing with high-power-density design of discrete EMI filters for power electronic converters. Some techniques are based on setting up a compact layout by using suitable winding structures and/or high performance magnetic materials for the inductor cores [85], [86]. Other approaches, starting from an accurate high frequency model of the system under investigation, propose the use of optimization algorithms to minimize either the volume of the whole EMI filter, i.e. related to common mode (CM) and differential mode (DM) sections, or the volume of some parts of it. It should be noted that a relevant computational effort is anyhow needed [87]. The use of heuristic procedures, mostly genetic algorithms (GA), to perform an EMI filter design oriented to power density maximization, is proposed in [88]. In those cases the high number of iterations, usually needed to obtain optimal or sub-optimal solutions, results in a time consuming procedure. A PC-based automatic EMI filter design method without any volume minimization implications is presented in [89]. Finally, a minimization of the DM EMI filter volume, utilizing some interpolated volumetric parameters, has been done in [90], where it is demonstrated that the selection of an optimal number of filter stages leads to the minimum occupied volume. However, this approach cannot be applied to minimize CM EMI filter volume.

It is worth noting that, once the filter topology has been chosen and the values of its components (Common Mode/Differential Mode inductors/capacitors) have been defined, there is a huge amount of possibilities for practical configurations. Moreover, the identification of the configuration leading to the best power density in terms of minimum volume/weight is a nontrivial task. According to a trial and error approach, the conventional design of EMI filters requires a significant effort in terms of time spent and it does not guarantee the optimal choice of filter components in order to obtain the maximum power density.

For this reason, an optimized design procedure of discrete EMI filters oriented to obtain high performing filters and high power density is presented in this chapter. This is ultimately the main focus of this PhD thesis.

The optimized design of EMI filters is based on an automatic rule-based computer aided procedure and presents easy implementation features and low computational demand. Both CM and DM sections of the EMI filter are considered within the procedure.

Moreover, to make the new design procedure more accessible to EMI engineers or scientists involved in investigation of filter performance/configurations/power density, a software tool based on the optimized design procedure has been developed, namely ODEF (*Optimized Design of EMI Filters*).

The optimized design procedure and the developed tool are described in the following sections.

4.2 Optimized Design Procedure

The optimized design procedure starts from the basic principle of the conventional EMI filter design illustrated in Section 3.4, introducing the additional objective of pursuing the best power density for the EMI filter. It is a rule-based algorithm that takes into account the main characteristics of the filter application: the power electronic circuits under study, the filter design constraints and databases with parameters extracted by datasheets of commercial components for the realization of EMI filters.

The overall concept of the optimized technique is summarized in Figure IV.1.

The following Input Data are needed to run the rule-based algorithm:

- *EMI filter topology*;
- n_{phase} : number of AC phases/DC lines of the power electronic system;
- U_N : nominal voltage of the power converter;
- I_{max_phase} : maximum operating current;
- I_{CM_max} , I_{DM_max} : maximum CM and DM currents;
- the filter design can be performed either on the basis of the measured CM/DM spectra (EMI_{CM} , EMI_{DM}), given as input and compared with the limits of a chosen standard, or explicitly giving

the required CM/DM attenuations (Att_{req_CM} , Att_{req_DM}) and the CM/DM harmonic frequencies to be attenuated ($f_{CM_att_h}$, $f_{DM_att_h}$);

- *Standard for C_y value selection*: the CM capacitance can be chosen either on the basis of SAE AES 1831 standard requirements or by explicitly setting the maximum ground leakage current;
- k_{vol} , k_{weight} : two coefficients provided by the designer allow to optimize the design assuming any linear combination of volume and weight as the objective function.

In order to properly select the most suitable components for the EMI filter, two databases of commercially available devices have been set up.

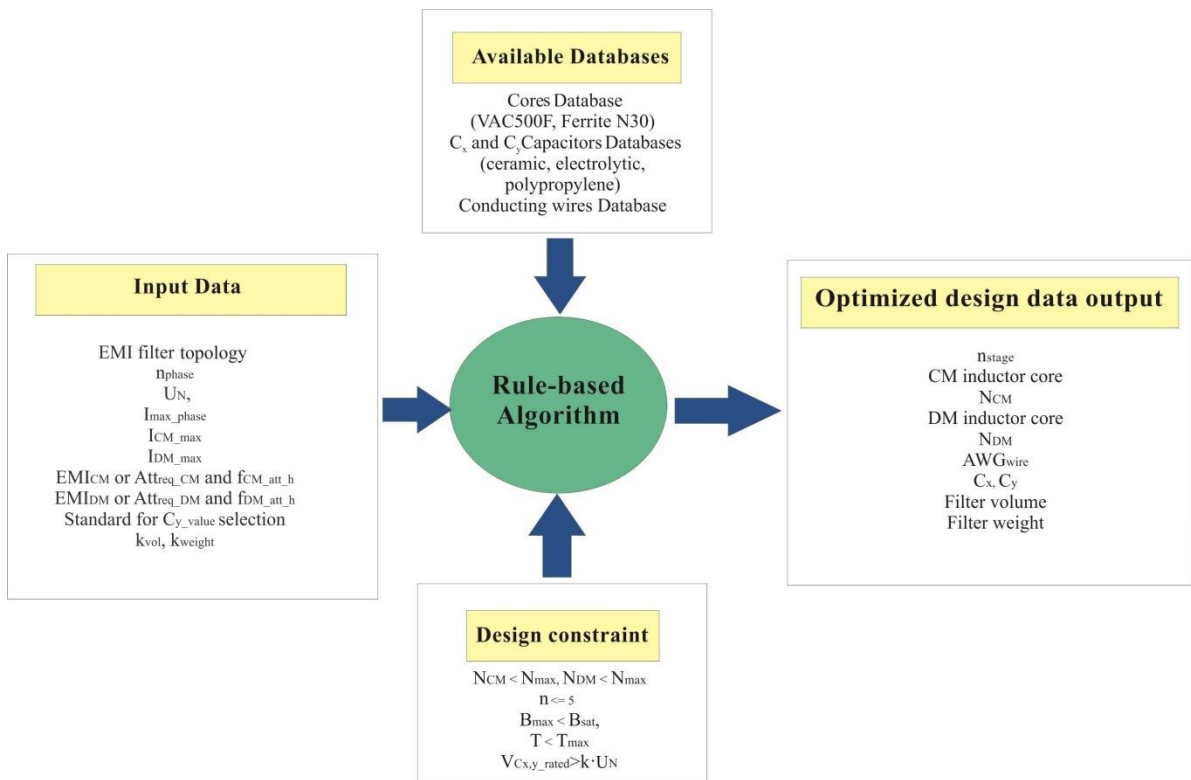


Figure IV.1 – Concept of the optimized EMI filter design procedure.

The first one is a database of magnetic cores, including 110 toroidal cores, with both nanocrystalline (Vitroperm 500F) and ferrite (N30) materials.

The database of commercial cores contains the following information:

- core material and model;
- geometric dimensions and weight;
- inductance factor A_L ($\mu\text{H}/1$ turn) at 10 kHz and saturation flux density value.

The cores' dimensions have been chosen so as to design EMI filters for applications able to manage both low powers and powers up to some kW.

In addition, a suitable database of capacitors, including Y-type (for the CM noise mitigation) and X-type (for the DM noise mitigation), has been built as well. As for Y-type capacitors, ceramic devices with different rated voltage levels have been included in the database. As far as the X-type capacitors are concerned, 160V, 250V and 400V aluminum electrolytic capacitors for applications with high ripple currents at high frequencies and polypropylene capacitors for EMI suppression, have been included.

The database of commercial capacitors contains the following information:

- brand, material, series, model and package;
- rated capacitance and voltage;
- geometric dimensions and weight.

In addition, a third database, including conducting wires, is provided. So, the volume/weight contribution given by the inductor wires (non-negligible when dealing with rated power of hundreds of watt and beyond) is included in the EMI filter calculations.

Once all the input data have been entered, the rule-based algorithm repeats the steps of the conventional design procedure for different configurations (e.g., varying core material and model, number of stages, etc.) and chooses the configuration exhibiting the best power density. Since multi-stage filter can occupy a smaller volume than single stage one, depending on the used components, the optimized design procedure considers the possibility to span a number of filter stages (n) ranging from 1 to 5. The evaluation of a maximum number of five stages is a reasonable choice, since it is very unlikely that a greater number of filter stages can allow to obtain a more compact filter than a single stage one.

In particular, the algorithm performs the filter design according firstly to CM requirements; then, DM requirements are fulfilled according to the steps described hereinafter. The different steps of the optimized procedure are summarized in Figure IV.2, whose symbols are defined as follows. AWG : conductor diameter expressed in American Wire Gauge unit; n : number of filter stages in range 1÷5; N_{max} : maximum number of turns for each core; C_y, C_x : capacitance of phase-to-ground/phase-to-phase capacitors; V_{rated}, C_{rated} : capacitors' rated voltage/capacitance; U_N : nominal voltage of the power converter; B_{max}, B_{sat} : maximum/saturation magnetic induction.

The first step is the selection of wire AWG on the basis of the maximum operating current value given by the designer as input data. Follows a computation of the maximum number of turns (N_{max}) for each core of the database.

A. CM section design

As for the CM section design, the procedure computes, for $n=1, \dots, 5$, the following quantities: the CM capacitance (C_y), the cutoff frequency, the CM inductance and the number of turns (N_{CM}) needed to set up the required inductance. Then, the C_y capacitor with the minimum volume is selected from the database according to the design constraint $V_{C_y} = k \cdot U_N$ where k is a multiplier factor (equal to 2.5 for DC systems and 4.2 for AC systems). Also the cores allowing the practical realization of the CM choke according to the required value of CM inductance (i.e., $N_{CM} < N_{max}$) are selected from the database, taking into account the further constraint related to the absence of saturation.

B. DM section design

Two different procedures allow the designer to compare the results obtained considering either the leakage inductance of the CM choke (No extra L_{DM}) or the use of separate DM inductors (Extra L_{DM}).

The first step, i.e., the evaluation of the cutoff frequency versus the number of stages, is common to both procedures. Then:

- The “No extra L_{DM} ” procedure computes, for $n=1, \dots, 5$, the leakage inductance of the feasible CM chokes and the corresponding required value of DM capacitance. After the computation of the C_{DM} capacitance, the corresponding capacitor with the minimum volume is selected from the database according to the design constraint $V_{C_x} = k \cdot U_N$.
- With the “Extra L_{DM} ” procedure, for $n=1, \dots, 5$, the DM inductance candidate values are obtained on the basis of the X-capacitors values in the database (ranging between 10nF and 330 μ F). Then, the number of turns for each DM core is calculated and the cores allowing a practical realization are selected from the database, according to the condition $N_{DM} < N_{max}$ and to the absence of saturation. Finally, the best pairs L_{DM} - C_x that allow to set up the DM section according to the design constraints $V_{C_x} = k \cdot U_N$, are selected.

As already underlined, the constraint on the absence of saturation of the magnetic core has been imposed in both the CM and DM section design procedures. In particular, the fulfillment of the condition $B_{max} < B_{sat}$ has been verified for the magnetic materials (nano-crystalline or ferrite) taken into account in the procedure. Thus the designed EMI filters are free from saturation issues with no degradation of the desired performance. Finally, the algorithm calculates the EMI filter volume and weight of all possible configurations and select the one with the best power density.

The algorithm allows a more extensive evaluation of EMI filter components and configuration impact on power density in terms of both volume and weight and, therefore, more effective results. Furthermore, it does not discard suboptimal designs, allowing to compare them with the best solution.

The automatic rule-based procedure can be easily implemented by using a common programming language, within either an open source or a commercial environment, and it does not require a long lasting execution time but it provides the real-time output data. Therefore, it can be advantageously

used both by EMI engineers for obtaining an optimized filter design and by scientists/experts for the evaluation of filter performance versus configuration and power density features. Moreover, to make the new design procedure more accessible to EMI designer, a software tool based on the optimized design procedure has been developed, namely ODEF (*Optimized Design of EMI Filters*) and described in the next section. All the design options, steps, outputs and design-related supplementary analyses are managed by ODEF tool in a user-friendly mode.

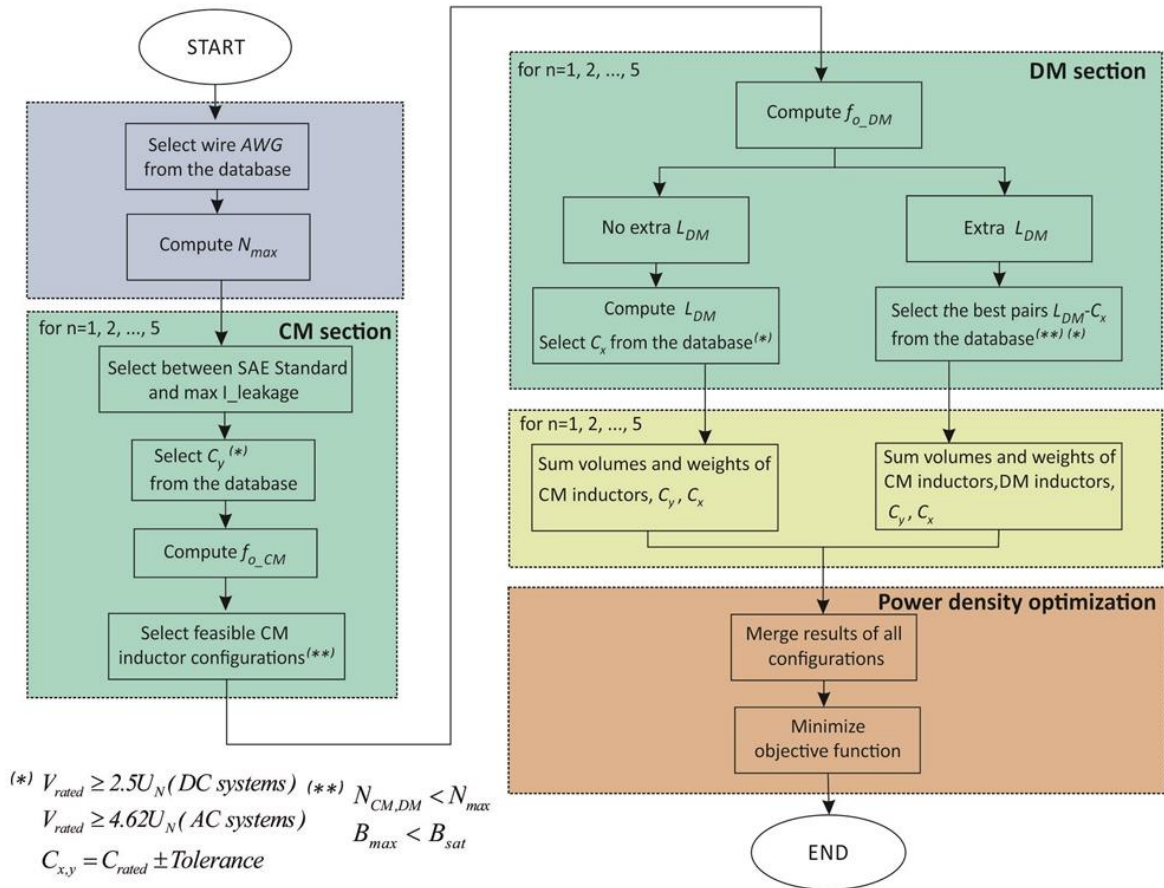


Figure IV.2 - Flowchart of the optimized EMI filter design procedure.

4.3 ODEF Application

ODEF is an interactive application running in Matlab® environment that enables a simple and fast selection of EMI filter components, circuit configuration and number of stages for achieving optimal power density. Furthermore, ODEF allows to compare the optimal EMI filter design to the suboptimal results, so as to leave the final choice to the designer.

ODEF application is distributed as freeware for noncommercial use. A first version of ODEF can be downloaded from www.issia.cnr.it/wp/?page_id=8070 (Figure IV.3) and an updated version v.2.0.

will be provided. The application has been designed using Matlab GUIDE to layout the user interface and by manually writing the code for the callback functions associated with each graphical object. It has a simple and intuitive user interface, which is organized in three tabs for increased usability, namely Noise Profile, Computation, Extra (Figure IV.4 - Figure IV.6). In particular, the main algorithm is executed interacting with the graphical objects of Computation tab, whereas the other tabs present additional features that complement the main algorithm.

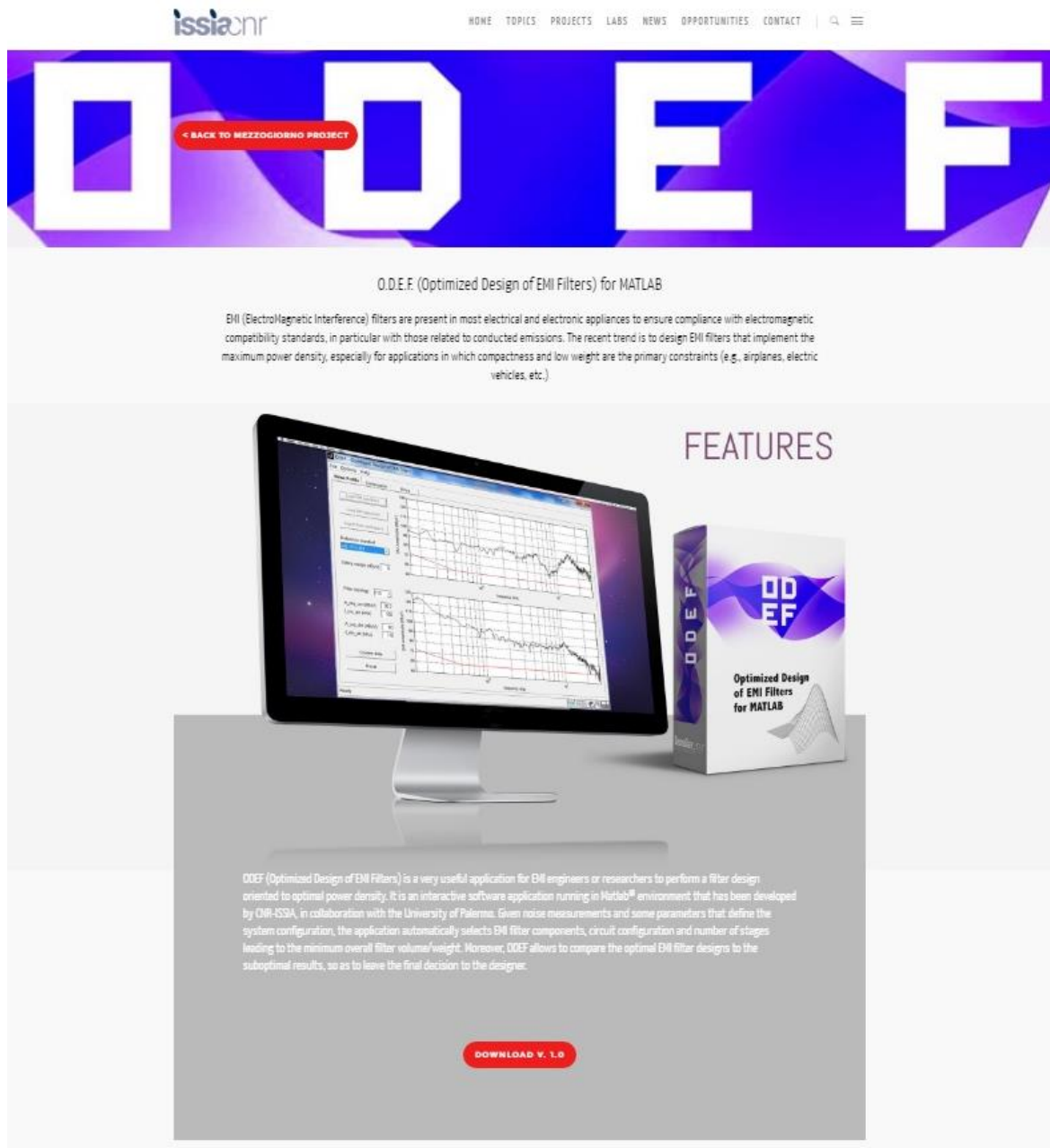


Figure IV.3 – Screenshot of the web page for ODEF application download.

A general description of the implementation of ODEF and the main functionality of the application will be given hereinafter.

A. Starting the application and defining inputs

After installation, the application is simply started typing ODEF at Matlab® prompt. A window will open, as shown in Figure IV.4. If the user already knows the required CM/DM attenuations and cutoff frequencies, he can directly switch to *Computation* tab and enter these values in the related fields of the third panel, together with filter topology (e.g., Γ , Π , T). The circuit schematic of the chosen filter topology will be shown in the upper right figure of the tab.

Then, the user can provide the other input quantities, filling the fields of the other panels. In particular, the system parameters to be entered in the first panel are the following: system type (frequency and number of phases), nominal voltage, the maximum load current and maximum values of the CM/DM noise currents. In the second panel, the user can choose how to determine the value of the CM capacitors: either according to SAE AS 1831 standard (20 nF for 400 Hz systems; 100 nF in the other cases) or imposing a maximum leakage current. Furthermore, in the *Extra_Ldm* panel the user can express his preference about the realization of the DM filter. Choosing *Always* or *Never* the algorithm will include in the search space only the DM filters realized using an extra DM inductor or exploiting the leakage inductance of the CM choke, respectively. For example, aiming to achieve an increased reliability, the user might want to force the use of extra DM inductors to be sure that electrolytic capacitors are not used for the realization of the DM filter. On the other hand, if *Auto* is selected, the search space will include DM filters realized according to both techniques. Finally, the volume and weight coefficients of the objective function, expressed in percentage, can be entered in the last panel. If the user does not know the required CM/DM attenuations and frequencies, he can open *Noise Profile* tab and load previously acquired CM/DM noise spectra in Excel® file format or import them from Matlab® workspace. The data will be plotted in the two graphs of the tab. Then, selecting an item from the related drop-down menu, the user can choose a reference standard, whose limit curve will be superimposed on the data as a red line. The following reference standards are available: MIL-STD-461F, EN55011 class A, EN55011 class B, DO160F cat. B, DO160F cat. L.

Finally, as soon as the user selects filter topology and safety margin, the application automatically computes the CM/DM harmonic frequencies to be attenuated and the corresponding required attenuations, fills the related text boxes and highlights the related points on the graphs with red circles. At this point, the user can confirm the data and switch to the *Computation* tab to provide the other input data, as previously described.

B. Executing the algorithm

When the user clicks on the *Compute* button of the *Computation* tab the algorithm described in Section 4.2 is executed, processing the input values and the database content. Then, the results are

shown in the *Results* panel of the same tab. In particular, the feasible filter configurations are arranged according to increasing values of the objective function and the *Configuration* drop-down menu is populated. When the user selects an item from this menu, the details about the chosen configuration, including the objective function's value, are shown in the *Results* panel. Besides the numerical values of the physical quantities (e.g., L_{CM} , C_x , C_y , etc.), other data are extracted from the databases, e.g., wire type and code, core material and type, capacitor brand and model, etc. The obtained filter configurations depend on the specific components of the chosen database, which can easily be modified or expanded. In the latter case the execution time of the algorithm will increase, as expected. Finally, a series of buttons allow to load/save either the complete input dataset, including the CM/DM spectra, or the sorted set of feasible configurations. In this way, saved information can be recalled at later time.

C. Plotting data

Sometimes, it is useful to compare suboptimal designs to the best solution returned by the algorithm. For example, it could happen that the best design is a two-stage filter, but the second best design is a one-stage filter, whose objective function's value is slightly higher than the global minimum. In such cases, the designer could choose the second best design. For this purpose, besides exploring the *Results* panel of the *Computation* tab, it is possible to exploit the features of the *Extra* tab. In particular, after selecting the number of configurations to consider among the entire feasible set, it is possible to generate a series of comparative plots, as those shown in Chapter V for the chosen case study.

Furthermore, it could be interesting to check whether the best design varies or not when the CM attenuation, imposed by the user, is higher than the minimum required value. Sometimes the best design remains the same, due to the discrete nature of the problem (discrete set of values for L and C, integer number of turns for the inductor windings, etc.). To this aim, a series of buttons of the *Extra* tab allow to load feasible configuration sets, previously saved after different runs of the algorithm, and to generate some plots that compare the best designs, as those shown in Chapter V to discuss the results for the chosen case study.

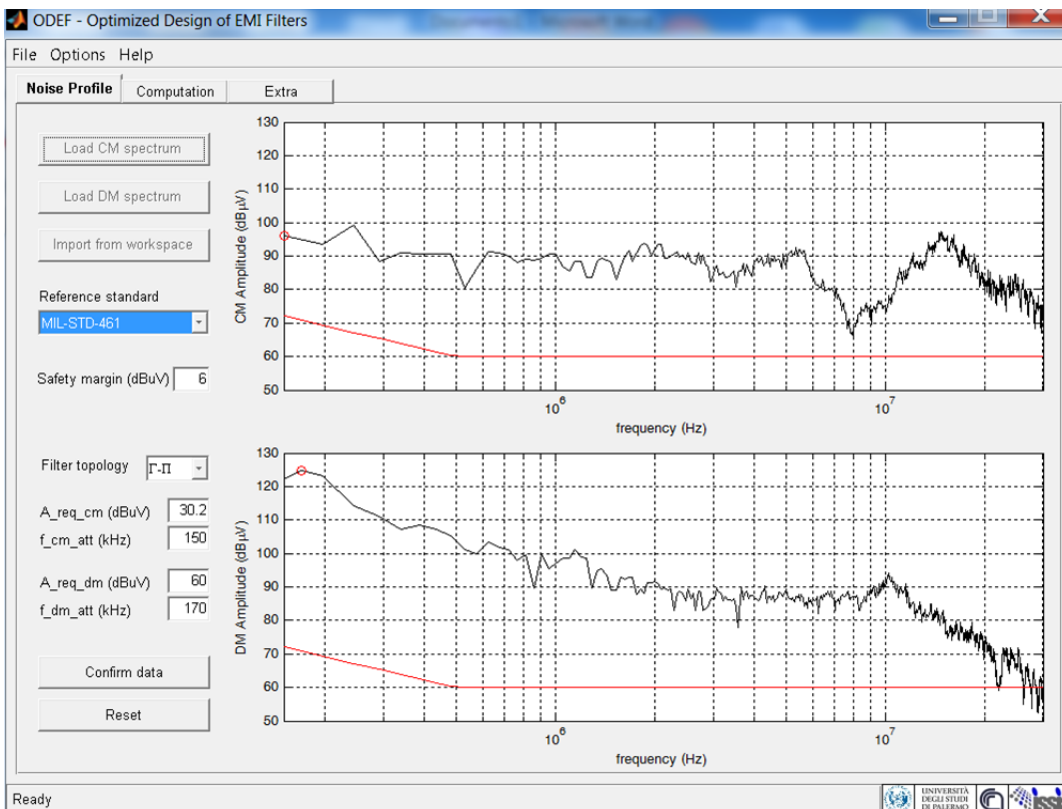


Figure IV.4 - Screenshot of ODEF application: *Noise Profile* tab.

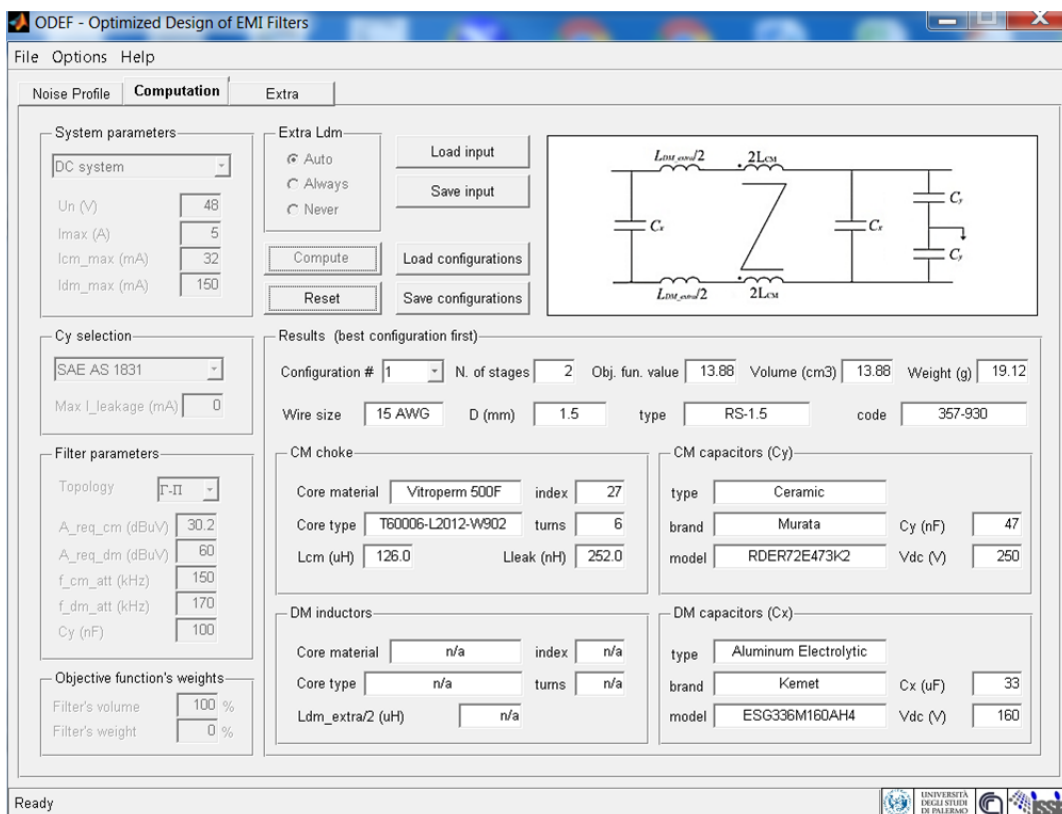


Figure IV.5 - Screenshot of ODEF application: *Computation* tab.

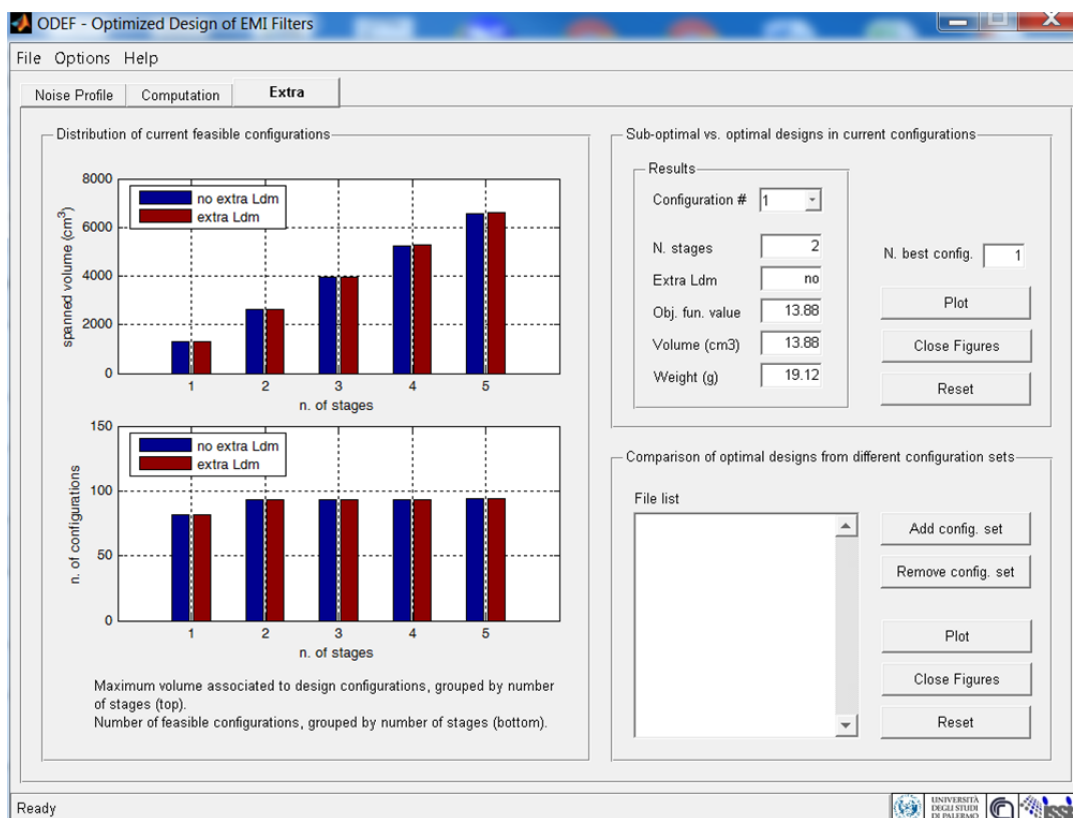


Figure IV.6 - Screenshot of ODEF application: *Extra* tab.

4.4 Summary

In this chapter a new optimized EMI filter design technique for the optimal and fast selection of discrete EMI filter components and configuration, aimed at obtaining the minimum volume/weight, has been presented. This technique has been implemented as a feedback to the demand of a wide range of applications in which the power density of power converter systems is a stringent design constraint. Therefore a filter design that implements the maximum power density is strongly desired.

The optimized procedure relies on a suitably devised rule-based algorithm and on databases of commercially available magnetic cores, capacitors and conducting wires. It takes as inputs some parameters that are computed from noise measurements and others that define the power electronic circuits under study system. Once all the input data have been entered, the rule-based algorithm repeats the steps of the conventional design procedure for different configurations (e.g., varying core material and model, number of stages, etc.) and chooses the configuration exhibiting the best power density. Easy implementation features and low computational demand characterize the rule-based algorithm.

On the basis of this procedure, an interactive software tool for the optimized design of discrete EMI filters in terms of power density, namely ODEF (*Optimized Design of EMI Filters*), has been developed . ODEF is an application running in Matlab® that also allows to compare the optimal EMI filter design to the suboptimal results, so as to leave the final choice to the designer.

CHAPTER V – Experimental Validation of the Optimized EMI filter Design Procedure

5.1 Introduction

In chapter 3, the basic steps of the general EMI filter design procedure and some considerations on the EMI filter performance and size due to the topology and to the components type have been presented. In the chapter 4 an optimized EMI filter design procedure which allows an optimal and fast selection of discrete EMI filter components and configuration, aiming to obtain the minimum volume or weight and high performance, has been presented.

In this chapter, an experimental assessment of the optimized technique is performed by using different suitably devised experimental setups. A comparison of the optimized filter obtained with the conventionally designed one, is carried out in terms of volume, weight and performance: the optimized design procedure allows to obtain the compliance of the power electronic system under study with the standard, using EMI filters with higher compactness and power density, with a low computational effort.

Furthermore, an analysis of the feasible configurations returned by the algorithm is performed, for some of the case studies, by a series of comparative plots generated by ODEF application; interesting results and a very considerable number of configurations are evaluated. This evaluation is practically cumbersome without the developed software tool.

5.2 Experimental setups

In order to validate the optimized EMI filter design procedure, an experimental investigation has been carried out on four suitable experimental setups:

- case study #1: inverter-fed induction motor drive (240W);
- case study #2: inverter-fed symmetric low power (7.2W) resistive load;
- case study #3: DC motor drive (30W) supplied by a DC/DC boost converter;
- case study #4: DC motor drive (190W) supplied by a DC/DC buck converter.

Figure V.1 shows a scheme of the experimental arrangement for the case studies.

It should be observed that PWM inverter-fed loads/induction motor drives supplied by a DC power grid, such as those considered in the first and second case study, are very common, for example either in vehicle applications (road vehicles, marine vehicles, aircrafts) either in DC distribution systems, such as those used in some residential/commercial smart buildings for energy saving [91], [92].

The third and fourth case study are typical applications for automotive environment in which the presence of low-power loads supplied with different voltage levels requires the use of DC/DC converters [93].

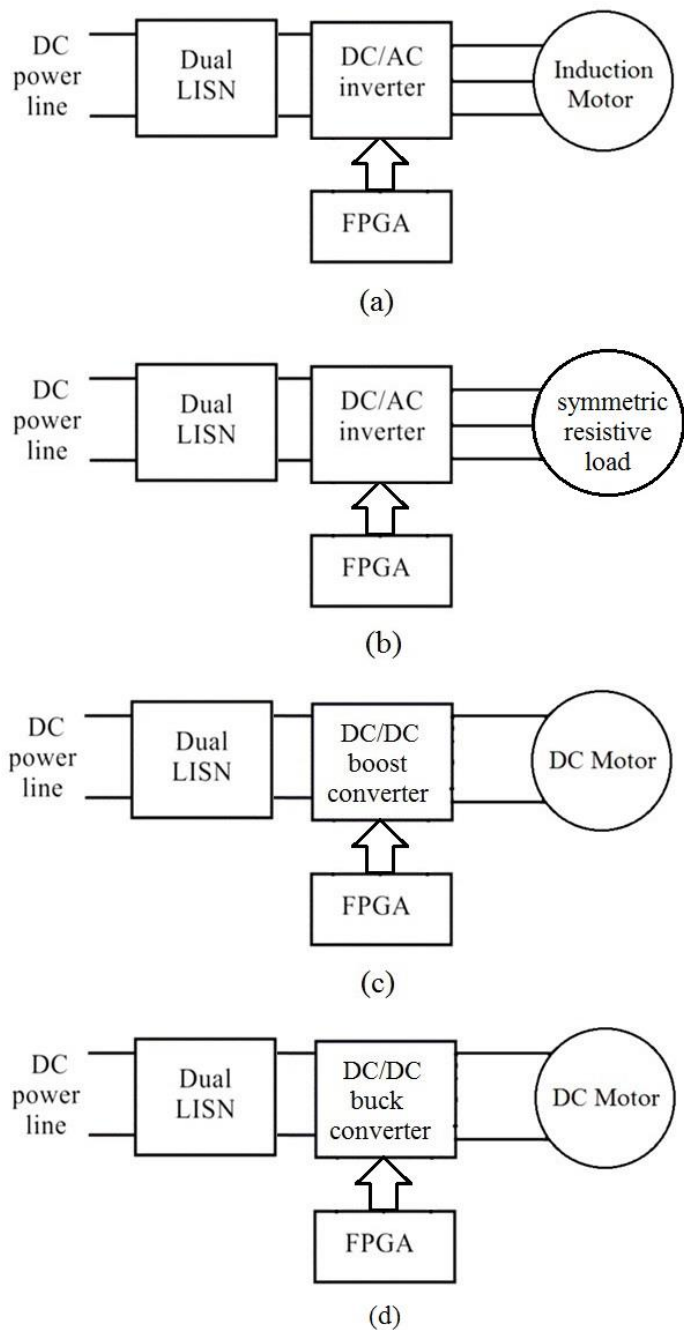


Figure V.1- Scheme of the experimental rigs: (a) case study #1; (b) case study #2; (c) case study #3; (c) case study #4.

In all case studies, the PWM modulation has been implemented on an Altera Cyclone III FPGA board [94], shown in Figure V.2 on the left. It includes an Altera FPGA EP3C25F324 controlled by a 50 MHz oscillator and it presents the following main features:

- 25K logic elements;
- 66 M9K memory blocks (0.6 Mbits);
- four PLLs (Phase-Locked Loop);
- 214 I/Os.

The board can be easily programmed in VHDL language and it represents a low-cost and high-performance platform that allows to implement a broad range of designs of different complexity.

The main features of the Cyclone III starter board are the low-power consumption, the availability of SSRAM and EEPROM memories and the expandability via the HSMC connector (High Speed Mezzanine Card), which allows the connection of expansion boards with different capabilities.

In the concerned cases, it was necessary to connect the Nial Stewart GPIB expansion board [95], equipped with different I/O connectors with its level-shifter to interconnect the 2.5V CMOS logic to 3.3V CMOS logic and TTL logic, and with 10-bit A/D and D/A converters with 8 channels each. This expansion board is shown on the right of the Figure V.2.

A further advantage of the Altera board consists of the the Cyclone III device can be configured via the on-board USB-Blaster™ or through the JTAG interface using an external programming cable (sold separately).

For the writing and the compiling code, the simulation, the debugging and the programming phases of the device, the Quartus II Web Edition software, which is a free valuable graphical development environment provided by Altera [96], has been used.

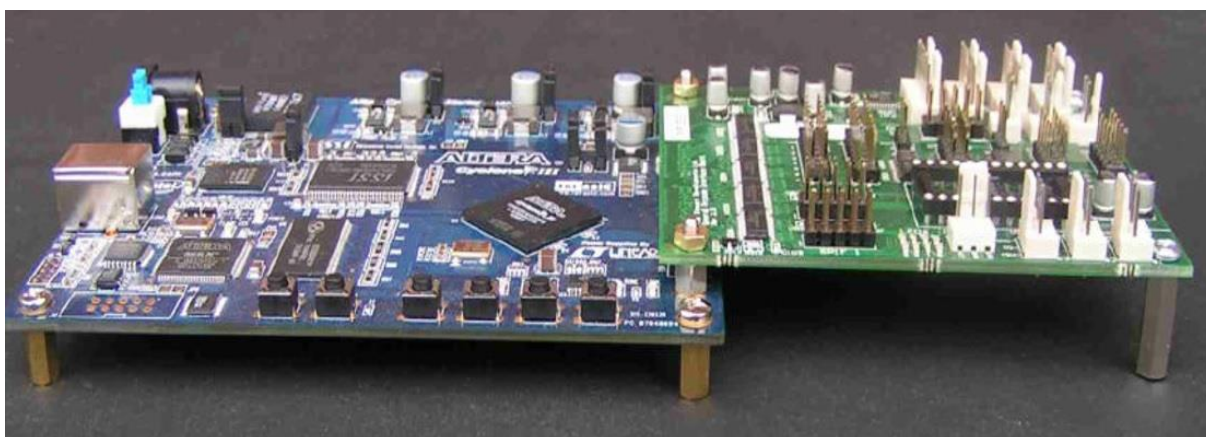


Figure V.2 - Cyclone III FPGA Starter Board equipped of the Nial Stewart GPIB expansion board used in the experimental setups.

The programming of the Altera Cyclone III FPGA board has allowed to obtain a system with the following characteristics:

- the PWM carrier frequency can be modified according to the output frequency (synchronous or asynchronous modulation);
- the startup and shutdown of the system is settled by means of acceleration and deceleration ramps with configurable time, allowing to gradually change the frequency even after unexpected changes of reference;
- the presence of START and STOP buttons with LED display;
- the possibility to use the RESET button to quickly disconnect the connected motor;
- the possibility to view on a 7-segment display (SSD) the following information: the frequency, the actual output frequency set point, the output voltage, the modulation index, the carrier frequency, the indication of a block due to the overmodulation, the overflow indication.

In the SSD board there are a rotary switch with four possible positions, a 7-segment display with four digits (SSD display) and all the circuitry necessary for the multiplexed driving, as shown in Figure V.3. The SSD board allows to display information given by the Altera board, selecting them by the rotary switch, and it connects to the DIP24 socket of the Nial Stewart board using a specific 26-pin flat cable. When an overflow condition occurs, the display shows "0.0.0.0.". The LED is used as the overmodulation block indicator. On overflow, the display shows "0.0.0.0.". The sign LED is used as the indicator of block condition due to overmodulation.

The system also includes the following components:

- a DB15-RCA cable to connect the Nial Stewart board to the driving inputs of the switching devices;
- a 1 k Ω linear multi-turn potentiometer to set the frequency reference; it needs to be connected to ADC0 input of the A/D converter in the Nial Stewart board.



Figure V.3 - Board with the display SSD used in the experimental setups.

A dual LISN with a voltage capability up to 600V, a RF current probe R&S EZ-17 that allows measurements in the frequency range 20 Hz – 100 MHz with a maximum DC current of 300 A, and an Agilent E4402 (9 kHz – 3 GHz) spectrum analyzer have been employed to measure the conducted

EMI. A Tektronix TDS7254B 2.5GHz - 20GS/s - 4 channels has been used for the time domain measurements.

In all case studies has been verified that the systems are characterized by high CM noise source impedance and low CM noise receiver impedance. Then according to the criterion of maximum impedance mismatching between the source and the receiver, a Γ network topology has been chosen for the CM filter. The noise source characterization for DM noise is more complex to define due to the DM input impedance of the motor drive. For this reason, a Π network topology has been chosen for the DM filter: if the real DM noise source impedance is high, a theoretical attenuation of 60 dB/dec is expected. Otherwise the theoretical attenuation from one of the capacitors C_x is insignificant and a lower attenuation could be expected (40 dB/dec) and consequently the value of the DM capacitors will be adjusted.

Moreover, the EMI filters performance has been verified against both military and civilian technical standards. Many standards exist to accommodate the wide variety of applications where EMI is an issue. Most of the standards differ either by their frequency range of application or the amplitude of the noise limits and whether the type of measured noise is voltage or current. They also have their own experimental and noise measurement setup as well as their own LISN circuit. However this Ph.D. thesis is based on the military standard 461F described in [75] and on the civilian standard CISPR 25 described in [97].

The MIL-STD-461F, entitled “Requirements for the control of electromagnetic interference characteristics of subsystems and equipment”, establishes interface and associated verification requirements for the control of the electromagnetic interference emission and susceptibility characteristics of electronic, electrical, and electromechanical equipment and subsystems designed or procured for use by activities and agencies of the Department of Defense (DoD) USA. Such equipment and subsystems may be used independently or as an integral part of other subsystems or systems. In particular the CE102 applicability of this standard has been taken into account; this requirement is applicable from 10 kHz to 10 MHz for all power leads, including returns, which obtain power from other sources not part of the EUT. Figure V.4 defines the maximum noise limit for the conducted EMI noise. It is important to mention that the basic curve is given for a voltage of 28 V, and as the voltage increases some relaxation of this limit is permitted. For this Ph.D. thesis, the basic curve is anyway considered in the comparison with the measured EMI in order to consider the most restrictive limits.

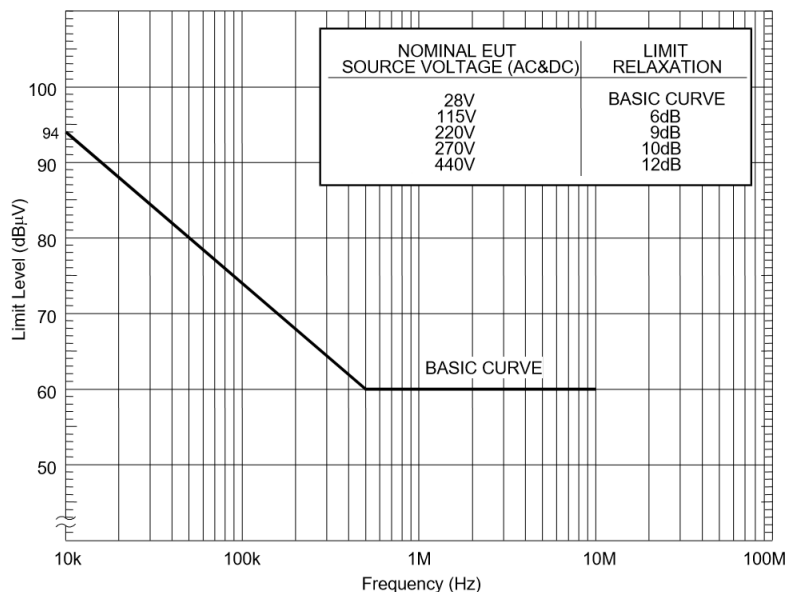


Figure V.4 - MIL-STD-461F: CE102 limit (EUT power leads, AC and DC) for all applications.

The CISPR 25 [97], entitled “Radio disturbance characteristics for the protection of receivers used on board vehicles, boats, and on devices – Limits and methods of measurement”, describes the limits and the procedures for the measurement of radio disturbances in the frequency range of 150 kHz to 1000 MHz. The standard applies to any electronic/electrical component intended for use in vehicles and devices. The limits are intended to provide protection for receivers installed in a vehicle from disturbances produced by components/modules in the same vehicle. The limits in this standard are recommended and subject to modification as agreed between the vehicle manufacturer and the component supplier. This standard is also intended to be applied by manufacturers and suppliers of components and equipment, to devices under test, which are to be added and connected to the vehicle harness or to an on-board power connector after delivery of the vehicle. Moreover the electromagnetic disturbance sources are divided into two main types:

- narrowband source whose emission has a bandwidth less than that of a particular measuring apparatus or receiver (e.g. vehicle electronic components which include clocks, oscillators, digital logic from microprocessors and displays);
- broadband source whose emission has a bandwidth greater than that of a particular measuring apparatus or receiver (e.g. electrical motors and ignition system).

The noise emission limits are referred to five different classes, in rising order of required reduction of the maximum electromagnetic disturbance level that the devices can produce on board. The class refers to a performance level agreed upon by the purchaser and the supplier and documented in the test plan. In the case studies the EMI source is a broadband source, therefore the noise limits (peak detector) for broadband conducted disturbances, shown in Figure V.5, have been considered.

The possible variation of the emission limits established by the standard, in later editions, does not affect in any case the optimized design procedure itself.

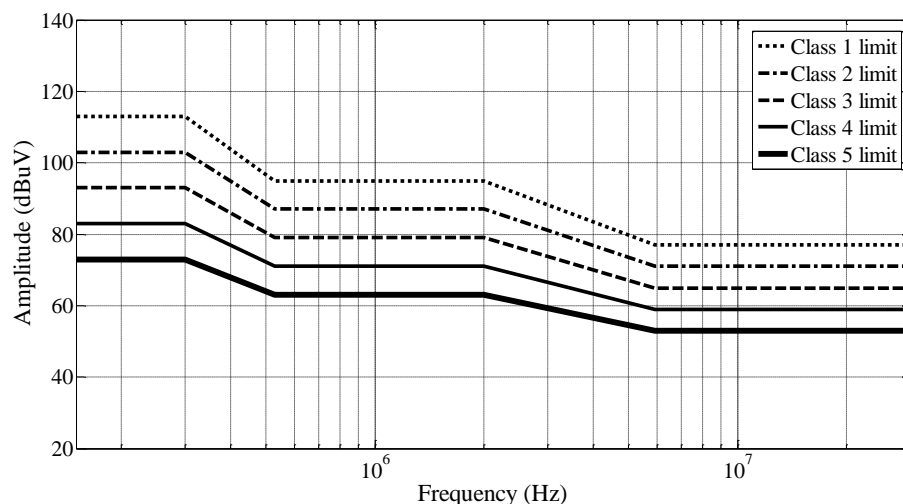


Figure V.5 - CISPR 25 [97]: Limits for broadband conducted disturbances (peak detector).

5.3 Case Study #1: inverter-fed induction motor drive

In the first case study, the conventional and optimized design of an EMI filter for a low voltage high current induction motor drives supplied by DC power grids are presented. A comparison of the optimized filter with the conventionally designed one has been carried out in terms of EMI filter configuration characteristics, size and performance. Furthermore, useful considerations on filter design result by an analysis of comparative plots of the best solution and suboptimal designs returned by the algorithm.

The test bench is composed of:

- a PWM IGBT voltage source inverter (VSI), realized by an intelligent module STGIPS10K60A;
- an Altera Cyclone III FPGA board equipped with a Nial Stewart GPIB expansion board, implementing the PWM modulator;
- a 48V induction motor with a rated power of 240W.

The switching frequency f_{PWM} is equal to 20 kHz.

The use of an intelligent module for the VSI allows a very compact layout of the power electronic stage. In Figure V.6 a view the experimental arrangement of the drive under study is shown.

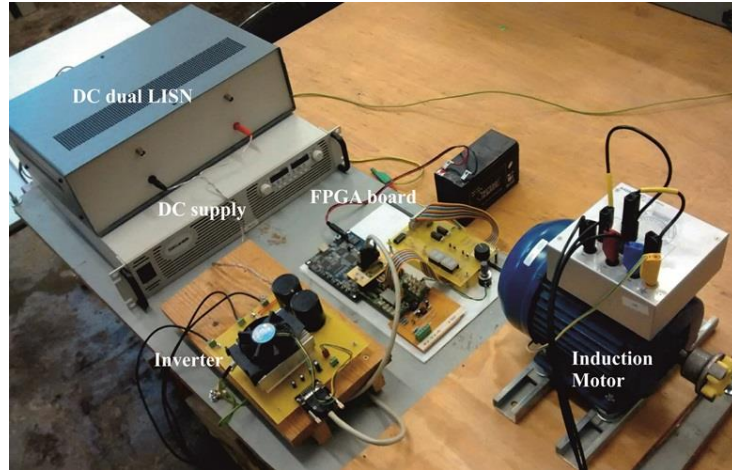


Figure V.6 - View of the PWM induction motor drive experimental setup.

Design, set up and comparison of optimized and conventionally designed EMI filter

Measured conducted disturbances have been compared with the limit reported in the MIL 461 F standard. As shown in Figure V.7, both the CM and DM emission profile exceeds the limit of the chosen reference standard. This calls for a suitable input EMI filtering.

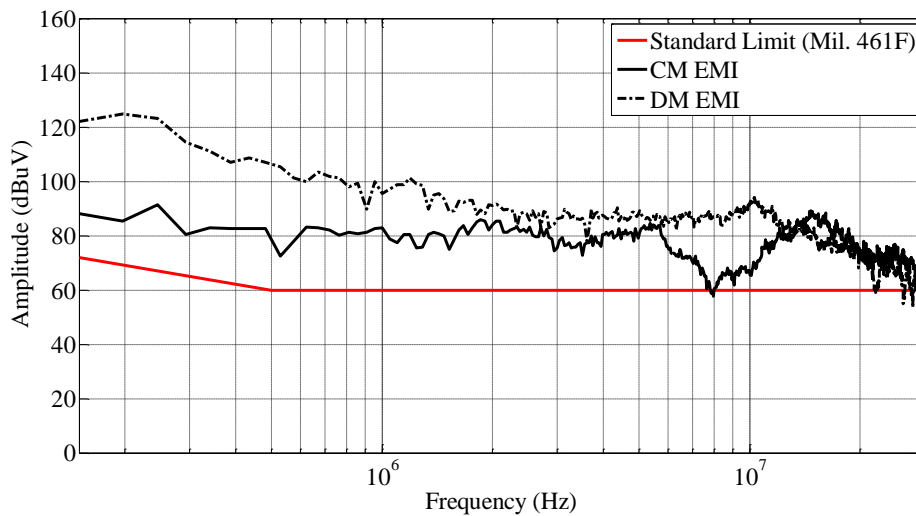


Figure V.7 – CM and DM EMI generated by inverter-fed induction motor drive.

On the basis of the conventional and optimized design procedures described in sections III.4 and IV.2, EMI filters have been set up. In particular, as for the filter realized according to the conventional procedure, the following data have been used:

- CM emission peak at the lowest frequency: 96dB μ V@150kHz;
- DM emission peak at the lowest frequency: 124dB μ V@200kHz;
- cut-off frequencies f_{o_CM} =12.5 kHz and f_{o_DM} = 18 kHz (according to the constraint $f_o < f_{PWM}$);

- $C_{CM}=200$ nF (maximum value allowed according to SAE AS 1831 Standard).

As regards the filter realized according to the optimized procedure, the measured CM/DM spectra, shown in Figure V.7, have been loaded into ODEF application and the automatic processing returned the following filter parameters:

- $Att_{req_CM} = 30$ dB μ V @ 150 kHz;
- $Att_{req_DM} = 60$ dB μ V @ 170 kHz.

Then, the input data shown in Table V.1 have been entered using the Computation tab of Figure IV.5 and the computation has been started. It is worth noting that the limit curve of the Military Standard 461F has been used as EMI limit standard and the SAE AS 1831 standard has been used for C_y selection in this case study.

Table V.1 INPUT DATA FOR ODEF APPLICATION – CASE STUDY #1.

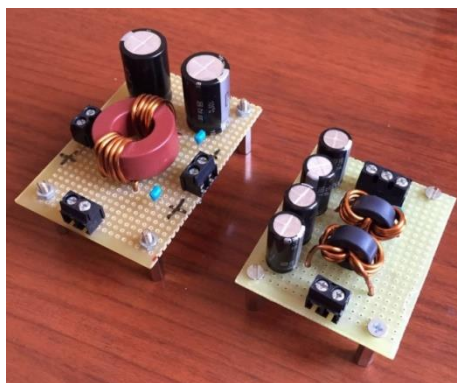
Filter topology	Γ -II
Reference standard	Military Standard 461F
System type	DC system
U_N	48 V
I_{max_phase}	5 A
I_{cm_max}	32 mA
I_{dm_max}	150 mA
C_y standard	SAE AS 1831
Volume coefficient	100%
Weight coefficient	0%
Extra_Ldm_mode	Auto

The conventional design procedure leads to a single stage configuration, whereas the optimized procedure selected a double stage configuration without separate DM inductors. A comparison of the optimized filter with the conventionally designed one has been carried out verifying their size and performance. Table V.2 summarizes the results obtained with the two procedures.

Evaluating the volume and weight of the two filters, it is possible to observe that the optimized design leads to a reduction in volume and weight. In particular, a reduction of 52% in volume and of 56% in weight is obtained. Figure V.8 shows the photo of the optimized EMI filter compared to the conventionally designed one: the higher compactness is evident.

Table V.2 COMPARISON BETWEEN OPTIMIZED AND CONVENTIONALLY-DESIGNED EMI FILTERS (CASE STUDY #1).

	<i>Conventional Design</i>	<i>Optimized Design</i>
Number of stages	1	2
$L_{CM}@10kHz$	0.8 mH	126 μ H (each stage)
CM inductor core dimensions (mm x mm x mm)	27.9x13.6x12.5	12x8.0x4.5 (each stage)
CM core $A_L@10kHz$	65.5 μ H (Vitroperm 500F, model T60006-L2025-W380)	28 μ H (Vitroperm 500F, model T60006-L2012-W902) (each stage)
Number of turns per CM winding	5	3 (each stage)
C_{CM}	200 nF	100 nF (each stage)
C_y	100 nF, ceramic, 250 V, (Murata RDER72E104K2)	47 nF, ceramic, 250 V, (Murata RDER72E473K2) (each stage)
$L_{DM}@10kHz$	1.6 μ H ($L_{leakage}=0.2\% L_{CM}$)	252 nH ($L_{leakage}=0.2\% L_{CM}$) (each stage)
C_{DM}	47 μ F, electrolytic, 400 V, (Panasonic EEUEE2G470)	33 μ F, electrolytic, 160 V, (Kemet ESG336M160AH4) (each stage)
Wire size	15 AWG	15 AWG
Volume	25.87 cm³	13.88 cm³ (all stages)
Weight	44 g	19.12 g (all stages)

**Figure V.8** - Photo of conventionally designed EMI filter (on the left) and optimized EMI filter (on the right), in case study #1.

Comparison of Optimized and Conventionally Designed EMI filter Performance

Finally, in order to evaluate the EMI filters mitigation performance, EMI measurements have been carried out without any filter, with the conventionally designed filter and with the optimized filter (Figure V.9). Limit curve relating to the EMI limit imposed by the Military Standard 461F is shown as well. It is possible to observe in Figure V.9 that both filters show a satisfactory behavior since the EMI filtered meet the limits imposed by the reference standard.

Therefore, despite the higher compactness and power density achieved, the optimized EMI filter still allows to obtain the compliance of the power electronic system under study with the reference standard.

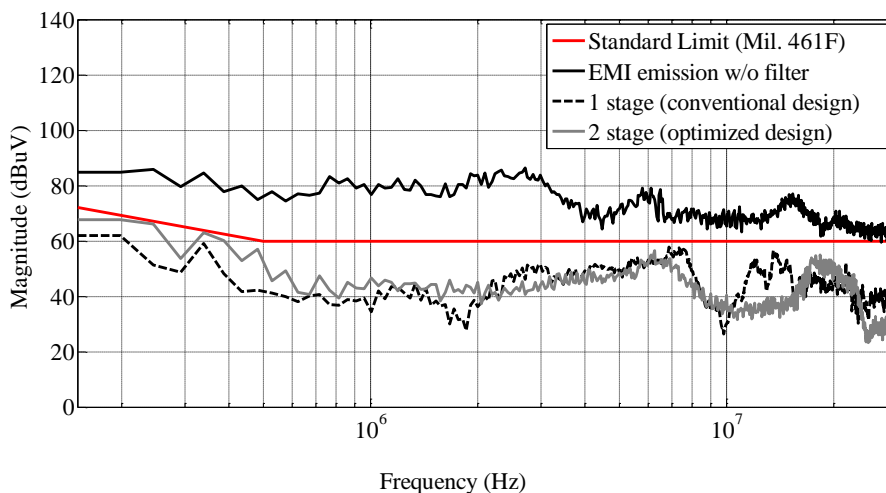


Figure V.9 - Comparison of optimized and conventionally designed EMI filter performance (case study #1).

Considerations on feasible configurations

As described in section 4.3, ODEF allows to compare the optimal EMI filter design to the suboptimal results, so as to leave the final choice to the designer. Moreover, after selecting the number of configurations to be considered among the entire feasible set in the *Extra* tab of ODEF application, it is possible to generate a series of comparative plots for the chosen case study.

In this case study the application selects the best design (2 stages, no extra L_{DM} , CM core index 27, total volume=13.88 cm³) among a total of 910 feasible configurations.

Finally, the features of the *Extra* tab have been used to analyze and compare the feasible configurations, which can be classified as shown in Figure V.10, according to the number of filter stages and to the presence/absence of the extra DM inductor. As shown in the figure, the search space is quite large and the filter volume reaches 6591 cm³ in the worst configuration. The feasible configurations selected by ODEF include both configuration with and without extra DM inductor. In addition it is very important to consider that the number of feasible configurations is related to the number of components in the database; so increasing the number of magnetic cores and capacitors in the database, the number of feasible configurations will increase. The evaluation by the designer of such considerable number of configurations is practically cumbersome without the software tool.

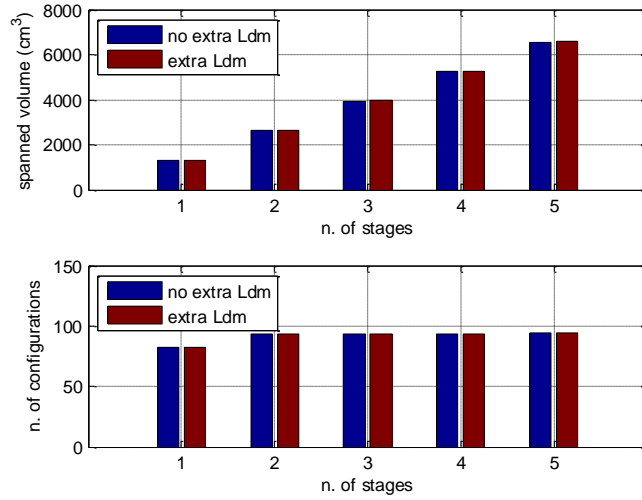


Figure V.10 - Distribution of all feasible configurations (case study #1).

In order to provide an insight into the configurations that belong to a small neighborhood around the optimal solution, the distribution of the 15 best designs is plotted in Figure V.11 and Figure V.12. The 15 best designs include 1-stage, 2-stage and 3-stage filter configurations with a volume range from about 14 cm³ to 21 cm³. In particular the plot shown in Figure V.12 helps the designer to compare the volume of different configurations.

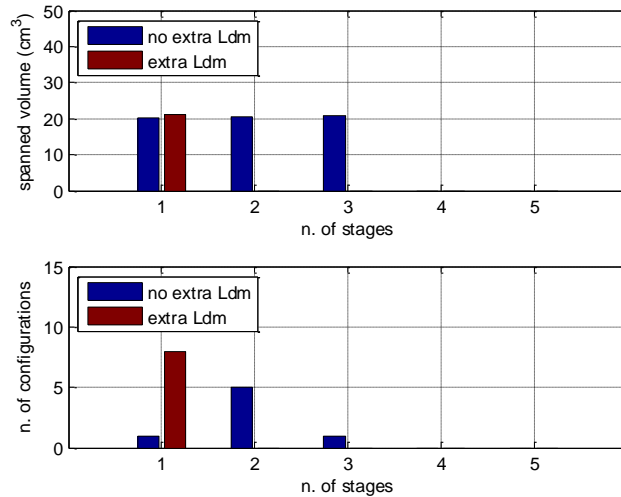


Figure V.11 - Distribution of the best 15 configurations (case study #1).

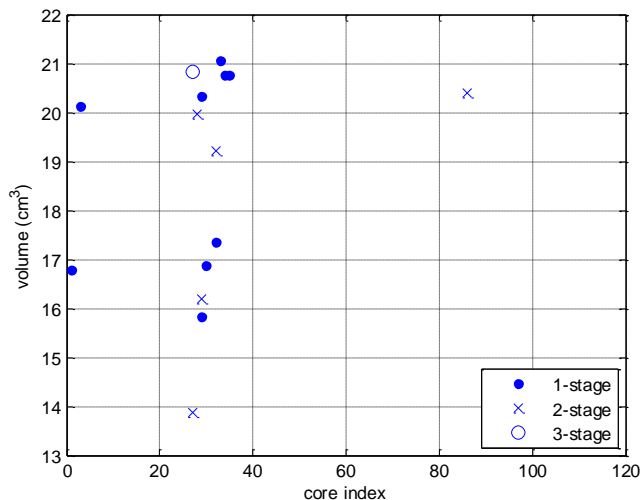


Figure V.12 - Scatter plot of the best 15 configurations (case study #1).

Furthermore, to evaluate the proximity of the returned solution to other configurations, Figure V.13 shows the volume of the best configuration for each number of stages and Figure V.14 presents the distribution of the best 100 configurations grouped for number of stages (50 for n=1, 29 for n=2, 11 for n=3, 8 for n=4, 2 for n=5). With reference to Figure V.14, the intersection of the curves related to 1-stage and 2-stage configurations demonstrates that the optimized design for achieving the best power density is a non-trivial problem. Therefore, it cannot effectively be managed by a trial-and-error approach.

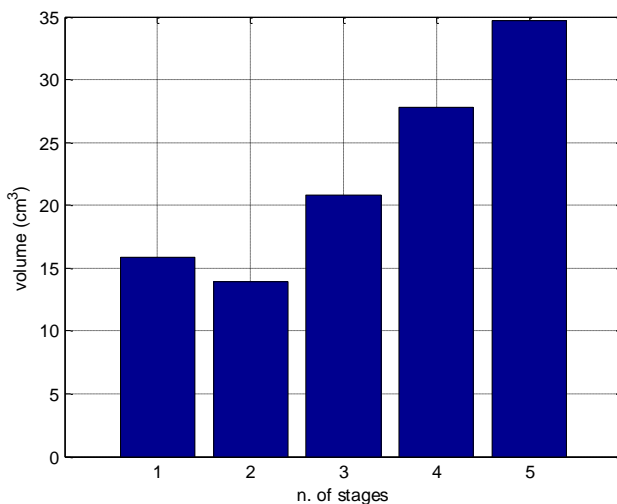


Figure V.13 - Volume of the best configuration for each number of stages (case study #1).

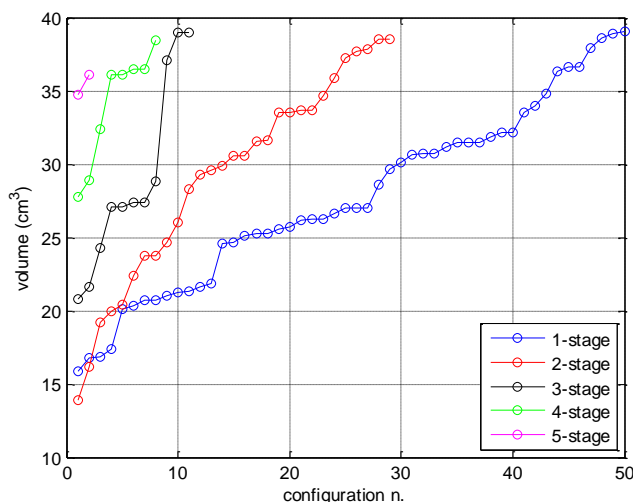


Figure V.14 - Distribution of the best 100 configurations for different n. of stages (case study #1).

As a further analysis, the design procedure has been repeated several times for increasing values of the desired CM attenuation, starting from the minimum required value and keeping the other input parameters constant. The following range has been swept: [30, 32, 34, 36, 38, 40, 42, 44, 46, 48, 50, 52, 54, 56] dB μ V.

Figure V.15 and Figure V.16 show the obtained results in terms of volume, number of stages and CM core index. In the considered case, the best configuration for each value of CM attenuation does not require the use of an extra DM inductor.

It is worth noting that, as Figure V.15 shows, the CM attenuation of the filter can be increased up to 40 dB μ V without increasing the design volume. This corresponds to an extra 10 dB μ V safety margin that allows obtaining a better filter performance, balancing further possible non-idealities in the filter realization.

Instead in Figure V.16, it is possible observe that the double stage configuration is the best configuration design for the evaluated CM attenuation range, except for a narrow range (42÷44 dB μ V) where the single stage configuration prevails.

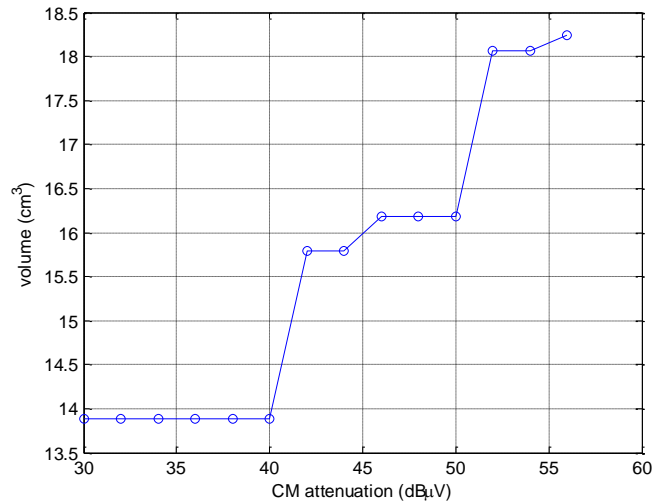


Figure V.15 - Volume variation of the best design for increasing CM attenuation (case study #1).

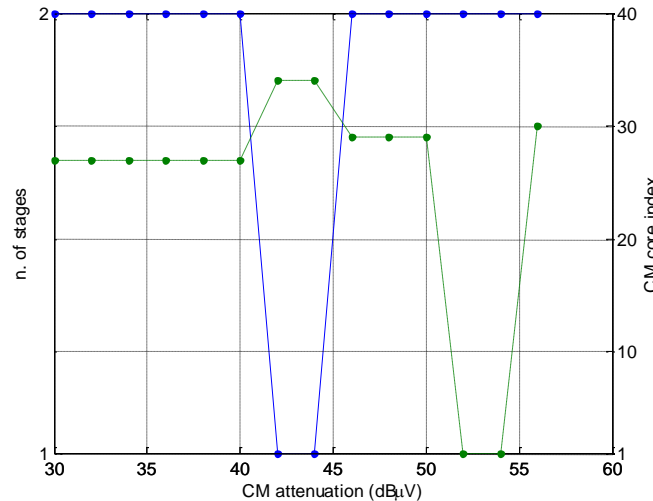


Figure V.16 - Number of stages of the best design for increasing CM attenuation (solid line). CM core index of the best design for increasing CM attenuation (dashed line). - case study #1.

5.4 Case study #2: inverter-fed symmetric low power resistive load

In the second case study, the conventional and optimized designs of an EMI filter for a symmetric low power resistive load supplied by DC power grid are reported. A comparison of the optimized filter with the conventionally designed one has been carried out in terms of EMI filter configuration characteristics, size and performance. In this case, the optimized filter configuration chosen is one of the feasible configurations proposed by ODEF. Even if it does not represent the best configuration which allows to obtain the EMI filter with the minimum volume; a configuration with the extra L_{DM} has been chosen to validate the design procedure with extra L_{DM} .

The test bench consists of a PWM IGBT Voltage Source Inverter that supplies a three phase resistive load with the following characteristics: rated voltage $U_N = 48\text{V}$, rated power $P_N = 7.2\text{W}$, maximum current $I_{max} = 150\text{mA}$. The VSI is based on a STGIPS10K60A power module and the switching frequency is equal to 20 kHz.

Design, setup and comparison of optimized and conventionally designed EMI filter

Figure V.17 shows the measured CM and DM EMI; both emission profiles exceed the limits of the standards that have been chosen as a reference. So a suitable input EMI filtering is necessary. It should be noted that the load has a significant impact on the noise emission profile. In fact, the test bench of case study #1 and #2 is the same and it differs only for the three phase load. The CM and DM EMI profiles shown in Figure V.7 and Figure V.17 are different; in particular, the high frequency noise contribution of the induction motor can be recognized in the spectrum.

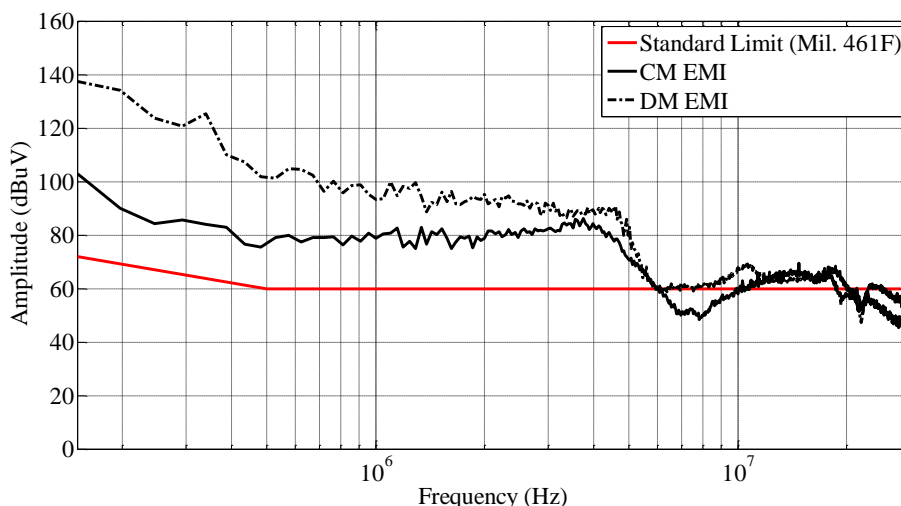


Figure V.17 - CM and DM EMI generated by inverter-fed symmetric low power resistive load.

A single stage EMI filter designed according to the conventional procedure has been realized and considered as a benchmark. It should be noted that the conventional design procedure, according to the constraint on the cutoff frequency lower than the power converter's switching frequency, leads to the same filter of the previous case study.

As regards the filter designed according to the optimized procedure, the measured CM/DM spectra, shown in Figure V.17, have been loaded into ODEF application and the automatic processing returned the following filter parameters:

- $Att_{req_CM} = 25 \text{ dB}\mu\text{V}@150 \text{ kHz}$;
- $Att_{req_DM} = 60 \text{ dB}\mu\text{V}@150 \text{ kHz}$.

Then, the input data shown in Table V.3 have been entered and the computation has been started.

Table V.3 INPUT DATA FOR ODEF APPLICATION – CASE STUDY #2.

Filter topology	Γ -II
Reference standard	Military Standard 461F
System type	DC system
U_N	48 V
I_{\max_phase}	150 mA
I_{cm_max}	45 mA
I_{dm_max}	60 mA
C_v standard	SAE AS 1831
Volume coefficient	100%
Weight coefficient	0%
Extra_Ldm_mode	Auto

In this case the optimized procedure selected a double stage configuration with separate DM inductors. A comparison of the optimized filter with the conventionally designed one has been carried out and Table V.4 summarize the results obtained with the two procedures.

Figure V.18 shows the photo of the optimized EMI filter compared to the conventionally designed one: the optimized filter is evidently more compact. Evaluating the volume and the weight of the two filters, it is possible to observe that the optimized design leads to a reduction in volume and weight. In particular, a reduction of 65% in volume and of 67% in weight is obtained. Despite the realized optimized filter is not the best configuration provided by ODEF, a considerable improvement in EMI filter power density is obtained.

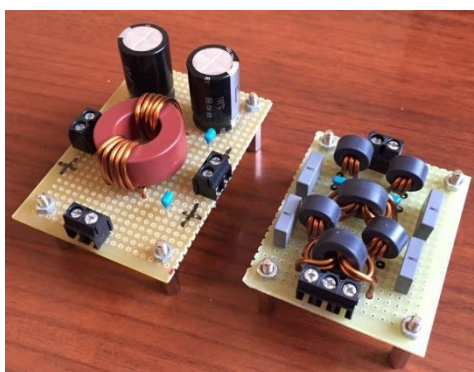


Figure V.18 - Photo of conventionally designed EMI filter (on the left) and optimized EMI filter (on the right), in case study #2.

Table V.4 COMPARISON BETWEEN OPTIMIZED AND CONVENTIONALLY-DESIGNED EMI FILTERS (CASE STUDY #2).

	<i>Conventional Design</i>	<i>Optimized Design</i>
Number of stages	1	2
$L_{CM}@10kHz$	0.8 mH	56 μ H (each stage)
CM inductor core dimensions (mm x mm x mm)	27.9x13.6x12.5	14.1x6.6x6.3 (each stage)
CM core $A_L@10kHz$	65.5 μ H (Vitroperm 500F, model T60006-L2025-W380)	28 μ H (Vitroperm 500F, model T60006-L2012-W902) (each stage)
Number of turns per CM winding	5	2 (each stage)
C_{CM}	200 nF	100 nF (each stage)
C_y	100 nF, ceramic, 250 V, (Murata RDER72E104K2)	47 nF, ceramic, 250 V, (Murata RDER72E473K2) (each stage)
$L_{DM}@10kHz$	1.6 μ H ($L_{leakage}=0.2\% L_{CM}$)	459 μ H (Extra L_{DM}) (each stage)
DM inductor core dimensions (mm x mm x mm)	n.a.	11.2x5.1x5.8 (two for each stage)
DM core $A_L@10kHz$	n.a.	25.5 μ H (Vitroperm 500F, model T60006-L2009-W914) (2 for each stage)
Number of turns per DM winding	n.a.	3 (each stage)
C_{DM}	47 μ F, electrolytic, 400 V, (Panasonic EEUEE2G470)	33 nF, polypropylene, 560 V, (Kemet 46KF23301P02) (each stage)
Wire size	15 AWG	21 AWG
Volume	25.87 cm³	9.88 cm³ (all stages)
Weight	44 g	14.42 g (all stages)

Comparison of Optimized and Conventionally Designed EMI filter Performance

EMI measurements have been carried out in order to evaluate the EMI filters mitigation performance. As shown in Figure V.19, both filters allow to obtain a fully compliant behavior concerning the standard limit in the whole frequency range. Then the optimized design procedure with extra L_{DM} has been validated.

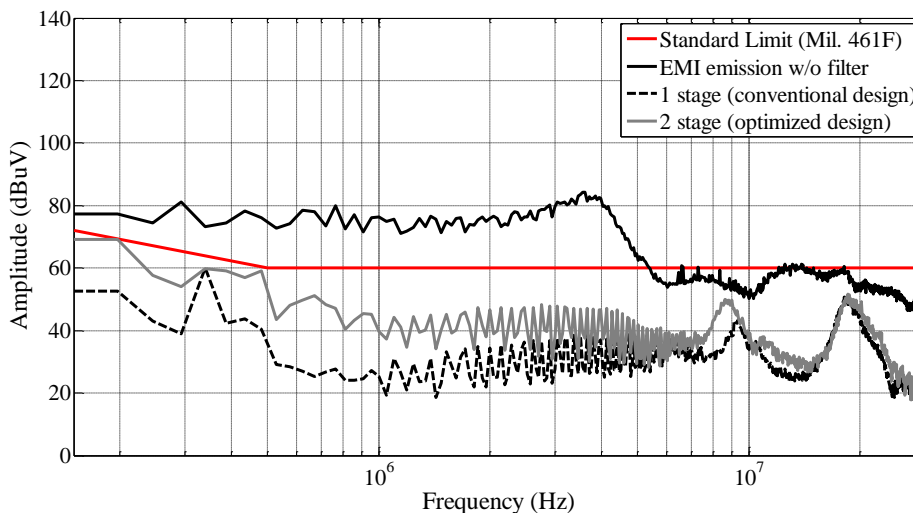


Figure V.19 - Comparison of optimized and conventionally designed EMI filter performance (case study #2).

5.5 Case study #3: DC motor drive supplied by a DC/DC boost converter

In the third case study, the conventional and optimized designs of an EMI filter for a DC motor drive supplied by a DC/DC boost converter are reported. A comparison of the optimized filter with the conventionally designed one has been carried out in terms of EMI filter configuration characteristics, size and performance. In this case, the best configuration given by the optimized design procedure without extra L_{DM} has been chosen as optimized filter configuration.

The DUT is composed of a voltage regulator based on a DC/DC boost converter and a DC motor drive with rated voltage $U_N = 12$ V, rated power $P_N = 30$ W and maximum current $I_{max} = 2.5$ A. The boost converter is based on the following devices: MURB820: Ultrafast Rectifier, IRFP150N: Power MOSFET, Inductor $320\mu\text{H}$, output capacitance $220\mu\text{F}$. The switching frequency is equal to 20 kHz.

Design, set up and comparison of optimized and conventionally designed EMI filter

The measured CM and DM EMI emission profiles (Figure V.20) have been compared with the limits imposed by the CISPR 25 because this standard is appropriate for the given DUT. Two limit curves are reported in Figure V.20: the Class 5 limit, which is the most stringent, and the Class 4 limit. Both CM and DM EMI exceed the limits of the standard that has been chosen as a reference.

EMI filters have been set up according to both design procedure.

In this case study, unlike the previous ones, the conventionally designed EMI filter does not take into account the constraint on cutoff frequency ($f_o < f_{PWM}$) to verify the filter efficiency without this rule.

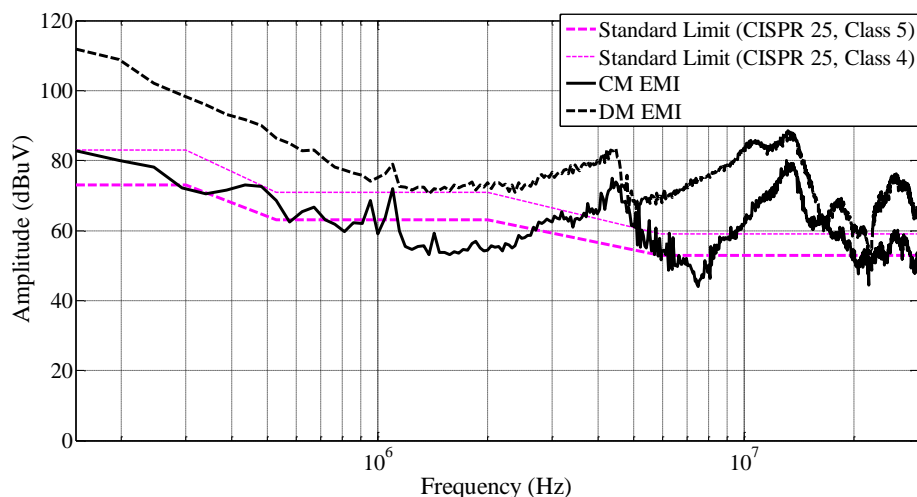


Figure V.20 - CM and DM EMI generated by a DC motor drive supplied by a DC/DC boost converter.

The following data have been used:

- CM emission peak at the lowest frequency: 82.8dB μ V@150kHz;
- DM emission peak at the lowest frequency: 111.9dB μ V@150kHz;
- cut-off frequencies: f_{o_CM} =56 kHz and f_{o_DM} = 25 kHz;
- C_{CM} =200 nF (maximum value allowed according to SAE AS 1831 Standard).

The following attenuations have been used for the optimized design procedure:

$$Att_{req_CM} = 16.8\text{dB}\mu\text{V}@150\text{ kHz};$$

$$Att_{req_DM} = 45.9\text{dB}\mu\text{V}@150\text{ kHz}.$$

Futhermore, the input data shown in Table V.5 have been used to run the optimized design algorithm. It is worth noting the maximum ground leakage current has been considered for C_y selection. Moreover, choosing *Never* in the *Extra_Ldm* panel, the algorithm included in the search space only the configurations with the DM filter realized using the leakage inductance of the CM choke.

Table V.5 INPUT DATA FOR ODEF APPLICATION – CASE STUDY #3.

Filter topology	Γ -II
Reference standard	CISPR25 Class 5
System type	DC system
U_N	12 V
I_{max}	2.5 A
I_{cm_max}	30 mA
I_{dm_max}	56.5 mA
C_y	102 nF (maximum ground leakage current = 0.85 mA)
Volume coefficient	100%
Weight coefficient	0%
Extra_Ldm_mode	Never

Also in this case study, the conventional design procedure leads to a single stage configuration, whereas the optimized procedure selected a double stage configuration. Table V.6 summarizes the design results. Evaluating the volume and weight of the two filters, it is possible to observe that the optimized design leads to a reduction of 38% in volume and of 41% in weight.

Table V.6 COMPARISON BETWEEN OPTIMIZED AND CONVENTIONALLY-DESIGNED EMI FILTERS (CASE STUDY #3)

	<i>Conventional Design</i>	<i>Optimized Design</i>
Number of stages	1	2
$L_{CM}@10kHz$	60 μ H	51 μ H (each stage)
CM inductor core dimensions (mm x mm x mm)	19x11x8.0	11.2x5.1x5.8 (each stage)
CM core $A_L@10kHz$	30 μ H (Vitroperm 500F, model T60006-L2017-W515)	25.5 μ H (Vitroperm 500F, model T60006-L2009-W914) (each stage)
Number of turns per CM winding	2	2 (each stage)
C_{CM}	200 nF	100 nF (each stage)
C_y	100 nF, ceramic, 100V, (Murata RDER72A104K1)	47 nF, ceramic, 100V, (Murata RDER72A473K1) (each stage)
$L_{DM}@10kHz$	120nH ($L_{leakage}=0.2\% L_{CM}$)	102 nH ($L_{leakage}=0.2\% L_{CM}$) (each stage)
C_{DM}	330 μ F, electrolytic, 160 V, (Panasonic EEUEE2C331)	68 μ F, electrolytic, 160 V, (Panasonic EEUEE2C680) (each stage)
Wire size	18 AWG	18 AWG
Volume	25.06 cm³	15.54 cm³ (all stages)
Weight	34.83 g	20.52 g (all stages)

The layout of the two filters is equal to those shown in Figure V.8. A comparison of the EMI filter components is shown in Figure V.21: the volume difference is more evident.

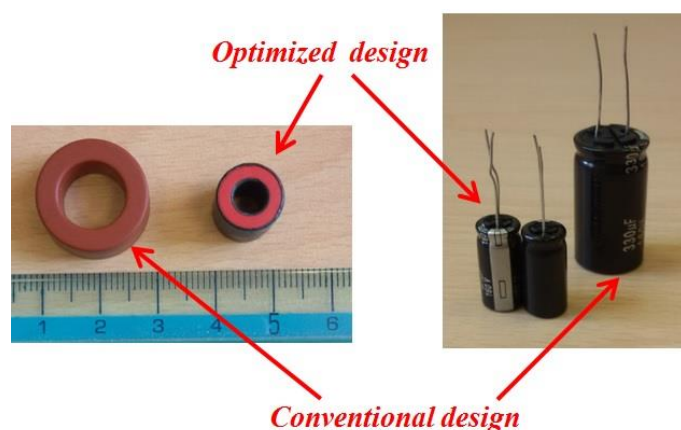


Figure V.21 – Comparison of components used to EMI filters setup (case study #3).

Comparison of Optimized and Conventionally Designed EMI filter Performance

In order to evaluate the EMI filters mitigation performance, EMI measurements have been carried out without any filter, with the conventionally designed filter and with the optimized filter (Figure V.22). Both filters show a satisfactory behavior since the mitigated EMI not exceed the applicable values imposed by the reference standard. In particular, the filters allow to obtain a fully compliant behavior with the Class 4 limits and an acceptable behavior for the Class 5 limits.

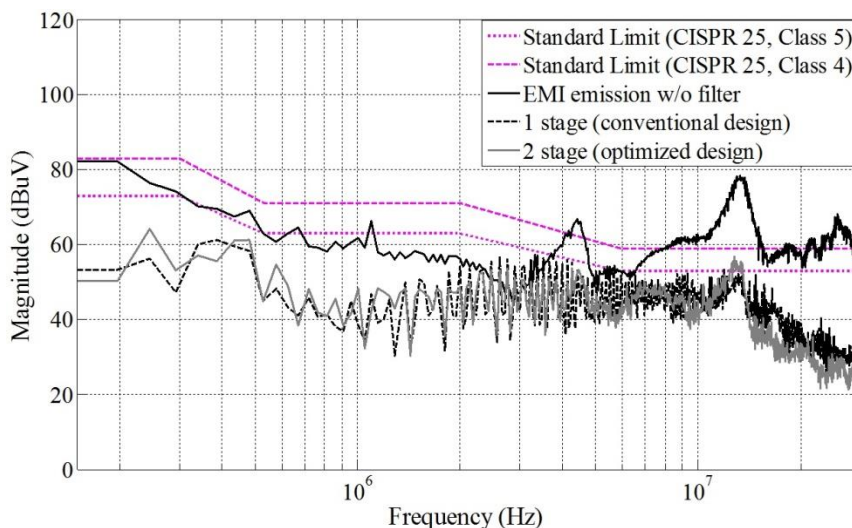


Figure V.22 - Comparison of optimized and conventionally designed EMI filter performance (case study #3).

Considerations on feasible configurations

In this case study the ODEF application selected the best design (2 stages, no extra L_{DM} , CM core index 26, total volume=14.54 cm³) among a total of 519 feasible configurations without extra L_{DM} (1038 feasible configurations taking into account also configurations with extra L_{DM}).

The features of the *Extra* tab have been used to analyze and compare the feasible configurations. The feasible configurations without extra L_{DM} can be classified as shown in Figure V.23, according to the number of filter stages. As the figure shows, the search space is quite large and the filter volume reaches 6300 cm³ in the worst configuration.

In order to provide an insight into the configurations that belong to a small neighborhood around the optimal solution, Figure V.24 and Figure V.25 show the distribution of the 30 best designs. The 30 best designs include 1-stage, 2-stage and 3-stage filter configurations with a volume range from about 15 cm³ to 22 cm³. In particular the plot shown in Figure V.25 helps the designer to compare the volume of the different configurations.

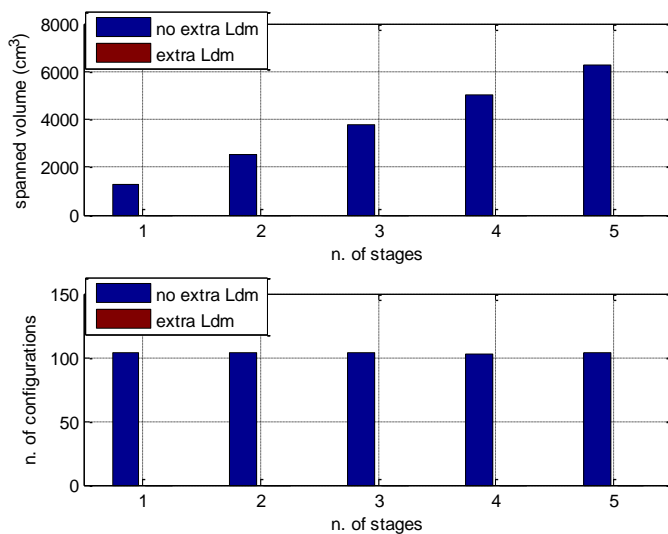


Figure V.23 - Distribution of feasible configurations without extra L_{DM} (case study #3).

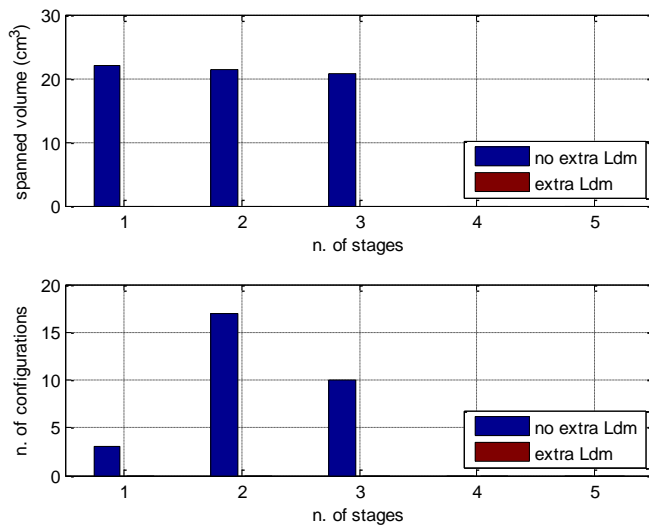


Figure V.24 - - Distribution of the best 30 configurations without extra L_{DM} (case study #3).

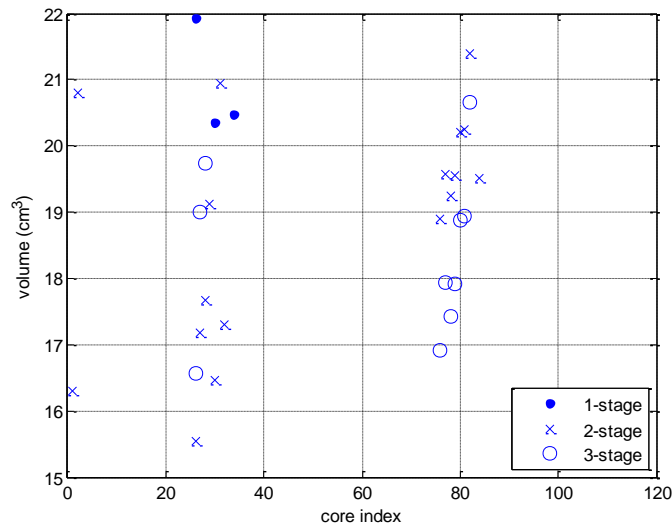


Figure V.25 - Scatter plot of the best 30 no extra L_{DM} configurations (case study #3).

Furthermore, to evaluate the proximity of the returned solution to other configurations, Figure V.26 shows the volume of the best configuration for each number of stages; it can be noted that the 2-stage and 3-stage configurations occupy a lower volume respect to the 1-stage configuration.

Figure V.27 presents the distribution of the best 100 configurations grouped for number of stages (32 for $n=1$, 26 for $n=2$, 20 for $n=3$, 14 for $n=4$, 8 for $n=5$): there are different intersection points of the curves related to 1-stage, 2-stage and 3-stage configurations. With reference to Figure V.27, it should be noted that 14 2-stage configurations and 9 3-stage configurations occupy a lower volume respect to the best 1-stage configuration. This occurs because the case study requires low attenuation for the CM noise ($16.8\text{dB}\mu\text{V}@150\text{ kHz}$) and high attenuation for the DM noise ($45.9\text{dB}\mu\text{V}@150\text{ kHz}$): then DM filter components have greater impact on the volume occupied by the EMI filter. Having chosen *Never* (Table V.5) the algorithm included in the search space only the DM filters realized using the leakage inductance of the CM choke. Since the DM required attenuation is high and $L_{DM}=L_{\text{leakage}}$ has generally a very low value, a high DM capacitance is required and the algorithm chooses the electrolytic capacitors. A multi stage configuration is preferable to reduce the value and consequently the size of electrolytic capacitors. Even if more components are required in the 2-stage and 3-stage configurations than in a single stage configuration, more compact filter configurations are obtained.

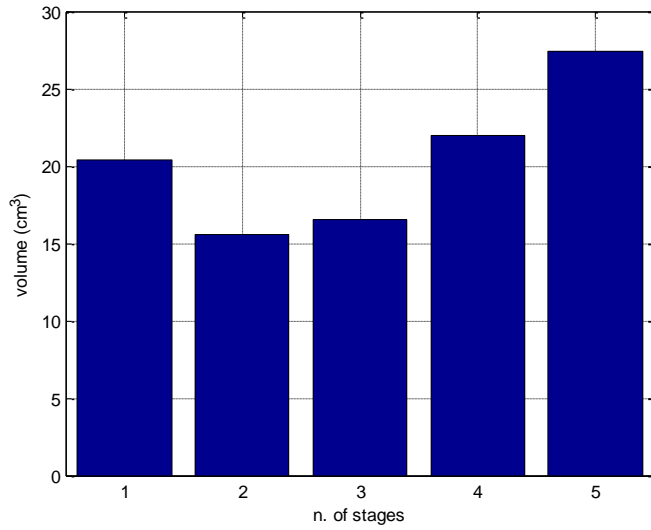


Figure V.26 - Volume of the best configuration for each number of stages (case study #3).

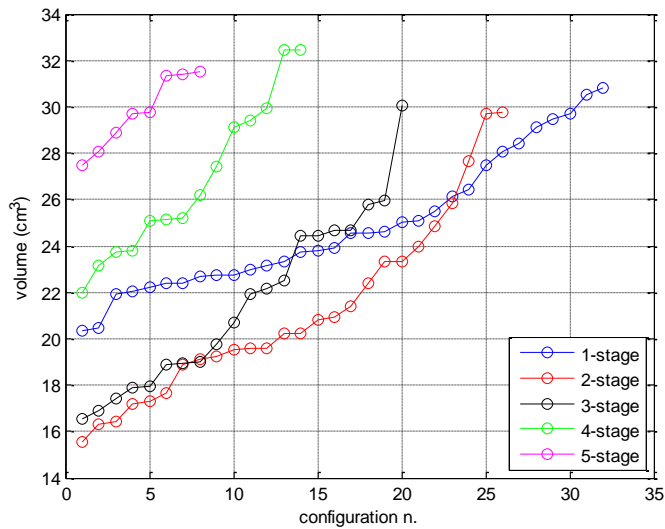


Figure V.27 - Distribution of the best 100 configurations for different n. of stages (case study #3).

5.6 Case study #4: DC motor drive supplied by a DC/DC buck converter

In this case study, the DUT is composed of a voltage regulator based on a DC/DC buck converter and a DC motor drive with rated voltage $U_N = 12V$, rated power $P_N = 190W$ and maximum current $I_{max} = 3.8A$. As far as the buck converter is concerned, two different converters with the following devices are considered:

- buck converter 1: SKM50GB123D: Power IGBT, Diode with forward voltage $V_F = 2.2V$ and maximum forward current $I_{Fmax} = 40A$, Inductor $500\mu H$, output capacitance $1000\mu F$;

- buck converter 2: STTH12R06: Ultrafast Rectifier, IRFP150N: Power MOSFET, Inductor 500 μ H, output capacitance 1000 μ F.

The switching frequency of both buck converter devices is equal to 10 kHz. The switching frequency value is limited by the maximum frequency at which the power IGBT can operate. The power MOSFET could operate at higher switching frequencies but, in order to maintain the same operating conditions, the same switching frequency has been maintained.

The effectiveness and usefulness of the optimized design procedure have been demonstrated in previous case studies by a comparison of the optimized filters with the conventionally designed one in terms of size and performance.

Then, in this case study, the EMI filter is designed according to the optimized procedure.

Optimized EMI filter design

At first the CM and DM EMI emission generated by the DC motor drive supplied by a DC/DC buck converter 1 have been evaluated. In a second step, CM and DM EMI generated by DC motor drive supplied by a DC/DC buck converter 2 have been measured and compared with those previously measured to evaluate as the converters, with the same topology but different switching devices, can influence the EMI generation.

The EMI profiles have been compared with the limits of the CISPR 25 that can be applied for the given DUT. Both the CM and DM EMI, shown in Figure V.28 exceed the limits of the reference standard.

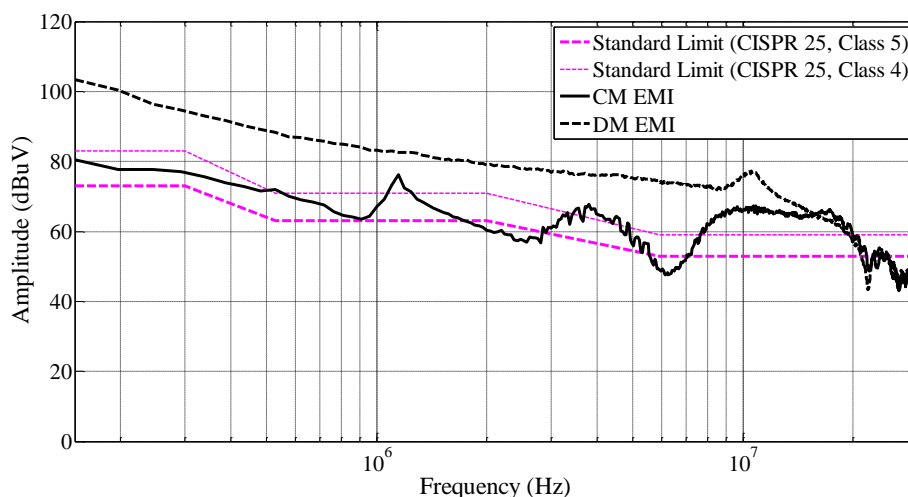


Figure V.28 - CM and DM EMI generated by DC motor drive supplied by the DC/DC buck converter 1.

The attenuation values used for the optimized design procedure are: $Att_{req_CM} = 14.4\text{dB}\mu\text{V}@150$ kHz, $Att_{req_DM} = 37.3\text{dB}\mu\text{V}@150$ kHz. Then, the input data shown in Table V.7 have been entered and

the computation has been started. Only the configurations with the DM filter realized using the leakage inductance of the CM choke have been evaluated.

The application selected the best design (2 stages, no extra L_{DM} , CM core index 26, total volume=11.91 cm³, total weight=16.61 g) among a total of 486 feasible configurations (except configurations with extra L_{dm}). All the details of the optimized EMI filter are given in Table V.8.

Table V.7 INPUT DATA FOR ODEF APPLICATION – CASE STUDY #4 WITH BUCK CONVERTER 1.

Filter topology	Γ -II
Reference standard	CISPR25 Class 5
System type	DC system
U_N	12 V
I_{max}	3.8 A
I_{cm_max}	39 mA
I_{dm_max}	46 mA
C_v	SAE AS 1831
Volume coefficient	100%
Weight coefficient	0%
Extra_Ldm_mode	Never

Table V.8 FEATURES OF THE OPTIMIZED EMI FILTER (CASE STUDY #4).

Number of stages	2
$L_{CM}@10kHz$	51 μ H (each stage)
CM inductor core dimensions (mm x mm x mm)	11.2x5.1x5.8 (each stage)
CM core $A_L@10kHz$	25.5 μ H (Vitroperm 500F, model T60006-L2009-W914) (each stage)
Number of turns per CM winding	2 (each stage)
C_{CM}	100 nF (each stage)
C_v	47 nF, ceramic, 100V, (Murata RDER72A473K1) (each stage)
$L_{DM}@10kHz$	102 nH ($L_{leakage}=0.2\% L_{CM}$) (each stage)
C_{DM}	47 μ F, electrolytic, 160 V, (Panasonic EEUEE2C470) (each stage)
Wire size	15 AWG
Volume	11.91 cm³ (all stages)
Weight	16.61 g (all stages)

Afterwards CM and DM EMI generated by DC motor drive supplied by a DC/DC buck converter 2 have been measured. As shown in Figure V.29, CM and DM EMI exceed the limit curves. In particular, Figure V.30 and Figure V.31 show a comparison between CM/DM EMI generated by the DC motor drive supplied by the buck converter 1 or by the buck converter 2. It should be noted that the EMI profiles are very similar until 10 MHz and 17 MHz, for CM and DM EMI respectively. Beyond these frequencies the EMI generated with the buck converter 2 are more relevant. However the emission peaks at the lowest frequency have the greatest impact on EMI filter design. Consequently, the EMI filter design according to CM and DM spectrum shown in Figure V.29 leads to the EMI filter with the same features given in Table V.8.

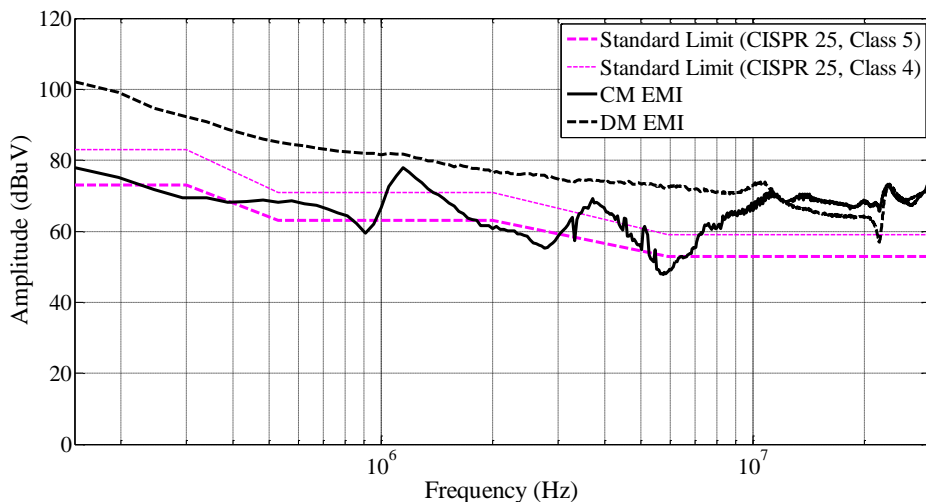


Figure V.29 - CM and DM EMI generated by DC motor drive supplied by the DC/DC buck converter 2.

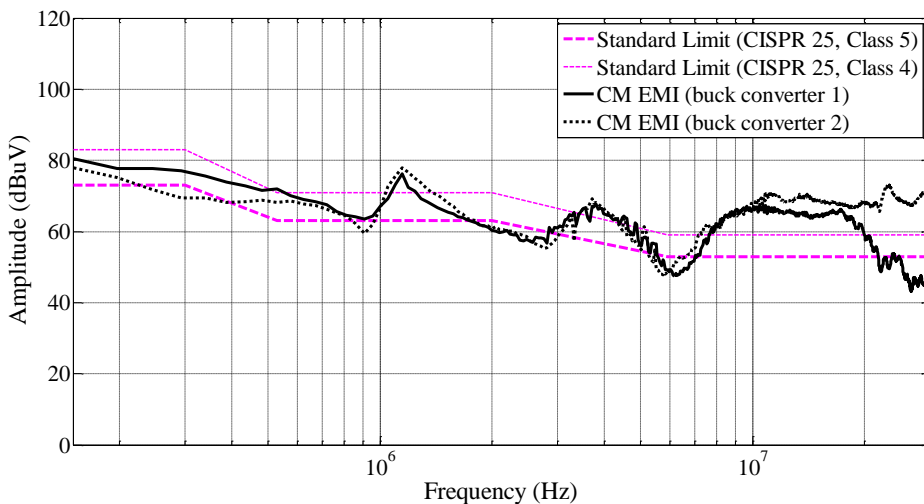


Figure V.30 – Comparison between CM EMI generated by the DC motor drive supplied by the buck converter 1 (solid line) or by the buck converter 2 (dashed line).

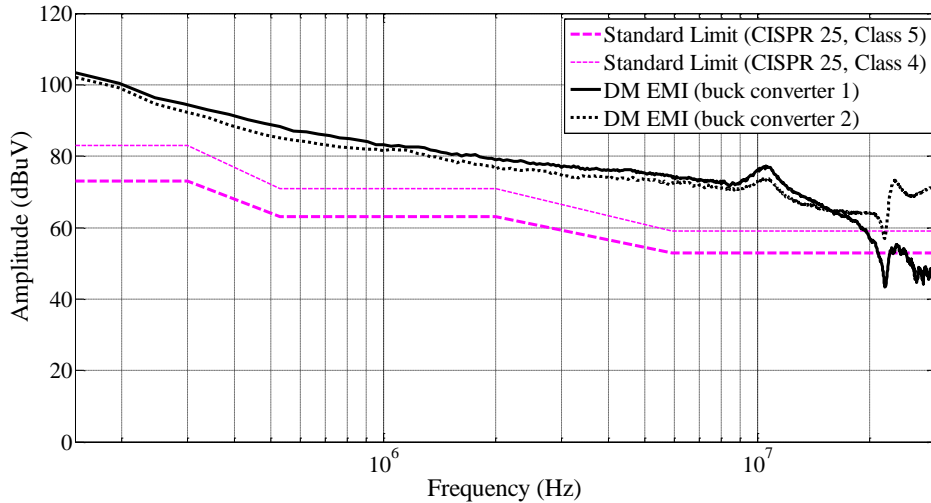


Figure V.31 - Comparison between DM EMI generated by the DC motor drive supplied by the buck converter 1 (solid line) or by the buck converter 2 (dashed line).

Evaluation of optimized EMI filter Performance

Finally, in order to evaluate the EMI filter mitigation performance with both DC/DC buck converter, EMI measurements have been carried out without filter and with the optimized filter (Figure V.32). The EMI filter shows a satisfactory behavior since the filtered EMI comply with the limits imposed by the reference standard in both cases.

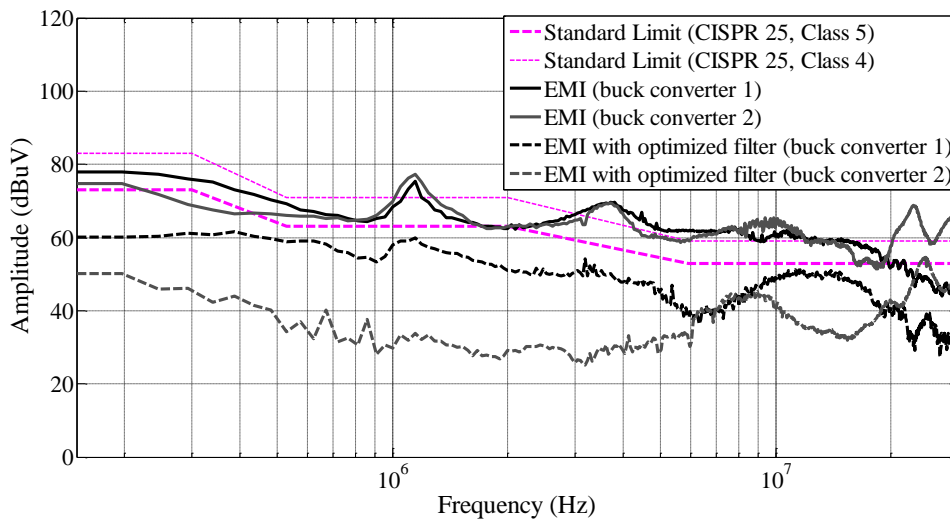


Figure V.32 – Measured EMI with and without EMI filter (case study #4).

CONCLUSIONS and FUTURE DEVELOPMENTS

The research conducted during the PhD course regards the power density issue in EMI filters used for mitigating EMI in power electronic systems. For this purpose, a broad research on commercially available materials, with which the discrete EMI filter components are realized (inductors and capacitors), has been conducted; moreover, their characteristics and performance at high frequencies (in particular in the range of frequencies of the conducted electromagnetic interference) have been evaluated.

With regard to the design issues, once the filter topology and component values have been defined, there are many practical configurations to realize the filter. The identification of the configuration leading to the best power density in terms of minimum volume/weight is a nontrivial task. The conventional EMI filter design requires a considerable computational effort and it could not guarantee the optimal choice of filter components in order to obtain the maximum power density. Then, an optimized design procedure of discrete EMI filters oriented at obtaining high performing filters with the minimum volume/weight, has been developed. The optimized procedure relies on a suitably devised rule-based algorithm and on databases of commercially available magnetic cores, capacitors and conducting wires. The optimized algorithm can be implemented by using a common programming language, within either an open source or a commercial environment, and it exhibits low computational demand. Therefore, it can be advantageously used both by EMI engineers for obtaining an optimized filter design and by scientists/experts for the evaluation of filter performance versus configuration and power density features. Moreover, to make the new design procedure more accessible to EMI designer, a software tool based on the optimized design procedure has been developed, namely ODEF (*Optimized Design of EMI Filters*). All the design options, steps, outputs and design-related supplementary analyses are managed by ODEF tool in a very intuitive and user-friendly fashion.

The optimized EMI filter design procedure has been validated experimentally, both in terms of performance and increased power density, in several case studies related to different power electronic converters configurations and different application fields. In addition to the compliance of the power electronic systems under study with the reference standards, the optimized procedure has allowed to achieve EMI filters with considerable higher compactness and power density compared to the conventional design. In particular, the EMI filters size comparison has been carried out for the following case studies.

- In the first case study, in which the conventional and optimized design of an EMI filter for a low voltage high current induction motor drives supplied by DC power grids have been presented, a reduction of 52% in volume and of 56% in weight has been obtained.
- In the second case study, the conventional and optimized designs of an EMI filter for a symmetric low power resistive load supplied by DC power grid have been reported. A reduction of 65% in volume and of 67% in weight has been obtained.
- The third case study has regarded a DC motor drive supplied by a DC/DC boost converter. The optimized design has led to a reduction of 38% in volume and of 41% in weight.

This thesis provides a considerable contribution to the power density improvement in power electronic converters with regard to the EMC compliance of these systems.

Future developments include the investigation of the use of inductors working in partial saturation and the approach with the digital active EMI filtering technique. The literature provide a few contributions on these approaches, so it would be interesting to conduct an investigation on these topics in order to analyze the possible developments and limits.

REFERENCES

- [1] Clayton R. Paul, "Introduction to electromagnetic compatibility," 2006, ISBN: 0471755001.
- [2] Mohan, Undeland, Robbins, "Power Electronic: Converters, Applications and Design", 1995.
- [3] V. Serrao, "Studio delle problematiche di compatibilità elettromagnetica negli azionamenti elettrici", Master Thesis, Dept. of Mechanical and Industrial Engineering, University of Roma Tre, Rome, IT.
- [4] A. Roch, "Behavioural Models for Common Mode EMI Filters", Master Thesis, Dept. of Electrical Engineering, Mathematics and Computer Science, University of Twente, The Netherlands, 2012.
- [5] Norma CEI 301-1 - Azionamenti elettrici - Dizionario, 1997.
- [6] Vocabolario Elettrotecnico Internazionale. Cap. 551 - Elettronica di potenza (Pubbl. CEI 02/91. Fascicolo 1468).
- [7] R. Redl, P. Tenti, J. Daan van Wyk Rand – *Power electronics' polluting effects* – Spectrum IEEE, 1997.
- [8] Millán, P. Godignon, X. Perpiñà, A. Pérez-Tomás, J. Rebollo, "A survey of Wide Bandgap Semiconductor Devices", IEEE Transactions on Power Electronics, vol. 29, pp. 2155 - 2163, May 2014.
- [9] P. Gammon, "Silicon and the Wide Bandgap Semiconductors, shaping the Future Power Electronics Device Market", 14th International Conference on Ultimate Integration on Silicon (ULIS), 19-21 March 2013.
- [10] K. Mainali, R. Oruganti, "Conducted EMI Mitigation Techniques for Switch-Mode Power Converters: A Survey", IEEE Transactions on Power Electronics, vol. 25, no. 9, pp. 2344-2356, September 2010.
- [11] L. Rossetto, S. Buso, and G. Spiazzi, "Conducted EMI issues in a 600-W single-phase boost PFC design" IEEE Transactions on Industry Applications, vol. 36, no. 2, pp. 578–585, March/April 2000.
- [12] M. Silva, N. Hensgens, J. Oliver, P. Alou, O. García, J. A Cobos, "New Considerations in the Input Filter Design of a Three-Phase Buck-Type PWM Rectifier for Aircraft Applications", IEEE Energy Conversion Congress and Exposition (ECCE 2011), 17-22 September 2011, Phoenix, AZ, USA.

- [13] F. Mihalič, D. Kos, “Reduced Conductive EMI in Switched-Mode DC–DC Power Converters Without EMI Filters: PWM Versus Randomized PWM”, *IEEE Transactions on Power Electronics*, vol. 21, no. 6, pp. 1783–1794, November 2006.
- [14] X. Yang, Y. Yuan, X. Zhang, P. R. Palmer, “Shaping High-Power IGBT Switching Transitions by Active Voltage Control for Reduced EMI Generation”, *IEEE Transactions on Industry Applications*, vol. 51, no. 2, pp. 1669–1677, March/April 2015.
- [15] X. Yang, Z. Long, Y. Wen, H. Huang, P. R. Palmer, “Investigation of the trade-off between switching losses and EMI generation in Gaussian S-shaping for high-power IGBT switching transients by active voltage control”, *IET Power Electronics*, vol. 9, iss. 9, pp. 1979–1984, 2016.
- [16] B. K. Bose, “Soft-switched Power Conversion for AC Motor Drives”, *IEEE Industrial Electronics Magazine*, vol. 1, Iss. 4, pp. 30-39, 2007.
- [17] C. Choochuan, “A Survey of Output Filter Topologies to Minimize the Impact of PWM Inverter Waveforms on Three-Phase AC Induction Motors”, *The 7th International Power Engineering Conference*, November/December 2005.
- [18] M. Hartmann, H. Ertl, J. W. Kolar, “EMI Filter Design for a 1 MHz, 10 kW Three-Phase/Level PWM Rectifier”, *IEEE Transaction on Power Electronics*, vol. 26, no. 4, pp.1192-1204, April 2011.
- [19] S. Ye, W. Eberle, Y. Liu, “A Novel EMI Filter Design Method for Switching Power Supplies”, *IEEE Transaction on Power Electronics*, vol. 19, no. 6, pp. 1668-1677, November 2004.
- [20] Y.C. Son, S.K. Sul, “Generalization of Active Filters for EMI Reduction and Harmonics Compensation”, *IEEE Transaction on Industry Applications*, vol. 42, no. 2, pp. 545-551, March/April 2006.
- [21] Y.C. Son, S.K. Sul, “A new active common-mode EMI filter for PWM inverter”, *IEEE Transaction on Power Electronics*, vol. 18, iss. 6, pp. 1309-1314, November 2003.
- [22] Y.C. Son, S.K. Sul, “Conducted EMI in PWM Inverter for Household Electric Appliance”, *IEEE Transaction on Industry Applications*, vol. 38, no. 5, pp. 1370-1379, September/October 2002.
- [23] M.C. Di Piazza, A. Ragusa, G. Vitale, “An Optimized Feedback Common Mode Active Filter for Vehicular Induction Motor Drives”, *IEEE Transaction on Power Electronics*, vol. 26, no. 11, pp. 3153-3162, November 2011.
- [24] D. Hamza, P. K. Jain, “Conducted EMI noise mitigation in DC-DC converters using active filtering method”, *IEEE Power Electronics Specialists Conference (PESC 2008)*, 15-19 June 2008, Rhodes, Greece.

- [25] Y. Sha, W. Chen, H. Qi, Y. Han, X. Yang, Y. Hao, “Research of active EMI filter for Gallium Nitride based high frequency resonant converter”, Asia-Pacific International Symposium on Electromagnetic Compatibility (APEMC 2016), vol. 1, pp. 491-494, 2016.
- [26] V. Tarateeraseth, “Enhancement of Operational Amplifier Gain Bandwidth Product used in Common-mode Active EMI Filter Compensation Circuit”, 10th International Conference on Electrical Engineering/Electronics, Computer, Telecommunications and Information Technology (ECTI-CON 2013), 15-17 May 2013, Krabi, Thailand.
- [27] T. C. Neugebauerand, D .J. Perreault, “Parasitic capacitance cancellation in filter inductors” IEEE Transaction on Power Electronics, vol. 21, no. 1,pp. 282–288, January 2006.
- [28] S. Wang, F. C. Lee, and W. G. Odendaal, “Cancellation of capacitor parasitic parameters for noise reduction application”, IEEE Transaction on Power Electronics, vol. 21, no. 4, pp. 1125–1132, July 2006.
- [29] S. Wang, “Characterization and cancellation of high-frequency parasitics for EMI filters and noise separators in power electronics applications”, Ph.D. dissertation, Virginia Polytechnic Institute and State University, Blacksburg, VA, 2005.
- [30] M. U. Iftikhar, D. Sadarnac, and C. Karimi, “Input filter damping design for control loop stability of DC-DC converters”, IEEE International Symposium on Industrial Electronics (ISIE 2007), 4–7June 2007, Vigo, Spain.
- [31] K. Louati, D. Sadarnac, C.Karimi, “Input filter influence on the control stability of DC/DC converters”, IEEE International Symposium on Industrial Electronics (ISIE 2004), 4–7 May 2004, Ajaccio, France.
- [32] D. Hamza, M. Qiu, “Digital Active EMI Control Technique for Switch Mode Power Converters”, IEEE Transaction on Electromagnetic Compatibility, vol. 55, no. 1, February 2013.
- [33] D. Hamza, M. Pahlevaninezhad, P.K. Jain, “Implementation of a Novel Digital Active EMI Technique in a DSP-Based DC–DC Digital Controller Used in Electric Vehicle (EV)”, IEEE Transaction on Power Electronics, vol. 28, no. 7, pp. 3126-3137, July 2013.
- [34] D. Hamza, Q. Mei, P.K. Jain, “Implementation of an EMI active filter in grid-tied PV micro-inverter controller and stability verification”, 38th Annual Conference on IEEE Industrial Electronics Society (IECON 2012), 25-28 October 2012, Montreal, Canada.
- [35] S. Wang, Y. Y. Maillet; F. Wang; D. Boroyevich; R. Burgos, “Investigation of Hybrid EMI Filters for Common-Mode EMI Suppression in a Motor Drive System”, IEEE Transaction on Power Electronics, vol. 25, no. 4, pp. 1034-1045, April 2010.

- [36] W. Chen; X. Yang; Z. Wang, "A Novel Hybrid Common-Mode EMI Filter With Active Impedance Multiplication", *IEEE Transactions on Industrial Electronics*, vol. 58, no. 5, pp. 1826-1834, May 2011.
- [37] X. Chang, W. Chen, Y. Yang, K. Wang, X. Yang, "Research and realization of a novel active Common-Mode EMI Filter", *IEEE Applied Power Electronics Conference and Exposition (APEC 2015)*, 15-19 March 2015, Charlotte, NC, USA.
- [38] Y. Chu, S. Wang, Q. Wang, "Modeling and Stability Analysis of Active/Hybrid Common-Mode EMI Filters for DC/DC Power Converters", *IEEE Transaction on Power Electronics*, vol. 31, no. 9, pp. 6254-6263, September 2016.
- [39] W. Chen, X. Yang, Z. Wang, "Analysis of insertion loss and impedance compatibility of hybrid EMI filter based on equivalent circuit model", *IEEE Transaction on Industrial Electronics*, vol. 54, no. 4, pp. 2057–2064, August 2007.
- [40] K. Koiwa, J. Itoh, "A Maximum Power Density Design Method for Nine Switches Matrix Converter Using SiC-MOSFET", *IEEE Transaction on Power Electronics*, vol. 31, no. 2, pp. 1189 - 1202, February 2016.
- [41] Y. Wang, S. W. H. de Haan, J. A. Ferreira, "Potential of improving PWM converter power density with advanced components", *13th European Conference on Power Electronics and Applications (EPE 2009)*, 8 - 10 September 2009, Barcelona, Spain.
- [42] U. Drogenik, J. W. Kolar, "Thermal Power Density Barriers of Converter Systems", *5th International Conference on Integrated Power Electronics Systems (CIPS 2008)*, 11 - 13 March 2008, Nuremberg, Germany.
- [43] T. Halder, "Power Density & Thermal Limits of The Flyback SMPS", *IEEE First International Conference on Control, Measurement and Instrumentation (CMI 2016)*, 2 - 10 January 2016, Kolkata, India.
- [44] J.W. Kolar, J. Biela, S. Waffler, T. Friedli, U. Badstuebner, "Performance Trends and Limitations of Power Electronic Systems", *6th International Conference on Integrated Power Electronics Systems (CISP 2010)*, 16 - 18 March 2010, Nuremberg, Germany.
- [45] B. Wen, D. Boroyevich, P. Mattavelli, "Investigation of Tradeoffs between Efficiency, Power Density and Switching Frequency in Three-Phase Two-Level PWM Boost Rectifier", *14th European Conference on Power Electronics and Applications (EPE 2011)*, 30 Aug. - 1 Sept. 2011, Birmingham, United Kingdom.
- [46] G. Di Capua, N. Femia, "A Novel Method to Predict the Real Operation of Ferrite Inductors With Moderate Saturation in Switching Power Supply Applications", *IEEE Transaction on Power Electronics*, vol. 31, no. 3, pp. 2456-2464, March 2016.

- [47] G. Di Capua, N. Femia, K. Stoyka, "Power Magnetics Volume and Weight Reduction in Aerospace Power Supply Units", IEEE 17th Workshop on Control and Modeling for Power Electronics (COMPEL 2016), 27 - 30 June 2016, Trondheim, Norway.
- [48] M. Danilovic, F. Luo, L. Xue, R. Wang, P. Mattavelli, D. Boroyevich, "Size and weight dependence of the single stage input EMI filter on switching frequency for low voltage bus aircraft applications", 15th International Power Electronics and Motion Control Conference (PEMC 2012), 4 - 6 September 2012, Novi Sad, Serbia.
- [49] A. C. Schittler, T. KleeB, M. Kazanbas, S. V. Araújo, P. Zacharias, "Considerations on the influence of the current ripple and switching frequency towards the differential mode EMI filter", 9th International Conference on Integrated Power Electronics Systems (CISP 2016), 8 - 10 March 2016, Nuremberg, Germany.
- [50] B. Wen, X. Zhang, Q. Wang, R. Burgos, P. Mattavelli, D. Boroyevich, "Comparison of three-phase ac-ac matrix converter and voltage dc-link back-to-back converter topologies based on EMI filter", IEEE Energy Conversion Congress and Exposition (ECCE 2013), 15 - 19 September 2013, Denver, CO, USA.
- [51] T. Sun, P. Markondeya Raj, J. Min, Z. Wu, H. Sharma, R. Tummala, T. Takahashi, K. Takemura, "Magnetic materials and design trade-offs for high inductance density, high-Q and low-cost power and EMI filter inductors", IEEE 66th Electronic Components and Technology Conference, 31 May - 03 Jun 2016, Las Vegas, NV, USA.
- [52] M. Ali, E. Labouré; F. Costa, "Integrated Active Filter for Differential-Mode Noise Suppression", IEEE Transactions on Power Electronics, vol. 29, no. 3, pp. 1053-1057, March 2014.
- [53] J. Biela, A. Wirthmuller, R. Waespe, M. Lobo Heldwein, K. Raggl, J. W. Kolar, "Passive and Active Hybrid Integrated EMI Filters", IEEE Transaction on Power Electronics, vol.24, no.5, pp. 1340-1349, May 2009.
- [54] X. Liu, C. K. Lee, S. Y. Hui, "An Integrated Planar EMI Filter for Ultra-high Frequency Power Converters", IEEE Power Electronics Specialists Conference (PESC 2007), 17-21 June 2007, Orlando, FL, USA.
- [55] M. Ali, E. Labouré; F. Costa, "Integrated hybrid EMI filter: Study and Realization of the active part", 15th European Conference on Power Electronics and Applications (EPE 2013), 02 - 06 September 2013, Lille, France.
- [56] X. Wu, Z. Wen, D. Xu, Y. Okuma, K. Mino, "Design and experiment research of integrated EMI filter based on flexible multi-layer foils", International Power Electronics Conference - ECCE ASIA (IPEC 2010), 21 - 24 Jun 2010 - Jun, Sapporo, Japan.

- [57] A. N. Racasan, C. Pacurar, C. Munteanu, V. Topa, D. D. Micu, C. Hebedean, "Modeling and mitigation techniques of the magnetic integrated structures parasitic capacitance", 47th International Universities Power Engineering Conference (UPEC 2012), 04 - 07 September 2012, Uxbridge, Middlesex, United Kingdom.
- [58] H. Huang; L. Deng, "Improving the high-frequency performance of integrated EMI filter with multiple ground layers", Asia-Pacific Symposium on Electromagnetic Compatibility (APEMC 2012), 21 - 24 May 2012, Singapore, Singapore.
- [59] H. Huang; M. Ye, "Parasitic capacitance cancellation of integrated EMI filter by splitting ground windings", IEEE Electrical Design of Advanced Packaging and Systems Symposium (EDAPS 2012), 09 - 11 December 2012, Taipei, Taiwan.
- [60] M. C. Di Piazza, A. Ragusa, G. Vitale, "Effects of Common-Mode Active Filtering in Induction Motor Drives for Electric Vehicles", IEEE Transaction on Vehicular Technology, vol. 59, no. 6, pp. 2664-2673, July 2010.
- [61] "Radio disturbance characteristics for the protection of receivers used on board vehicles, boats, and on devices – Limits and methods of measurement", CISPR 25, 2002.
- [62] J. Stahl; D. Kuebrich; A. Bucher; T. Duerbaum, "Characterization of a modified LISN for effective separated measurements of common mode and differential mode EMI noise", IEEE 3rd Energy Conversion Congress and Exposition (ECCE 2010), 12-16 September 2010, Atlanta, Georgia, USA.
- [63] S. Wang, F.C. Lee, W.G. Odendaal, "Characterization, Evaluation, and Design of Noise Separator for Conducted EMI Noise Diagnosis", IEEE Transactions on Power Electronics, vol 20, no. 4, pp. 974 - 982, July 2005.
- [64] Taub, "Principles Of Communication Systems", McGraw-Hill Education, 2008.
- [65] M. Kumar, V. Agarwal, "Power Line Filter Design for Conducted Electromagnetic Interference Using Time-Domain Measurements", IEEE Transactions on Power Electronics, vol 48, no. 1, pp. 178 - 186, Feb. 2006.
- [66] Y.S. Lee, Y.L. Liang, M.W. Cheng, "Time Domain Measurement System for Conducted EMI and CM/DM Noise Signal Separation", IEEE PEDS 2005.
- [67] S. Cannizzaro, M.C. Di Piazza, M. Luna, G. Vitale, G. Calogero, I. Citro, "Parameter identification and real-time J-V curve reconstruction of polymer PV and dye-sensitized cells using non-iterative algorithms", European PV Solar Energy Conference and Exhibition, (EU PVSEC 2014), 22-26 September 2014.
- [68] R. L. Ozenbaugh, T. M. Pullen "EMI filter Design", 3rd Ed. CRC Press, 2012.

- [69] F. Luo, D. Dong, D. Boroyevich, P. Mattavelli, and S. Wang, "Improving High-Frequency Performance of an Input Common Mode EMI Filter Using an Impedance-Mismatching Filter", *IEEE Transactions on Power Electronics*, vol 29, no. 10, pp. 5111 -5115, October 2014.
- [70] J. Xue; F. Wang; X. Zhang; D. Boroyevich; P. Mattavelli, "Design of output passive EMI filter in DC-fed motor drive", *27th Annual IEEE Applied Power Electronics Conference and Exposition (APEC 2012)*, 5-9 Feb. 2012, Orlando, Florida, USA.
- [71] M. C. Di Piazza, G. Giglia, M. Luna, G. Vitale. "EMI Filter Design in Motor Drives with Common Mode Voltage Active Compensation", *IEEE 23rd International Symposium on Industrial Electronics (ISIE 2014)*, 1-4 June 2014, Istanbul, Turkey.
- [72] L. Tihanyi, "Electromagnetic compatibility in power electronics", 1995, Butterworth Heinemann, Sarasota, FL, USA.
- [73] F.Y. Shih, D.Y. Chen, Y.P. Wu, Y.T. Chen, "A Procedure for Designing EMI Filters for AC Lines Applications", *IEEE Transactions on Power Electronics*, vol 11, no. 1, pp.170 - 181, 1996.
- [74] SAE AS 1831:1997 (R2010) Characteristics And Utilization Of Electrical Power, 270 V DC, Aircraft.
- [75] "Requirements for the control of electromagnetic interference characteristics of subsystems and equipment", *Military Standard 461F*, Dec. 2007.
- [76] Yoann Y. Maillet, "High-Density Discrete Passive EMI Filter Design for Dc-Fed Motor Drives", Master Thesis, Dept. of Elect. Eng., Virginia Polytechnic Institute and State University, Blacksburg, VA, 2008.
- [77] T. Kut, A. Lücken, S. Dickmann, D. Schulz, "Common mode chokes and optimisation aspects", *Advances in Radio Science journal*, vol. 12, pp. 143–148, 2014.
- [78] H. Schwenk, J. Beichler, W. Loges, C. Scharwitz, "Actual and Future Developments of Nanocrystalline Magnetic Materials for Common Mode Chokes and Transformers", *International Exhibition and Conference for Power Electronics, Intelligent Motion, Renewable Energy and Energy Management (PCIM Europe 2015)*, 19 – 21 May 2015, Nuremberg, Germany.
- [79] J. Petzold, "Advantages of softmagnetic nanocrystalline materials for modern electronic applications", *Journal of Magnetism and Magnetic Materials*, vol. 242-245, Issue PART I, pp. 84-89, April 2002.
- [80] Vitroperm EMC Products online available online:
http://www.vacuumschmelze.com/fileadmin/Medienbibliothek_2010/Downloads/KB/Vitroperm_EMV_EN_full.pdf.

- [81] G. L. Skibinski, R. J. Kerkman, D. W. Schlegel, "EMI Emissions of Modern PWM AC Drives", *IEEE Ind. Electron. Magaz.*, pp.47-81, Nov./Dec.1999.
- [82] M. Silva, N. Hensgens, J. Oliver, P. Alou, "New considerations in the input filter design of a three-phase buck-type PWM rectifier for aircraft applications", *IEEE Energy Conv. Congr. Exp.*, pp. 4087 – 4092, 2011.
- [83] M.C. Di Piazza, A Ragusa, G Vitale, "Power-loss evaluation in CM active EMI filters for bearing current suppression", *IEEE Trans. Ind. Electron.*, vol. 58, pp. 5142-5153, 2011.
- [84] J. W. Kolar, U. Drogenik, J. Biela, M. L. Heldwein, H. Ertl, T. Friedli and S. D. Round, "PWM Converter Power Density Barriers", *Power Conversion Conference (PCC '07)*, Nagoya, 2007.
- [85] G. Ala, M. C. Di Piazza, G. C. Giaconia, G. Giglia, G. Vitale, "Design and performance evaluation of a high power density EMI filter for PWM inverter-fed induction motor drives", *IEEE Trans. Industry Applications*, vol. 52, pp. 2397-2404, 2016, DOI: 10.1109/TIA.2016.2518129.
- [86] Y. Maillet, Rixin Lai, Shuo Wang, Fei Wang, R. Burgos, D. Boroyevich, "High-Density EMI Filter Design for DC-Fed Motor Drives", *IEEE Trans. Power Electron.*, vol. 25, no. 5, pp. 1163-1172, May 2010.
- [87] B. Toure, J.L. Schanen, L. Gerbaud, T. Meynard, J. Roudet, R. Ruelland "Optimal EMC Modeling of Drives for Aircraft Applications: Modeling Process, EMI Filter Optimization, and Technological Choice", *IEEE Trans. Power Electron.*, vol. 28, pp. 1145-1156, March 2013.
- [88] F. Wang, W. Shen, D. Boroyevich, S. Ragon, V. Stefanovic, M. Arpilliere, "Design Optimization of Industrial Motor Drive Power Stage Using Genetic Algorithms", *Power Electronics and Motion Control Conference (IPEMC 2006)*, 2006.
- [89] Huang-Jen Chiu, Tian-Fu Pan, Chun-Jen Yao, and Yu-Kang Lo, "Automatic EMI Measurement and Filter Design System for Telecom Power Supplies", *IEEE Trans. Instrum. Meas.*, vol. 56, pp. 2254-2261, Dec. 2007.
- [90] K. Raggl, T. Nussbaumer, J.W. Kolar, "Guideline for a Simplified Differential-Mode EMI Filter Design", *IEEE Trans. Ind. Electron.*, vol. 57, pp. 1031-1040, March 2010.
- [91] S. Anand, B. G. Fernandez, "Optimal voltage level for DC microgrids", in *Proc. 36th Annual Conference on IEEE Industrial Electronics Society (IECON 2010)*, pp 3034-3039, 2010.
- [92] H. Kakigano, N. Nomura, T. Ise, "Loss evaluation of DC distribution for residential houses compared with AC system", in *Proc. of International Power Electronics Conference (IPEC)*, pp 480-486, 2010.
- [93] S. Saponara, P. Tisserand, P. Chassard, D. My-Ton, "DC/DC Converter Integrated Architecture for 48V Supplies in Micro/mild Hybrid Vehicle Electrical Engine Control Module", *IEEE 16th*

- International Conf. on Environment and Electrical Engineering (EEEIC 2016), 7-10 June 2016, Florence, Italy.
- [94] Altera. Cyclone III FPGA Starter Board Reference Manual. October 2007.
https://www.altera.com/products/boards_and_kits/dev-kits/altera/kit-cyc3-starter.html
- [95] Nial Stewart Developments Ltd. HSMC General Purpose Interface Board (GPIB) User Guide.
<http://www.nialstewartdevelopments.co.uk/products.htm>
- [96] Altera. Introduction to the Quartus® II Software. Version 9.1.
<https://www.altera.com/downloads/software/quartus-ii-we/91.html>
- [97] “Radio disturbance characteristics for the protection of receivers used on board vehicles, boats, and on devices – Limits and methods of measurement”, CISPR 25, 2002.
- [98] Ferrites and Accessories, EPCOS Data Book 2013.
<https://en.tdk.eu/download/519704/069c210d0363d7b4682d9ff22c2ba503/ferrites-and-accessories-db-130501.pdf>

PUBLICATIONS

- [1] G. Ala, M. C. Di Piazza, G. C. Giaconia, G. Giglia, G. Vitale, “Design and performance evaluation of a high power density EMI filter for PWM inverter-fed induction motor drives”, IEEE Transaction on Industry Applicatons, vol. 52, pp. 2397-2404, 2016, DOI: 10.1109/TIA.2016.2518129.
- [2] G. Ala, G. C. Giaconia, G. Giglia, M. C. Di Piazza, M. Luna, G. Vitale, P. Zanchetta, “Power Density Improvement by Optimized Design of EMI filters for Power Electronic Converters”, submitted to IEEE Transaction on Industry Applicatons.
- [3] G. Ala, M. C. Di Piazza, G. C. Giaconia, G. Giglia, G. Vitale, “Design and performance evaluation of a high power density EMI filter for PWM inverter-fed induction motor drives”, IEEE 15th International Conf. on Environment and Electrical Engineering (EEEIC 2015), 10-13 June 2015, Rome, Italy.
- [4] G. Ala, G. C. Giaconia, G. Giglia, M. C. Di Piazza, M. Luna, G. Vitale, P. Zanchetta, “Computer Aided Optimal Design of High Power Density EMI Filters”, IEEE 16th International Conf. on Environment and Electrical Engineering (EEEIC 2016), 7-10 June 2016, Florence, Italy.
- [5] G. Ala, G. C. Giaconia, G. Giglia, M. C. Di Piazza, M. Luna, G. Vitale, P. Zanchetta, “Optimized Design of High Power Density EMI Filters for Power Electronic Converters”, IEEE International Conf. on Electrotechnical, Electronics, Automation, IT and Telecommunications Society (AEIT 2016), 5-7 October 2016, Capri, Italy.
- [6] G. Ala, G. C. Giaconia, G. Giglia, M. C. Di Piazza, M. Luna, G. Vitale, P. Zanchetta, “ODEF: an Interactive Tool for Optimized Design of EMI Filters”, IEEE 42nd International Conference on Industrial Electronics Society (IECON 2016), 24-27 October 2016, Florence, Italy.
- [7] G. Ala, M. C. Di Piazza, E. Francomano, G. C. Giaconia, G. Giglia, G. Vitale (2015). Filtri EMI compatti nei convertitori elettronici di potenza. In atti della XXXI Riunione Nazionale dei Ricercatori di Elettrotecnica - 17-19 giugno 2015, Genova.
- [8] G. Ala, M. C. Di Piazza, G. C. Giaconia, G. Giglia, M. Luna, G. Vitale, P. Zanchetta (2016). Progettazione ottimizzata di filtri EMI a elevata Power Density per convertitori elettronici di potenza. In atti della XXXII Riunione Nazionale dei Ricercatori di Elettrotecnica - 15-17 giugno 2016, Palermo.